Integration of Storage Devices into Power Systems with Renewable Energy Sources

Final Project Report

Power Systems Engineering Research Center

Empowering Minds to Engineer
the Future Electric Energy System

Integration of Storage Devices into Power Systems with Renewable Energy Sources

Final Project Report

Project Team

George Gross, Project Leader
Alejandro Dominguez-Garcia
University of Illinois at Urbana/Champaign

Chanan Singh and Alex Sprintson
Texas A&M University

PSERC Publication 12-24

September 2012

For information about this project, contact:

George Gross
Department of Electrical and Computer Engineering
University of Illinois at Urbana-Champaign
1406 W. Green Street
Urbana, IL 61801
Email: gross@illinois.edu

Power Systems Engineering Research Center

The Power Systems Engineering Research Center (PSERC) is a multi-university Center conducting research on challenges facing the electric power industry and educating the next generation of power engineers. More information about PSERC can be found at the Center's website: http://www.pserc.org.

For additional information, contact:

Power Systems Engineering Research Center
Arizona State University
527 Engineering Research Center
Tempe, Arizona 85287-5706
Phone: 480-965-1643
Fax: 480-965-0745

Notice Concerning Copyright Material

Acknowledgements

This is the final report for the Power Systems Engineering Research Center (PSERC) research project titled “Integration of Storage Devices into Power Systems with Renewable Energy Sources” (project S-40). We express our appreciation for the support provided by PSERC’s industry members and by the National Science Foundation under the Industry / University Cooperative Research Center program.

We wish to thank the following Industry Team Members whose advice we acknowledge: N. Bhatt, EPRI; F. Galvan, Entergy; M. Patel, PJM; L. Min, EPRI; X. Luo, NE-ISO; and Doug Bowman, Southwest Power Pool.

Executive Summary

The recent advances in the state of the art of storage technology have led to wider deployment of storage technologies in today's electricity networks. This project developed models, simulation methodologies and control strategies for analyzing the effects of storage integration into grids at the transmission and distribution levels and for their effective operations in those grids. The advancements reported here explicitly make use of storage as a system resource that provides the flexibility to mitigate the effects of variable renewable energy sources, improves the overall system reliability, and has the ability to provide energy- and capacity-based ancillary services.

The research was performed in four separate parts with two focusing on the transmission level integration of storage resources and the other two on the distribution grid integration. The scope of work and the results are presented in the four parts. The following is a summary of each of the four parts.

Part 1: Simulation of Energy Storage in a System with Integrated Wind Resources

Wind is a clean and renewable source of energy with zero fuel costs. However, wind generation outputs are highly variable, intermittent and with rather limited controllability by the operator. The wind speed patterns present a key challenge to integration of wind resources since the wind may not blow when the system most needs the wind resource output or blow in hours of surplus generation, creating concerns about "spilling" wind energy due to the insufficiency of the load demand. The basic tool operators use to manage the wind variability is the raising of the reserve levels, which, typically, results in increasing the overall production costs. As such, the full economic and environmental benefits of harnessing wind energy cannot be realized. Such situations create excellent applications for utility-scale storage to facilitate the improved harnessing of the wind resources by storing wind energy for release during peak-load hours so as to displace the costly energy from polluting generating units. We have developed a stochastic simulation methodology to emulate the behavior of power systems with integrated wind and storage resources. This methodology is able to evaluate the impacts of storage integration into a grid with wind resources, taking explicitly into account various sources of uncertainty, wind variability and intermittency and the impacts of the time varying transmission constraints on the deliverability of the electricity to the loads. The methodology may be used to quantify the variable effects of large-scale power systems with storage and intermittent wind resources operating in a market environment. There is a broad range of applications of the simulation methodology to planning, investment, transmission utilization and policy formulation and analysis studies for systems with integrated storage and variable energy sources. In addition, the methodology is very useful in the study of a broad array of *what if* questions.

The simulation methodology – based on the deployment of Monte Carlo simulation techniques – uses systematic sampling mechanisms to compute the realizations of the various stochastic processes used to represent the sources of uncertainty and to construct the so-called sample paths. The approach uses an hour as the smallest indecomposable unit of time and uses the realizations of the stochastic processes at these discrete sub-periods. A salient characteristic is the ability to capture effectively the synergies between variable energy resource outputs and storage units so as to include the impacts of storage integration into power systems with multi-site wind farms. We have developed a storage scheduler to determine, given the initial state of the system and its forecasted evolution, the optimal trajectory of the state of each integrated

storage unit for each hour in the scheduling period with the objective to maximize the system total social surplus over that period. We simulate the clearing of the hourly transmission-constrained day-ahead markets by solving the *DCOPF* problem that is used to represent each hourly market. As such, the approach explicitly represents the chronology of time-dependent phenomena and transmission network constraints that influence the deliverability of the energy. The methodology is capable to account for the spatial correlation among the stochastic processes representing the variable energy resources as well as the correlation with the loads and over time. We also devoted much attention to ensure the computational tractability of the tool so as to allow the simulation over longer-term periods.

The presented results of representative case studies effectively illustrate the synergies among wind and storage resources. Our studies indicate that the deepening penetration of wind resources in systems with integrated storage resources contributes to significantly reducing the *LMP*s and the expected wholesale purchase payments and provides marked improvements in the system reliability. The presence of utility-scale *MWweek* storage units indeed accentuates such benefits, particularly at deeper wind penetrations where it tends to attenuate the "diminishing return" effects of installing more wind capacity. The case study results discussed the impacts that the siting of a storage unit can have on certain nodes and even the entire system performance. Furthermore, our studies on the integration of multiple storage units show that it is more beneficial, in general, to implement smaller distributed storage units into the network rather than the installation of a single large storage unit.

Part 2: Modeling and Simulation to Study the Impacts of Storage on the Reliability of Composite Power Systems with Wind Farms

Many countries, including the United States, have set targets to include a significant share of wind and solar resources into their energy portfolios. However, wind power is highly variable and uncertain because of its intermittent and fluctuating characteristics. Storage devices offer substantial benefits to system operations by providing the flexibility to mitigate the effects of variable renewable energy sources and the ability to provide energy- and capacity-based ancillary services. The basic objective of this effort is to develop modeling and simulation methodology to study the impacts of storage on the reliability of power systems when wind farms are integrated into the composite system.

To develop realistic models for the composite system, it is important to construct good models for the subsystems. The reliability models of conventional generation have been well developed. However, the models for the wind farms are inadequate and lack realism. As such, we devote the first subsection to describe the work done to improve the wind farm models. We then discuss in the subsequent sections the modeling and simulation methodology to study the effect of storage on the reliability of the composite power system and the optimization scheme developed for the optimal storage deployment to manage the variable characteristics of wind using sensitivity analysis.

We present several studies to illustrate the use of the methodology incorporating the improved wind farm models and the storage optimization scheme. We make use of Monte Carlo simulation, based on next event form of sequential approach. We evaluate the Loss of Load Expectation (LOLE) and the Expected Energy Not Supplied (EENS) indices to assess the system reliability, making extensive use of National Renewable Energy Laboratory wind data. We

investigate and analyze the results on the IEEE Reliability Test System (RTS) under different scenarios.

Part 3: Integration of Electric Energy Storage into a Distribution Level Grid with Integrated Renewable Energy Resources

We investigate the reliability and economic impacts of energy storage and renewable energy integration into the distribution level grid. We examine various operational strategies of the distribution grid integrated energy storage and renewable energy resources, making use of a dedicated reliability and economy framework. We construct the methodology for optimizing the energy storage size and its operation to achieve optimal reliability and economy. A key focus is on the scheduling and operation of distribution systems with energy storage so as to effectively harness the major benefits of electric energy time-shift, power supply capacity and transmission congestion relief imparted by the deployment of energy storage. We analyze the solution of the effective scheduling of the energy storage by a load aggregator who participates in the day-ahead and the real-time balancing markets. The judicious application of a Model Predictive Control-based approach allows the scheduling of the storage so as to minimize the energy costs of the load aggregator across the two markets. We investigate the impacts of the price and load forecast uncertainties on the energy costs.

We investigate the adequacy and economy characteristics of distribution grid integrated energy storage and renewable energy resources under different operational strategies. The use of the operational flexibility in the storage deployment results in a wide range of results for the tightly coupled economic benefits and reliability impacts. We discuss in detail these impacts in the load aggregator case utilization of energy storage for the minimization of the energy purchase costs. We construct an assessment framework, based on sequential Monte Carlo simulation approach, to evaluate the reliability and economic impacts. We illustrate its application to study the distribution system reliability enhancement in an islanding operation with renewable and storage energy power supplies.

We also investigated how to effectively take advantage of the multi-purpose benefits of energy storage deployment. In this context, we study a multi-objective approach to design energy storage implementation in distribution systems. A modified particle swarm optimization approach is proposed for the design of energy storage utilization in distribution systems, where not only the energy storage capacity and power are determined but also the energy storage operation strategy.

Part 4: Algorithms for Decentralized Control of Distributed Storage Resources

The objective of this research is to enable the effective utilization of distributed storage resources (DSRs) connected at the distribution level voltage at various places in the network. The basic concept is to develop appropriate coordination mechanisms to deploy DSRs for the provision of frequency response services. Such a task needs to be accomplished with the minimum amount of communications among the dispersed devices and the aggregating entity of these resources. A potential application of the mechanism is to the aggregation of battery vehicles in a single parking lot or in multiple parking lots during the day and to the aggregation of battery vehicles that are charged during the night at disparate locations on the network.

Two possible communication and control architectures exist to enable the effective coordination of DSRs – either completely centralized control architecture or distributed architecture. In

centralized control architecture, each DSR is commanded from a central controller. To implement this centralized architecture, it is necessary to overlay a communication network connecting the central controller with each distributed resource, and requires knowledge of the DSRs that are available on the distribution side at any given time. An alternative is to implement a completely distributed architecture where DSRs react to local signals and signals provided by neighboring DSRs. This distributed architecture has the potential to offer several advantages over its centralized counterpart: i) it is more economical because it does not require communication between a centralized controller and the various devices, ii) it does not require complete knowledge of the DSRs, and iii) it can be more resilient to faults and/or unpredictable behavioral patterns by the DSRs. Such a solution may rely on inexpensive and simple communication protocols, e.g., ZigBee technology, that provides the required local exchange of information for the distributed control approach to work. In this research, we pursue this distributed approach, providing algorithms that enable utilization of distributed resources for grid support.

In the setting we consider, each DSR can only exchange information with storage devices in its immediate neighborhood, and is endowed with a processor that can perform simple computations. We assume that the individual ability of each DSR is upper bounded by known capacity limits. Communication links between DSRs can be asymmetric, i.e., DSR *j* may be able to send information to DSR *i*, but not necessarily the other way, so that the information exchange between DSRs in the system can, in general, described by a directed graph. Our focus is on linear iterative algorithms in which a DSR *j* maintains a set of values that are updated to be weighted linear combinations of the device's previous values and the values of the DSRs that can send information to DSR *j*. A convergence analysis of the algorithms is presented, followed by the discussion of a modification that enhances the resiliency of the algorithms when the communication links are imperfect. We describe the development of a hardware testbed comprised of low-complexity devices equipped with wireless transceivers that implements the algorithms. We conclude by illustrating the efficacy of the algorithms by utilizing the hardware testbed to demonstrate each of the distributed algorithms.

In the setting we consider, each DSR can only exchange information with storage devices in its immediate neighborhood, and is endowed with a processor that can perform simple computations. We assume that the individual ability of each DSR is upper bounded by known capacity limits. Communication links between DSRs can be asymmetric, i.e., DSR j may be able to send information to DSR, but not necessarily the other way, so that the information exchange between DSRs in the system can, in general, described by a directed graph. Our focus is on linear iterative algorithms in which a DSR j maintains a set of values that are updated to be weighted linear combinations of the device's previous values and the values of the DSRs that can send information to DSR j. A convergence analysis of the algorithms is presented, followed by the discussion of a modification that enhances the resiliency of the algorithms when the communication links are imperfect. We describe the development of a hardware testbed comprised of low-complexity devices equipped with wireless transceivers that implements the algorithms. We conclude by illustrating the efficacy of the algorithms by utilizing the hardware testbed to demonstrate each of the distributed algorithms.

Principal Outcomes

The project efforts resulted in improved ability to exploit the increased flexibility imparted by storage applications to the power system through the development of appropriate models, methodologies and control strategies. The major results include:

- The development of a comprehensive stochastic simulation methodology to quantify the economic, environmental emission and reliability variable effects of storage integration into power systems with integrated intermittent renewable resources;
- A practical approach for the analysis of various problems and issues in system planning, operations, investment analysis, decision-making under uncertainty and policy formulation concerning bulk power system operations in the smart grid environment under deepening penetration levels of renewable resources;
- The effective deployment of energy storage to manage the A Model Predictive Control-based approach is developed to study the potential to better manage the energy cost of a load aggregator with EES in a market mechanism consisting of day-ahead market and real-time balancing market is explored.
- An assessment framework based on sequential Monte Carlo simulation approach is developed to assess the reliability and economic impact of proposed operation strategies.
- A multi-objective optimization methodology to construct Pareto-optimal solutions for conflicting objectives in the optimal design of storage utilization;
- An optimization methodology for the assessment of the impacts of storage on the reliability of a composite system with integrated variable energy sources;
- More realistic modeling of wind farm power production for use in reliability assessment;
- A distributed control architecture for distributed storage resources and associated robust and convergent algorithms that adhere to the communication topology;
- A hardware testbed comprised of low-complexity devices with wireless- transceiver-based implementation of the algorithms for the coordination of distributed storage resources.

Project Publications

1. N. Maisonneuve and G. Gross, "A production simulation tool for systems with integrated wind energy resources", *IEEE Transactions on Power Systems*, vol. 26, no. 4, pp. 2285 – 2292, Nov. 2011.
2. Y. Degeilh, J. Descloux and G. Gross; "Simulation of Energy Storage in a System With Integrated Wind Resources", Proceedings of the *17th Power Systems Computation Conference*, Stockholm, Sweden, Aug. 2011.
3. Y. Degeilh, F. Cadoux, N. Navid and G. Gross, "Impacts of ramp capability constraints in electricity markets with the participation of renewable resources," Proc. Of IEEE PES General Meeting, July 21-25, 2012, San Diego.

4. Y. Xu and C. Singh, "Adequacy and Economy Analysis of Distribution Systems Integrated with Electric Energy Storage and Renewable Energy Resources," IEEE Transactions of Power System, to appear.

5. Y. Xu and C. Singh, "Multi-Objective Design of Energy Storage in Distribution Systems Based on Modified Particle Swarm Optimization," Proc. of IEEE PES General Meeting, San Diego, July 21-25, 2012.

6. Y. Xu, L. Xie and C. Singh, "Optimal Scheduling and Operation of Load Aggregators with Electric Energy Storage Facing Price and Demand Uncertainties," Proc. of North American Power Symposium, August 4-6, Boston, September 2011.

7. Y. Xu and C. Singh, "Distribution Systems Reliability and Economic Improvement with Different Electric Energy Storage Control Strategies," Proc. Of IEEE PES General Meeting, Detroit, July 24-29, 2011.

8. Y. Xu, L. Xie and C. Singh, "Optimal Scheduling and Operation of Load Aggregator with Electric Energy Storage in Power Markets," Proc. of North American Power Symposium, Arlington, TX, September 26-28, 2010.

9. H. Kim, C. Singh and A. Sprintson, "Simulation And Estimation Of Reliability In A Wind Farm Considering The Wake Effect, " IEEE Transactions on Sustainable Energy, vol.3, no.2, pp. 274-282, April 2012.

10. H. Kim, C. Singh and A. Sprintson, "Comparison of wake models for reliability analysis," Proc. of International Conference on Probabilistic Methods Applied to Power Systems, Istanbul, Turkey, June 10-14, 2012.

11. H. Kim and C. Singh, "Comparison of clustering approaches for reliability simulation of a wind farm," Proc. of IEEE PES International Conference on Power Systems Technology, Auckland, New Zealand, October 30-November 2, 2012.

12. H. Kim and C. Singh, "Reliability simulation in wind farm with different wind turbines," Proceedings of National Power Systems Conference, Decemeber 12-14, 2012, V aranasi, India.

13. C. N. Hadjicostis, A. D. Domínguez-García, and N. H. Vaidya, "Resilient Average Consensus in the Presence of Heterogeneous Packet Dropping Links," in Proc. of the IEEE Control and Decision Conference, Maui, HI, December 2012.

14. S. T. Cady and A. D. Domínguez-García, "Distributed Generation Control of Small-Footprint Power Systems," in Proc. of North American Power Symposium, Champaign-Urbana, IL, September 2012.

15. A. D. Domínguez-García, C. N. Hadjicostis, and N. H. Vaidya, "Resilient Networked Control of Distributed Energy Resources," IEEE Journal on Selected Areas in Communications: Smart Grid Communications Series, vol.30, no.6, p p.1137-1148, July 2012.

16. A. D. Domínguez-García and C. N. Hadjicostis, "Distributed Algorithms for Control of Demand Response and Distributed Energy Resources," in Proc. of the IEEE Control and Decision Conference, Orlando, FL, December 2011.

17. S. T. Cady, A. D. Domínguez-García, C. N. Hadjicostis, “Robust Implementation of Distributed Algorithms for Control of Distributed Energy Resources,” in Proc. of North American Power Symposium, Boston, MA, August 2011.

Student Theses

1. Z. Zheng, “Impacts of Energy Storage Siting on Power System”, Senior Thesis, submitted to the Department of Electrical and Computer Engineering, University of Illinois, Urbana, IL, May 2012.

2. Y. Degeilh, “Stochastic Simulation of Power Systems with Variable Energy Resources,” under preparation and to be submitted to the Department of Electrical and Computer Engineering, University of Illinois, Urbana, IL to meet the Ph. D. degree requirements, 2013.

3. Y. Xu, "Integration of Electric Energy Storage into Distribution Systems with Renewable Energy Resources", Ph.D. Thesis, Texas A&M University, 2012.

4. H. Kim, "Reliability Modeling and Simulation of Composite Power Systems with Wind Farms and Storage Techniques", Ph.D. Thesis, Texas A&M University, 2013.

5. S. T. Cady, "Robust implementation of algorithms for distributed generation control of small-footprint power systems," M.S. Thesis, University of Illinois at Urbana-Champaign, May 2012.

Part 1

Simulation of Energy Storage in a System with Integrated Wind Resources

George Gross
Yannick Degeilh, Doctoral Student
University of Illinois at Urbana/Champaign

For information about Part 1, contact:

George Gross
Department of Electrical and Computer Engineering
University of Illinois at Urbana-Champaign
1406 W. Green Street
Urbana, IL 61801
Email: gross@illinois.edu

Power Systems Engineering Research Center

The Power Systems Engineering Research Center (PSERC) is a multi-university Center conducting research on challenges facing the electric power industry and educating the next generation of power engineers. More information about PSERC can be found at the Center's website: http://www.pserc.org.

For additional information, contact:

Power Systems Engineering Research Center
Arizona State University
527 Engineering Research Center
Tempe, Arizona 85287-5706
Phone: 480-965-1643
Fax: 480-965-0745

Notice Concerning Copyright Material

Table of Contents

List of Figures

List of Tables

1. Introduction

Wind is widely viewed as a clean and renewable source of energy with zero fuel costs and zero emissions. However, wind generation outputs are highly variable, intermittent and only controllable by t he operator to a limited extent. The wind speed variable/intermittent nature presents major challenges in the integration of wind resources as the wind may fail to blow when the system actually needs the wind generation output and so make it difficult to use the wind resource at such times. Indeed, a very frequent phenomenon in many regions with wind resources is the pronounced output of wind generation, due to the appropriate wind speeds, in the low-load hours and rather low or near zero outputs, due to the low wind speeds, during the peak-load periods. Such a mismatch of the generation and load due to the wind speed patterns, coupled with the limited controllability over wind resources, implies that the full potential of grid integrated wind resources may not be realized. Moreover, there are serious concerns about the "spilling" of wind energy during low load conditions due to the insufficient load demand. Indeed, in such cases, the grid is unable to harness all the benefits from the use of the wind energy to meet the demand. The basic mechanism that system operators use to manage the wind variability and intermittency is to raise the reserve levels. Such operational tactics, typically, lead to increases in the overall production costs and emissions, notwithstanding the zero fuel costs and emissions of the wind resources. It is precisely such situations that create excellent applications of utility-scale storage resources, with *MWweek* storage capability, to improve the utilization of the wind resources by storing wind energy whenever produced for release during peak-load hours so as to displace the costly energy from polluting generating units. While storage resources are highly costly investments, their effective management – charge-discharge schedule and operations – impacts considerably the total costs since they influence the variable portion of the costs. As such, power system engineers need appropriate tools for the effective deployment of such resources so as to ensure that the improved harnessing of variable generation units is realized. A particularly acute need is a practical simulation tool that can reproduce with good fidelity the expected variable effects in systems with variable energy resources (*VER*), such as renewable and storage units. Such a tool allows the quantification of the variable effects and is useful in power system planning, operations and investment analysis. We describe in this part of the Final Report the development of a comprehensive and sufficiently general methodology – the models and the simulation approach – that forms the basis of the simulation tool, which is capable to provide answers to a broad range of planning, investment, emission reduction quantification and reliability improvement questions. In addition, the methodology allows engineers to analyze issues in the areas related to the economically efficient and effective utilization of storage devices in the grid.

We developed the stochastic simulation approach of systems with integrated wind and storage resources with the ability to take explicitly into account

- The market structure;
- The various sources of uncertainty, wind variability and intermittency;
- The coordinated operation of multiple integrated storage units; and

- The impacts of the time varying transmission constraints on the deliverability of the electricity to the loads in the evaluation of the expected production costs, expected emissions and reliability indices.

The methodology allows the quantification of the variable effects of large-scale power systems with storage and intermittent *VER*s. The conventional probabilistic simulation approach cannot be used to capture the time-varying nature and the inter-temporal effects required in the simulation of the storage and intermittent *VER*s. Consequently, the representation of the loads and resources in the system requires that stochastic-process-based models be used. The methodology is capable to account for the spatial correlation among the stochastic processes representing the *VER*s as well as the correlation with the loads and over time. We also devoted much attention to ensure the computational tractability of the tool so as to allow the simulation over longer-term periods.

The approach uses an hour as the smallest indecomposable unit of time and uses the realizations of the stochastic processes at these discrete sub-periods. In addition, a snapshot representation of the grid is used to represent the transmission-constrained day-ahead markets (*DAM*s). The modeling of the storage operations takes into account arbitrage possibilities in the charging and discharging of the units and storage cycle efficiency characteristics. The simulation methodology – based on the deployment of Monte Carlo simulation techniques – uses systematic sampling mechanisms to compute the realizations of the various stochastic processes and to construct the so-called sample paths. A salient characteristic is the ability to capture effectively the synergies between *VER* outputs and storage units so as to include the impacts of storage integration into power systems with multi-site wind farms in the assessment of the reliability, emission and economics metrics. We compute such metrics using the outcomes of the hourly *DAM*s. We obtain the market clearing results of the transmission-constrained hourly *DAM*s by determining the solution of the optimal power flow using a linearized *DC* model – the so-called *DCOPF* problem [1]. Based on the sample paths used as inputs into the *DCOPF* problem, we construct the approximations to the various economic, emission and reliability metrics. These metrics include the hourly expected locational marginal prices (*LMP*s), congestion rent contributions, revenues of the generators, payments made by buyers, either energy charged into or discharged by storage, and the emission, the *LOLP* and the *EUE* contributions. We note that in all these metrics, we implicitly account for the effects of the deliverability of the electricity. From the hourly values, we then determine the values for the simulation periods, which are then used to determine the metric values for the study period. The methodology is able to capture the seasonal effects in loads and wind speeds, the impacts of maintenance scheduling and the ramifications of new policy initiatives. For the performance of various policy studies, we also provide weekly unit commitment schedules that allow the user to specify the weekly reserves requirements. These features are essential in the analysis of the substitutability of conventional generation by renewable resources and storage technologies under deepening penetration levels. There is a broad range of applications of the simulation methodology to planning, investment, transmission utilization and policy formulation and analysis studies for systems with integrated storage and *VER*s. A very useful feature of the tool is the ability to quantitatively assess the impacts of deepening penetration of wind and storage technologies.

There are five additional sections in this volume of the Final Report. We devote the next section to describe the key features of the modeling and the construction of the Monte Carlo simulation technique used in the methodology we developed. In section 3, we discuss the issues in the

modeling and scheduling of energy storage resources. We outline, in section 4, the various steps used in the implementation of the methodology to ensure computational tractability in the study of large-scale systems over longer time periods. In section 5, we provide a list of applications of the methodology and illustrate with the results of representative case studies. We conclude in section 6 with some summary remarks and directions for future work.

2. The Monte Carlo Simulation of Power Systems with Integrated Wind and Storage Resources

We start out the discussion of the simulation approach by setting the stage with a description of the time frame definition. The study period of the simulation is partitioned into non-overlapping simulation periods, whose union covers the entire study period. We define each simulation period in such a way that the system resource mix and its unit commitment, the transmission grid, the operating policies, the market structure and the seasonality effects have uniform characteristics over its entire duration. While there are many choices for the study period, to make this discussion concrete, we specify each simulation period to be of one-week duration. We further decompose each simulation period into its constituent sub-periods, where a sub-period is the smallest indecomposable unit of time in the models deployed. We choose the sub-period to be of one-hour duration. Such a choice represents a compromise between the needed level of detail for a realistic representation of the power system and market operations behavior and the computational resources to carry out all simulation studies that constitute the study period.

The incorporation of the time-dependent storage and *VER*s cannot be accommodated in the conventional probabilistic simulation framework [2, 3]. The modeling of the highly variable and intermittent characteristics of the *VER*s and the various sources of uncertainty, both of a climatological and geographic nature, with which they are associated, require that we represent them as discrete-time indexed stochastic processes defined at each sub-period in the simulation period. As such, we also need to represent the loads and the conventional resources by such stochastic processes. A salient feature of the methodology is the fact that the models are capable to account for the spatial correlation among the stochastic processes representing the *VER*s as well as the correlation with the loads and over time. Clearly, since the storage operations are dependent on the *VER* and conventional resource outputs, we represent each storage unit by a similar stochastic process. An important feature of the simulation scheme is the ability to capture effectively the synergies between *VER* outputs at multi-site locations and storage units so as to include the impacts of storage integration in the emulation of the side-by-side power system and market operations. We next briefly discuss the representation of uncertainty in the wind resources, the loads and the conventional resource capacity availabilities by discrete-time stochastic processes.

We represent the daily patterns of the multi-site wind speeds and the resulting power outputs by discrete-time indexed stochastic processes defined for each hour of the day. We use the collected wind speed data to determine the corresponding wind power output patterns at the multiple locations for each day in a specific season and classify the patterns into groups with “similar” patterns [4]. From the categorized groups, we approximate the joint probability distributions of the daily multi-site wind output pattern stochastic processes so as to explicitly take into account the spatial and temporal correlations of the wind power outputs. While the discussion here is in terms of wind resources, the simulation scheme is general and can accommodate any other *VER*s, such as solar units.

We model the system load as a discrete-time indexed stochastic process defined over a week for each hour of the week. We assume that the time-indexed random variables making up such stochastic process are statistically independent. The immediate consequence is that the joint probability distribution of the stochastic process can be decomposed into the product of the marginal probability distributions of the time-indexed random variables. As such, we gather weeks of hourly data to construct the marginal probability distributions of the system load for each hour of the week. In the simulation, we assume that each buyer bids a specified, constant fraction of the system load. This representation allows us to capture the correlation with the time-varying *VER* output patterns.

We model a conventional generator as a multi-state unit whose transition times between its states, such as the failed, a nonnegative number of derated and the fully operational states, are characterized by independent exponentially-distributed random variables. We use a discrete-state Markov chain to represent the underlying stochastic process [5]. We make the assumption that the conventional generator stochastic processes are statistically independent from one another. The parameters of the exponentially-distributed transition time random variables of each Markov chain of a unit are based on historical data for the performance of the units.

A key element in the Monte Carlo simulation is the construction of the sample paths of the stochastic processes that represent the resources – supply and demand – in the power system. A sample path contains the realizations of the time-indexed random variables that constitute the stochastic process. We use independent sets of random numbers for sampling purposes in the sample path construction. The sampling is done to be consistent with the correlations among the time-indexed random variables. In this way, we are able to represent the interactions between *VER* outputs at multi-site locations and storage units over time. For the conventional units, we obtain the sample path of the available capacity of each unit by drawing samples from the associated Markov chain over the one-week simulation period. The sampled available capacity of a unit determines the maximum power output the unit may offer into the *DAM* of that hour.

The simulation uses the sample paths to determine the outcomes of each of the 168 transmission-constrained *DAM*s, one for of each hour in the simulation period. The realizations on the so-called "driver" sample paths, as seen on Fig.1, correspond to a particular hour of the simulation and provide the information for the construction of the offers of the sellers and the bids of the buyers in the corresponding *DAM*. We use a snapshot representation of the transmission network, with the time-varying characteristic of the network captured by the nodal injections – outputs of all the supply sources at a node – and nodal withdrawals – loads at a node – as determined by the realizations on the corresponding "driver" sample paths. We use a *DC* power flow to represent the real power balance relationships at the nodes of the network. We determine the hourly *DAM* clearing results from the solution of the optimal power flow (*OPF*) problem corresponding to that hour's realizations on the sample paths associated with the collection of stochastic processes. The *DCOPF* problem solution for the *DAM* then provides the realization for that hour of the values of the market outcomes that we use in the evaluations of the metrics. Since the variables that provide the inputs into the market clearing are random, so are the corresponding output variables that we use to characterize the performance of the side-by-side power system and market operations. The values of the metrics of interest – such as the *LMP*s, congestion rent contributions, revenues of the generators, payments made by buyers, either the energy charged into or the energy discharged by storage, and the emission, the *LOLP* and the *EUE* contributions – obtained from the clearing of a particular hour *h DAM* clearing results

provide the realizations from which we construct the corresponding sample paths of the "outcome" stochastic processes that represent those metrics. The simulation thus captures the time-dependent and uncertain nature of these metrics. Figure 1 depicts the conceptual procedure – in practice called simulation run – through which we obtain a sample path for each metric of interest represented by the associated "outcome" stochastic process. We note that, although not explicitly shown in the diagram of Fig. 1, some stochastic processes are multi-dimensional and their realizations at each time-indexed value are a vector. For example, a realization of the daily wind power output pattern at time-index h is a vector of the power outputs of the wind farms at the different sites.

We carry out multiple simulation runs in order to create the sample paths from which we estimate the expected values of the metrics. Each simulation run corresponds to a sample path. We determine the number of simulation runs from the statistical accuracy requirements we specify for the estimation of these expected values. This accuracy is a function of the confidence interval with which the expected value is determined. We construct the confidence interval for the true expected value of each time-indexed random variable corresponding to the metric stochastic process making use of the standard deviation of the sample mean estimator. The confidence interval width is inversely proportional to the square root of the number of sample paths used, i.e., the number of simulation runs. Hence, we determine the number of simulation runs from the confidence interval width corresponding to the specified statistical accuracy of the expected value estimate [6].

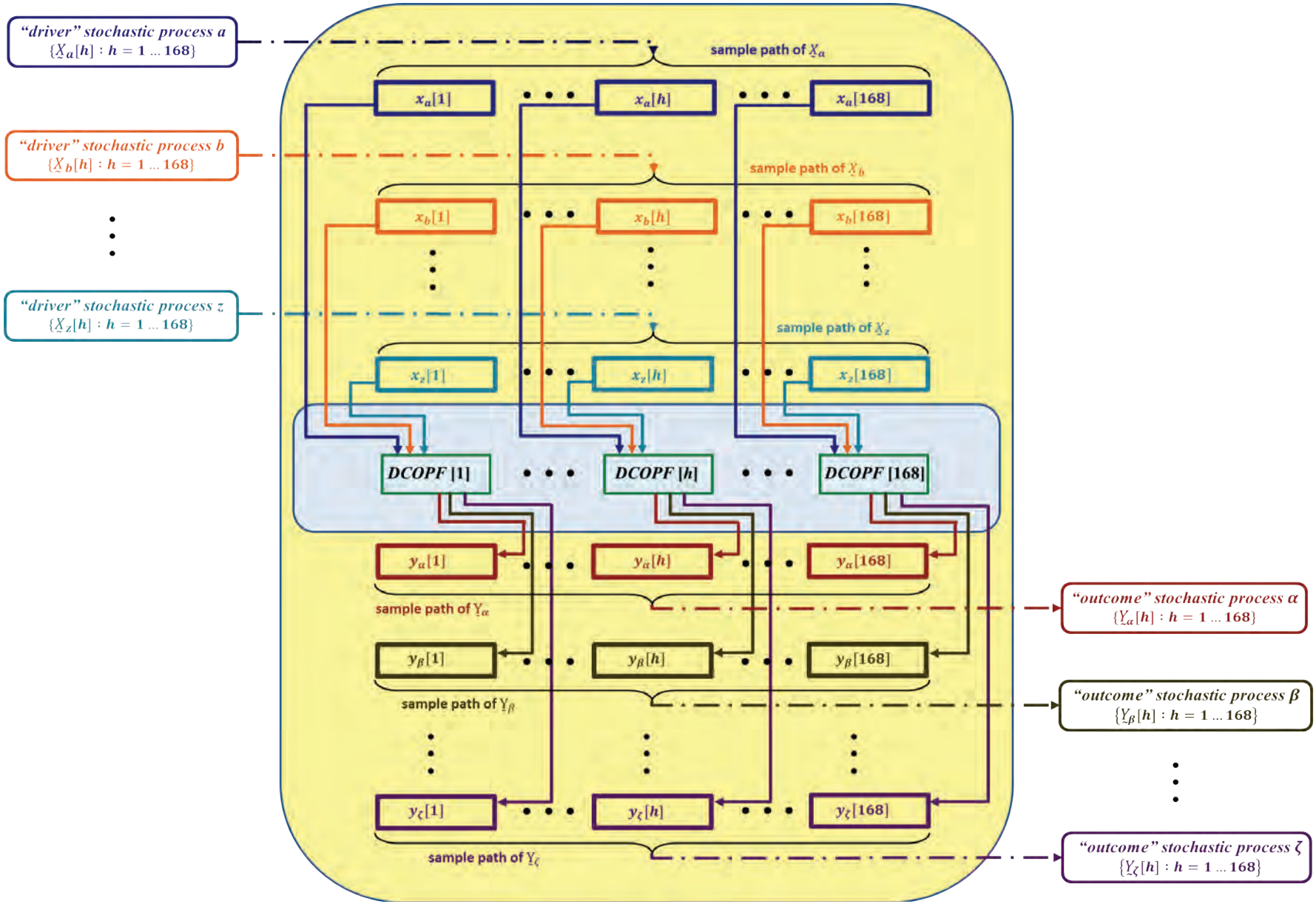

Figure 1: Conceptual representation of a single simulation run for the set of "driver" sample paths and the set of resulting "outcome" sample paths

We use the sample paths of the market outcome discrete time-indexed stochastic processes to determine the values of the economic, reliability and emission metrics. For each hour of the simulation period, we estimate the expected values of the random variables using the realizations in the sample paths corresponding to that hour. In this way, we compute for that hour the expected *LMP*s, the contribution to congestion rents, the revenues of the generators, the payments made by the buyers, either the expected energy delivered or the expected energy displaced by storage, as well as, the contributions to the expected emissions, *LOLP* and the *EUE*. The repeated evaluation of the metrics allows us to assess the variation from hour to hour of each metric during the simulation period. The weekly values of the metrics, with the exception of the *LMP*s, are obtained by summing up the hourly contributions over all the hours in the week. Other metrics that may be of interest can also be evaluated using this procedure. Also, we can use the sample paths to approximate the joint probability distributions of all the stochastic processes that are defined from the market outcomes. Thus, the Monte Carlo simulation provides the ability to estimate virtually any metric that measures the performance of the side-by-side power system and market operations. Also, as the Monte Carlo simulation allows the approximation of the joint probability distributions of all the stochastic processes, such approximation may be used in the evaluation of all probability-based measures that are of interest.

3. Storage Modeling and Scheduling

The incorporation of the models for the simulation of utility-scale *MWweek* storage units increases the complexity of the methodology development. These models represent the storage operations that occur across multiple hours and thus impact, and are impacted by, the hourly *DAM* outcomes. Indeed, a storage unit may be, at any point in time, either a generator, a load or idle. Moreover, for a storage unit to act as a generator is only possible once it has been charged. The implication is that the unit acts as a load in some of the preceding hours. In our simulation, we consider utility-scale storage units that are controlled by the Independent Grid Operator (*IGO*). The *IGO* operates the storage units so as to maximize the total social surplus over time, i.e., the sum of the hourly social surpluses as determined by the outcomes of the hourly *DAM*s. Under such premises, the *IGO* must be able to schedule each storage unit operations over multiple hours, while accounting for the available resources in those specific hours, including the intermittent outputs of the *VER*s and the operations of the other storage units. We assume that the final charge in each storage unit equals its initial charge. In this way, all the charged energy must be discharged during the simulation period.

We have developed a storage scheduler to assist with the decisions to determine the status of each storage unit, by taking full advantage of arbitrage opportunities in their operations, in a power system with integrated wind resources. We model the construction of such a storage schedule as a multi-period economic dispatch optimization that explicitly represents the inter-hourly constraints imposed by storage operations with the objective to maximize storage utilization for the benefit of the system over the period. The scheduler may be run at any hour to make use of the information to determine the status of each storage unit based on the current state of the system and its forecasted evolution. The scheduler indicates for each hour of the scheduling period the status of each storage unit – idle, charging or discharging – and provides the associated charge/discharge energy. The produced schedule determines the optimal operations of the storage units should so as to provide maximal benefits to the system in terms of

economics and reliability. As such, the schedule specifies the hours in which to charge (discharge) each storage unit during the low-load (peak-load) conditions.

We use the scheduler to provide an initial storage schedule at the beginning of the simulation period so as to provide the appropriate information for the hourly *DAM*s. We may rerun the scheduler at different points in the simulation period, as deemed necessary. For example, whenever the realized current state is considerably different from that forecasted, we rerun the scheduler for the remaining hours in the simulation period. The most recent schedule determines the way each storage unit participates in the hourly *DAM*s during the remaining periods of the simulation period. Whenever the storage unit is not idle, the schedule-determined charge/discharge energy is used to formulate the unit's bid or offer in the *DAM*. The storage unit participates in the hourly *DAM*s as a buyer (seller) to charge (discharge) with the scheduled energy providing the limiting value of the bid (offer). The bid price of a charging unit is set very high – typically at the value of loss of load (*VOLL*) so as to ensure the storage unit is charged. The offer price of a discharging unit is set to zero so as to encourage the use of the stored energy to displace the output of more expensive and dirty conventional units. While the outcomes of the hourly *DAM*s may deviate from the schedule in the realized operations of the storage units due to unforeseen load of loss or excessive congestion events, we observe, in general, the hourly *DAM*s tend to follow the storage schedule rather faithfully.

The procedures described above on the deployment of the scheduler and the participation of the storage units in the *DAM*s provide the means used to construct their sample paths to explicitly include their impacts in the side-by side power system and market operations. The actual impacts are determined from the sample paths of the market outcome metrics.

4. Implementation Aspects of the Monte Carlo Simulation

We discuss in this section the steps taken to ensure the computational tractability of the simulation approach. This is an important requirement due to the large-scale nature of the power systems and the need to run the simulation for longer-term periods. An important step in improving the computational tractability of the simulation approach is the selection of the representative simulation periods. Rather than simulate each of the 52 weeks of a year, we take advantage of the fact that several weeks in a season have similar wind and load patterns and the resources have the same planned outages in terms of the maintenance schedule. The identification of the representative weeks reduces the number of simulation periods to be run, thereby cutting down the computational efforts required to assess the power system economics, reliability and environmental impacts. The results of each representative week are multiplied by the total number of weeks to determine their contribution to the annual figures.

A second way to reduce the computational burden is the deployment of variance reduction techniques in the Monte Carlo simulation. We have investigated the use of various variance reduction techniques, including control variants, stratified sampling, common random numbers and antithetic variables. We make use of the stratification of daily wind patterns possible with the regime categorization developed earlier [4]. These techniques are effective in reducing the number of sample paths to obtain the desired statistical accuracy. The gains in computational tractability with these techniques are not large and they vary depending on the particular market outcome stochastic process.

Also, as the *DCOPF* solution is that of a linear program, the solution times may be reduced by the use of appropriate starting solutions [7, 8]. We implemented such a scheme in the simulations we run.

The proposed simulation approach also lends itself well to parallel processing. Each representative week may be simulated on a different core/computer. Additional parallelization is achievable also for the simulation of a representative week. Indeed, it is possible to parallelize the simulation runs in a simulation period by sampling the stochastic processes that represent the supply and demand resources. The stored sample paths allow their processing in parallel and can be then recombined to provide the results for the evaluation of the metrics for the 168 hours.

5. Applications of the Methodology and Case Studies

The proposed simulation approach is designed to be very versatile so as to be able to answer a wide range of *what* if questions. It may be used in a broad range of planning and operations analysis, investment decision-making and risk assessment, and policy formulation/analysis processes. We list a number of representative application areas, along with relevant examples, that can reap major benefits from the use of the proposed simulation approach. We have grouped the areas into eight broad classes and they are listed below in an unranked order together with some representative examples:

- Resource planning studies
    - year of commissioning of a wind farm or storage plant
    - siting of a storage unit
    - transmission utilization under increased *ADRR* implementation
- Production costing issues
    - impacts of various penetration levels of wind and/or storage resources
    - impacts of increases in fossil fuel prices
- Transmission utilization issues
    - impacts of renewable storage integration on transmission utilization
    - identification of frequently-congested transmission lines for use in the construction of portfolios of financial transmission rights
- Environmental assessments
    - identification of generation resource mixes to reduce CO_2 emissions by a specified fraction and a specified point in time
    - wind and storage resource synergies in terms of CO_2 emission impacts
- Reliability analysis
    - assessment of the effective load carrying capability of renewable resource addition requirements
    - evaluation of the reserves in a power system with deepening levels of renewable penetration

- Investment analysis
  - assessment of the expected returns of wind resource investments
  - risk assessment of investments to deepen the penetration of renewable resources
  - assessment of transmission investments to integrate renewable resources
- Policy formulation and analysis
  - incorporation of a *cap and trade* carbon market in the US
  - assessment of the impacts of policies aimed at providing financial incentives for the retrofitting of old and dirty generation units
- Broad range of questions
  - sensitivity studies on storage sizing
  - selection of remuneration schemes for *ADRR*s
  - scenario analysis of the impacts of future technology developments
  - various *what if* questions

This list of topics is, by no m eans, all inclusive and the methodology is sufficiently comprehensive and has wide flexibility to be applied to numerous other areas not included above.

We have tested the methodology on a large number of test systems and under a wide range of conditions. For the purposes of illustrating its application, we select three representative studies to investigate some issues of interest in the integration of storage batteries into a grid with integrated wind resources. All these studies are performed on a modified version of the IEEE-118 bus test system [9]. All the results are for a single year of simulation so as to allow the discussion to focus on the key thrusts of the application discussed. Additional details on the test system and the scope of the studies may be found in [10].

The first study is concerned with the determination of the impacts of a utility-scale storage nominal capacity on a power system with integrated wind resources. In this study, the aggregated nameplate capacity of wind power was fixed at roughly 30 % of the annual peak load of 8,021 *MW*. The storage unit reservoir (capability) was limited to 5,000 *MWh*. We ran sensitivity studies with different nominal storage capacity values ranging from 0 to 400 *MW* as indicated in Table 1.

Table 1: Storage capacity sensitivity studies

case	*storage capacity (MW)*
A	***0***
B	**200**
C	**300**
D	**400**
E	**500**

The following are the main findings of the study results:

- The storage unit always tends to charge in the low load hours so it can discharge during the peak load hours.
- Storage utilization increases as the nominal capacity grows as illustrated in Fig. 2.

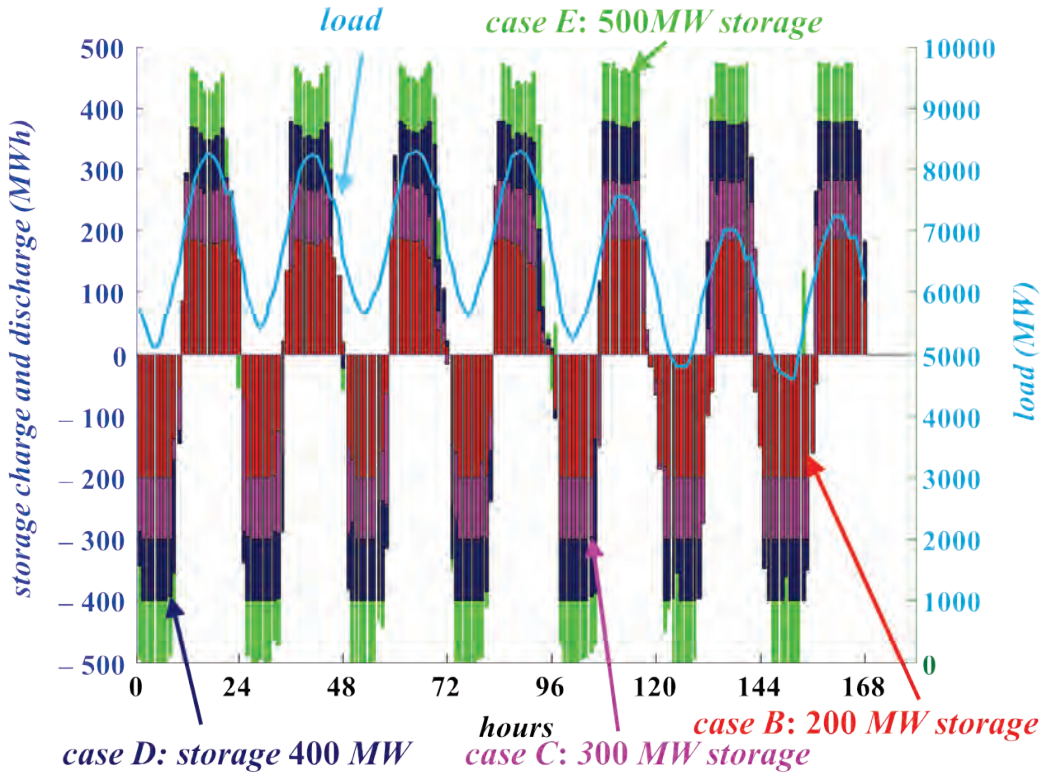

Figure 2: Average hourly storage utilization

- The total expected wholesale purchase payments by the buyers decrease as the storage nominal capacity increases. For a nominal capacity of 400 *MW* – about 5% of the annual peak load – the expected annual savings are 11.5% below the payments in the case without a storage unit. This is the case shown in Fig. 3. This decrease is primarily due to the fact that the storage unit displaces expensive thermal units in the peak load hours, thereby lowering the *LMP*s in the affected hours.

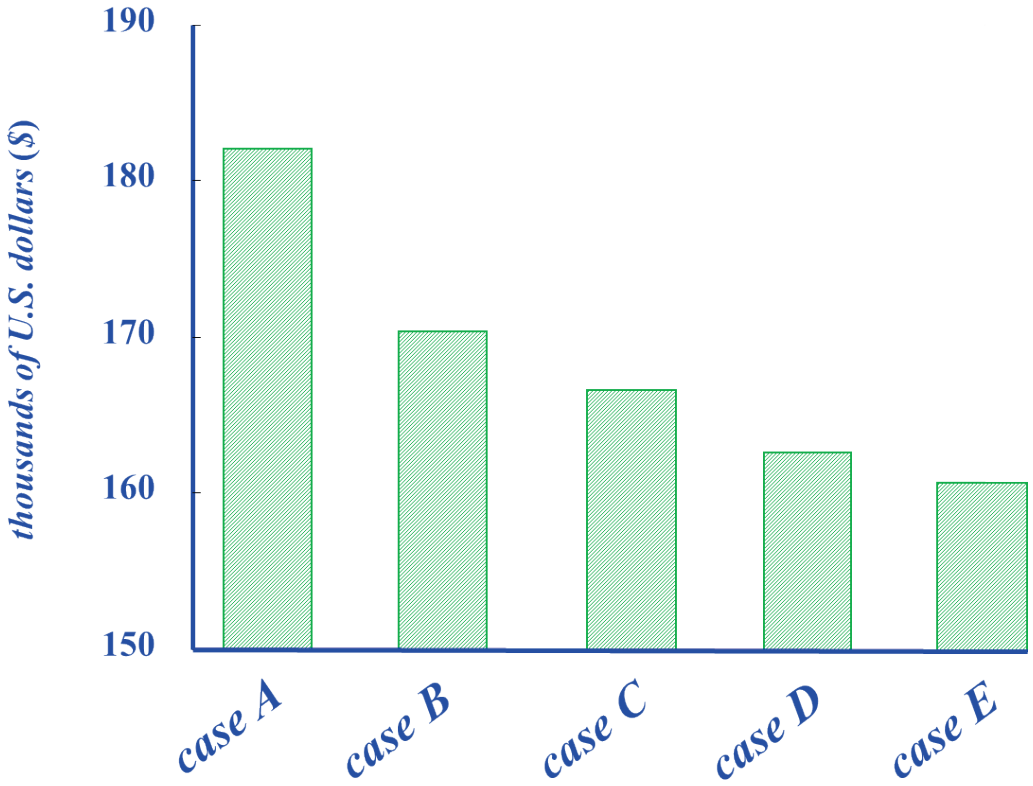

Figure 3: Expected weekly wholesale purchase payments

- The expected congestion rents tend to decrease slightly as the nominal capacity increases. The storage location at the particular node in the network reduces the system congestion.
- The expected CO_2 emissions do not vary significantly with changes in the nominal storage capacity. They largely depend on the generation mix of the considered power system, more specifically on the emission rates of the conventional units displaced by the storage unit and the emission rates of those units used to charge the storage.
- Both the *LOLP* and the *EUE* decrease as the storage nominal capacity increases, indicating an improvement in system reliability. Fig. 4 shows both the annual *LOLP* and *EUE* for the different values of storage capacity.

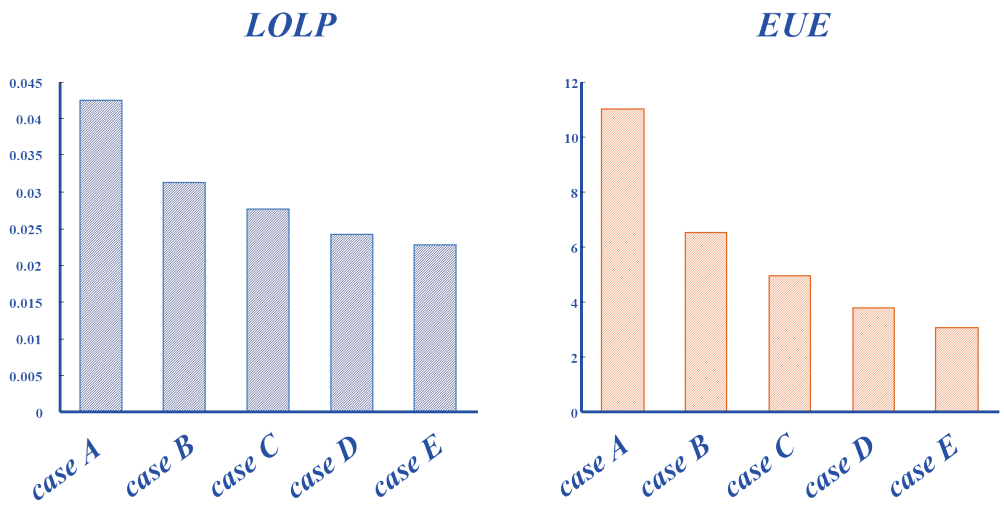

Figure 4: Annual reliability indices

- The reductions in the expected total wholesale purchase payments, expected congestion rents, the *LOLP* and the *EUE* become less pronounced as the nominal storage capacity increases, indicating diminishing returns with increased capacity.

These sensitivity studies are effective in providing some insights into the utility of a single storage resource and in indicating the limitations that may arise.

We discuss a second representative study, which investigates the impacts of deepening wind penetration in a power system with *or* without an integrated utility-scale storage unit. In this study, the storage nominal capacity is fixed at 400 *MW*, but the nameplate wind capacity increases from 0 to 2720 *MW* in increments of 680 *MW* as shown in Table 2. The maximum nameplate capacity is about one third about of the annual peak load of 8090.3 *MW*. We maintain constant reserve margins throughout the study.

Table 2: Wind penetration sensitivity studies

case	*total installed wind nameplate capacity in MW*
F	***0***
G	**680**
H	**1,360**
I	**2,040**
J	**2,720**

We briefly summarize the key findings of the study:

- The deeper penetrations of wind resources tend to reduce the *LMP*s, total expected wholesale purchase payments, the expected CO_2 emissions and to improve the system reliability. For illustrative purposes, we provide in Fig. 5 the average hourly *LMP* duration curve at bus 80. We present in Fig. 6 the corresponding annual reliability indices.

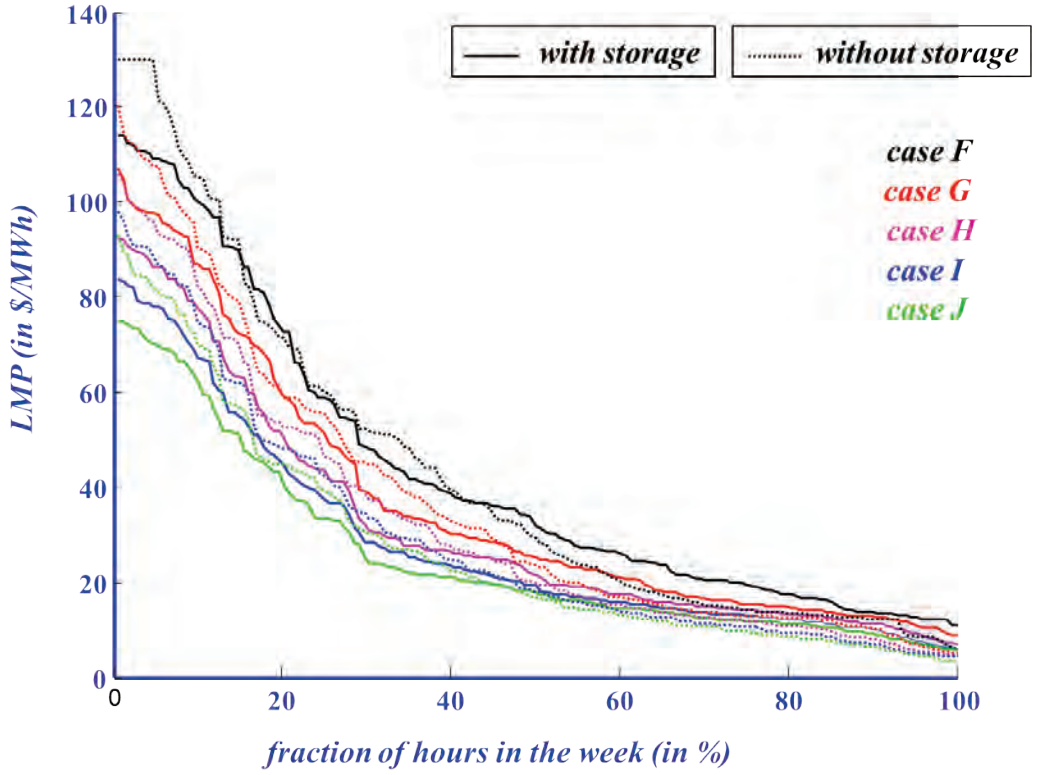

Figure 5: Average hourly *LMP* duration curve at bus 80

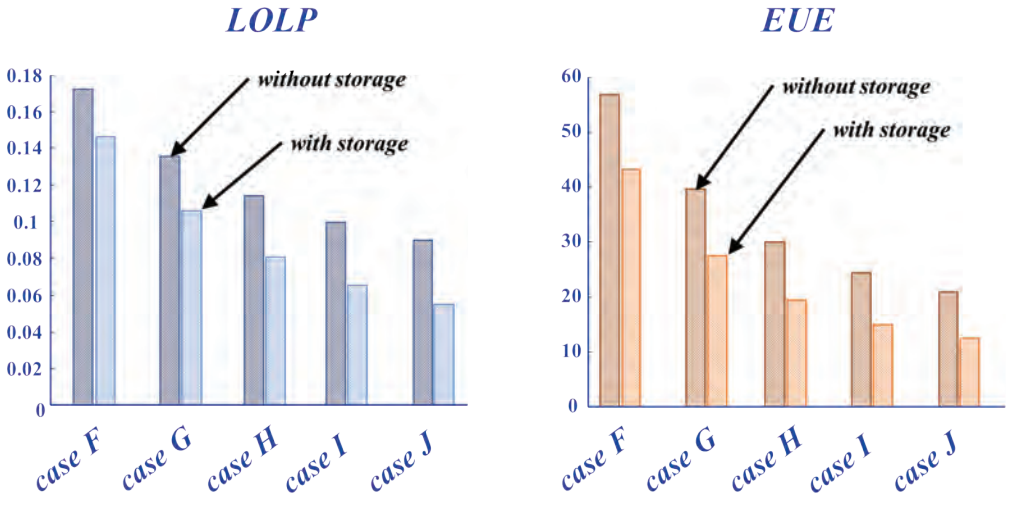

Figure 6: Annual reliability indices

- We can readily observe that the storage resource works in synergy with the wind resources: the integration of the storage unit increases the benefits due to deepening wind penetration, particularly in terms of the expected wholesale purchase payments and the improved reliability indices.
- The expected CO_2 emissions need not be reduced as a result of the storage unit integration. Indeed, they may increase slightly under some cases. Such an outcome is primarily due to the fact that the hourly aggregated wind power output cannot cover the base load and therefore the energy charged into the storage unit relies on the fossil fuel fired conventional generation. A representative plot of CO_2 emissions for the 5 case studies is shown in Fig. 7.

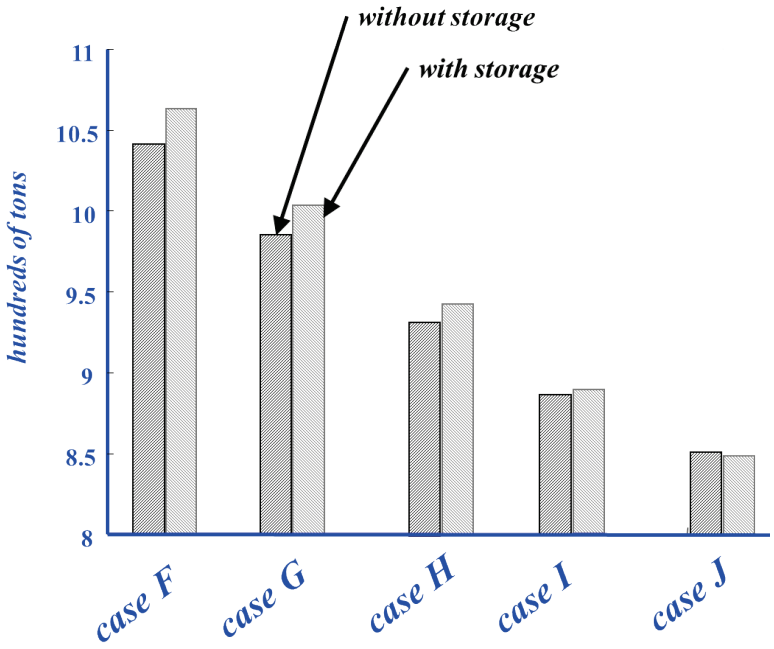

Figure 7: Weekly expected CO_2 emissions

- Similarly to the first study, we observed diminishing returns on all metrics of interest as the penetration of wind resources deepens. However, the integration of the utility scale storage unit tends to attenuate the "diminishing returns" effects and makes the deeper penetration of wind resources more attractive.

This study serves to provide some useful insights into the benefits attainable with storage integration, particularly for deepening penetrations of intermittent resources.

We focus on a third study, in which we examine the impacts on the power system of the location of a utility-scale *MWweek* storage resource. More specifically, we investigate the nature of the impacts of siting the storage unit electrically farther and farther away – in terms of intermediate nodes - from the most important load center in the network on the *LMP* at the load center, as well as on the expected total system wholesale purchase payments, the *LOLP*, and the expected congestion rents. The detailed results are reported in [11]. We highlight below some of the key findings of the study:

- The location of the utility-scale *MWweek* storage unit impacts acutely the power flows in the vicinity of the load center and may result in congestion in the transmission lines in the neighborhood of its location. As a result, the *LMP*s are affected. This location-dependent phenomenon is illustrated in Figs. 8. and 9 where the average hourly *LMP* at the most important load center closely follows the hourly average congestion rents depending on the location of the storage plant (the nodes where the storage plant is located are one node away from the considered load center).

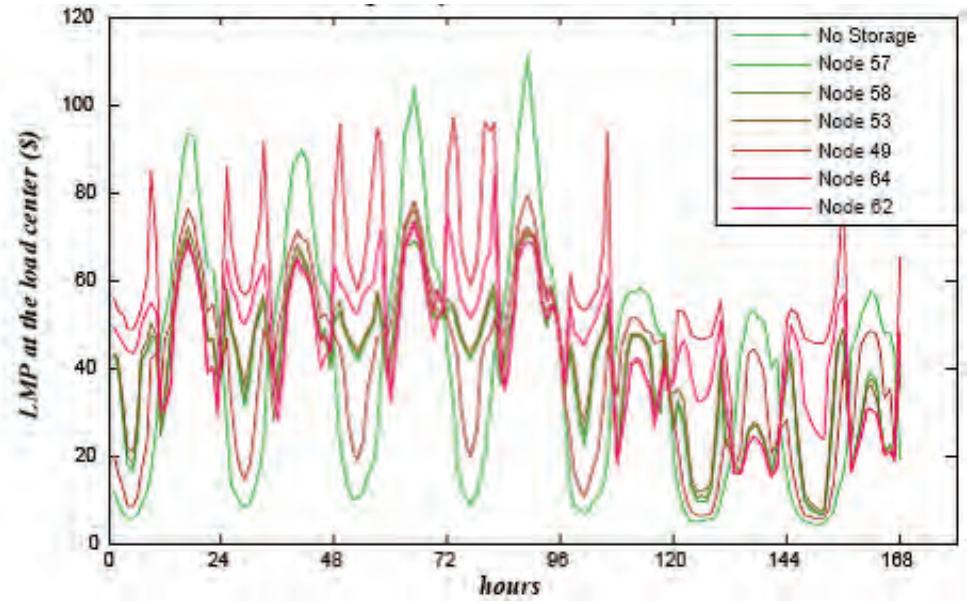

Figure 8: Average hourly *LMP* at the load center

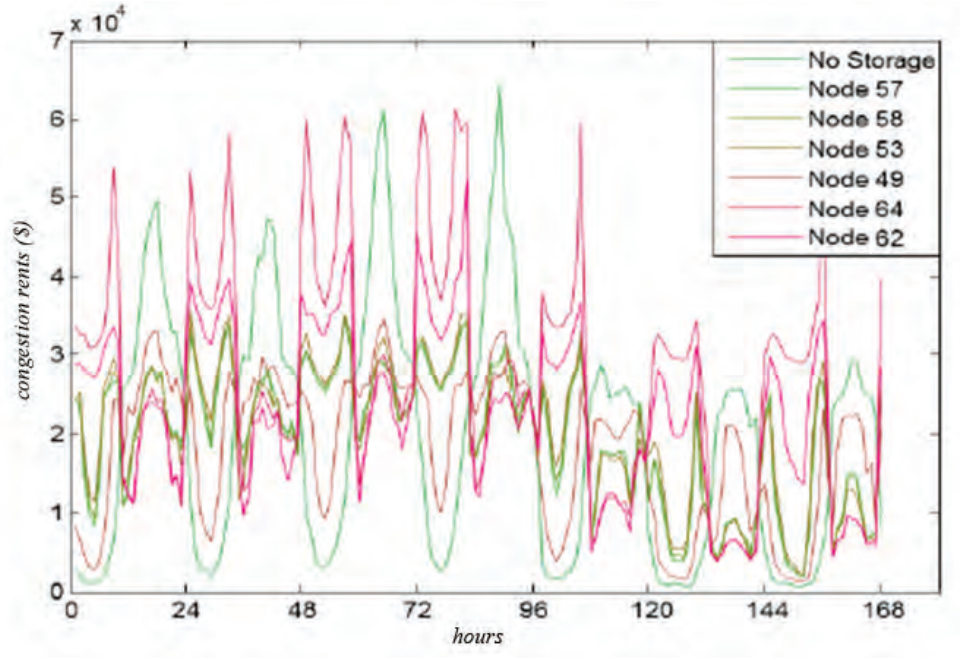

Figure 9: Average hourly congestion rents

- The load center *LMP* is strongly correlated with the congestion pattern in the power transfer corridor that connects the center to certain nuclear power plants. Indeed, the location of the storage plant near the nuclear plants may result in congestion on that corridor during the low-load hours due to the charging energy from the nuclear units. However, the location is beneficial during peak-load hours as the storage plant relieves congestion during those hours, when it provides energy to the load center. Exactly the opposite congestion pattern conditions arise with the location of the storage unit near the nuclear power plant.
- In general, the siting of the storage unit in the vicinity – one or two nodes away – of the load center is more beneficial, in terms of economics and reliability, than farther away. The only exceptions are for the location at the nodes near the nuclear power plants, notwithstanding the fact that these sites are three nodes removed from the load center. We display the results of some sensitivity studies for the storage location in Figs. 10 and 11.

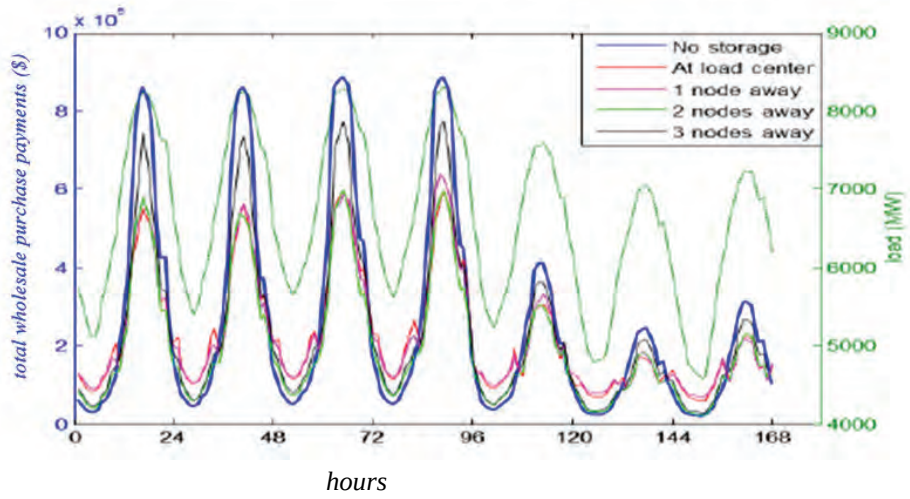

Figure 10: Average hourly purchase payments

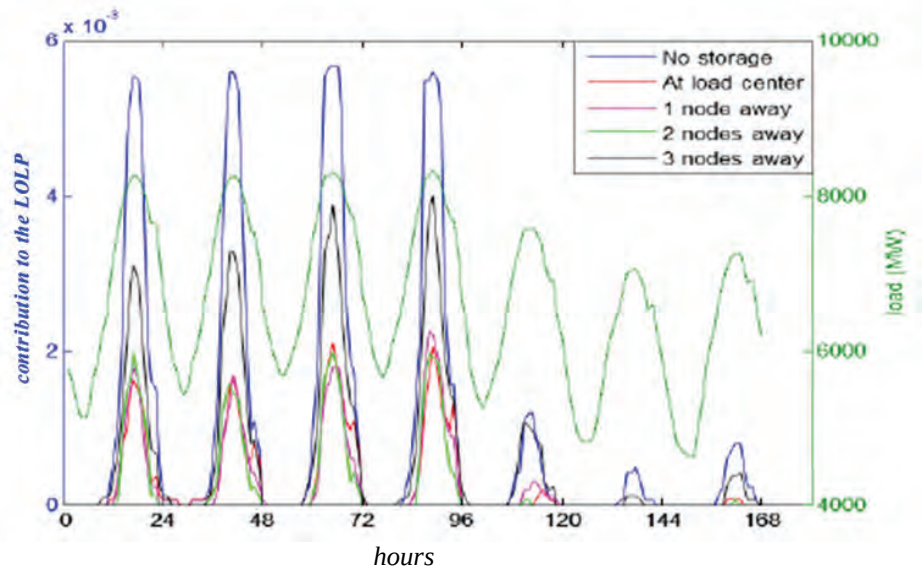

Figure 11: Average hourly contributions to the LOLP

The key conclusion from this study is that storage plant siting must be determined on a case-by-case basis. While the objective to locate the storage unit so as to avoid giving rise to new congestion patterns near the most important load center is reasonable, so are the objectives to provide access to the cheap energy for charging the storage in the low-load hours and to the energy discharged to serve load during the peak-load hours. Since these objectives may compete, it is not always possible to meet them in the same system.

We discuss our experiences with the simulation of power systems with multiple integrated storage units. In the case studies presented in Table 3, we integrate a total storage capacity of 1000 *MW* with 25,000 *MWh* of reservoir capability distributed over multiple storage units:

Table 3: Multiple storage sensitivity studies

case	*total number of storage units*	*storage unit capacity in MW*	*storage unit capability in MWh*
K	**1**	**1,000**	**25,000**
L	**2**	**500**	**12,500**
M	**3**	**333**	**8,333**
N	**4**	**250**	**6,250**
O	**5**	**200**	**5,000**

Our key findings from such case studies are the following:

- The impacts of the storage resources in such a system largely depend on the locations of the individual storage units. Storage units that are located close to one other in the network – within two nodes – may vie for the same charging energy, thereby limiting the benefits they may bring in terms of improving the power system performance.

In general, it is better to have many smaller storage units dispersed all over the network rather than a single big storage unit. Virtually, all the metrics of interest, particularly, the average hourly congestion rents as illustrated in Fig. 12 or the average hourly *LMP* at the most important load center as illustrated in Fig. 13, improve under a geographic diversification strategy for the siting of the storage units. Note that we display duration curves rather than chronological ones for the sake of clarity.

There are some other findings in terms of efficiency characteristics that are difficult to generalize.

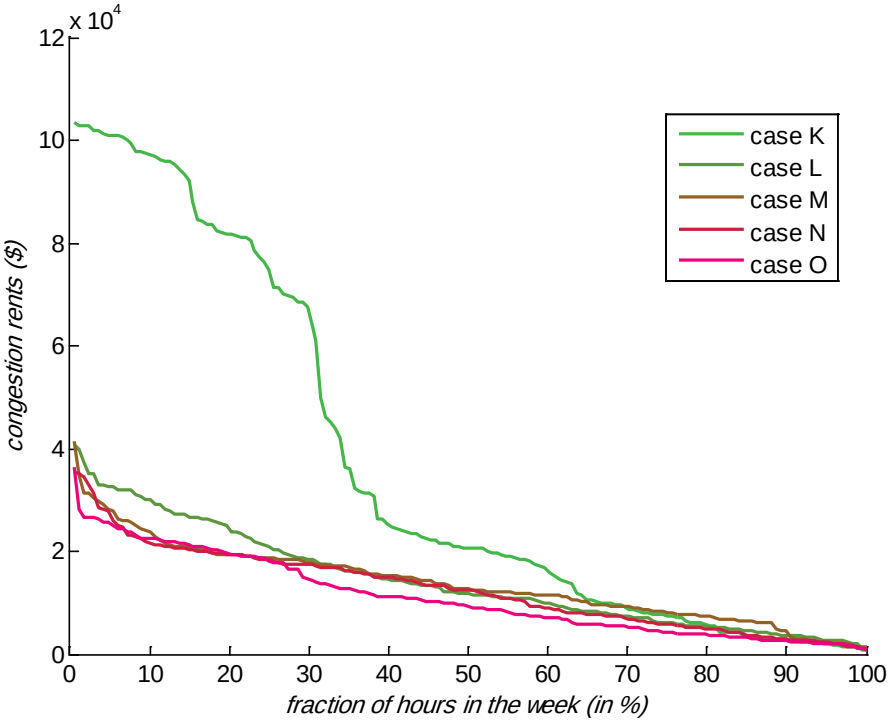

Figure 12: Average hourly congestion rent duration curve

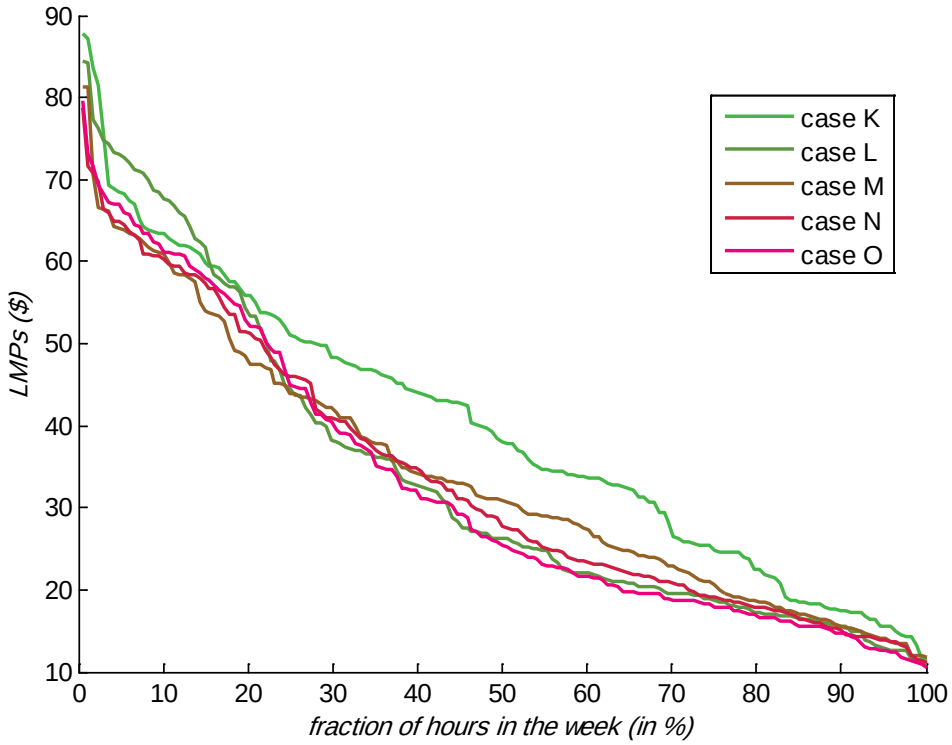

Figure 13: Average hourly *LMP* duration curve at the load center

We also share some additional observations related to the way we deploy the tunable elements in the Monte Carlo simulation and the implementation issues. In the deployment of the storage scheduler, our experience indicates that the shortest scheduling horizon must exceed 48 hours in order to avoid possible distortions in the results brought by shorter duration periods. We observe that the storage schedule is not particularly sensitive to errors in the forecasted system state evolution and so, in general, it is not necessary to rerun the scheduler it in too many cases. For example the mere fact that the sampled wind power outputs deviate from their expected values or that the sampled load values differ from their expected values are not sufficient factors to rerun the scheduler. The same is true for a conventional unit that unexpectedly transitions to another state. The more frequent running of the scheduler had insignificant effect on the values of the metrics.

In the construction of the sample paths for the stochastic processes that represent the multi-site wind output patterns for a day, we found that the use of 7 sample paths, one for each day of the week, was adequate to obtain from those realizations, the values of the wind resource capacities to be offered into the hourly *DAM*s.

The number of sample paths is difficult to specify a priori for an arbitrary system. For the test system in the case studies discussed in this section, the use of 100 sample paths, in other words 100 simulation runs, was adequate to obtain statistically accurate estimates of all the metrics of interest. In the simulation of the test system used for the case studies discussed, we use 16 representative weeks out of the annual 52, to obtain the above results without perceptible impacts to the annual values of the metrics.

6. Conclusions

In this project, we have developed a stochastic simulation methodology for the quantification of the variable effects in systems with variable energy resources (*VER*), such as wind, into which energy storage units are integrated. The attention to computational tractability allows such quantification to be performed over longer-term periods. The methodology can assess impacts of wind and storage resource integration on the variable economic, reliability and emission effects of the power system in a market environment. The simulation approach explicitly represents the time-varying nature and the uncertainty of the wind, load and storage resources together with the side-by-side interactions of the hourly transmission-constrained *DAM*s and the power system operations. We make extensive use of Monte Carlo simulation techniques to systematically sample the stochastic processes associated with the wind resources, loads and conventional generator available capacities. We have developed a storage scheduler to determine, given the initial state of the system and its forecasted evolution, the optimal trajectory of the state of each integrated storage unit for each hour in the scheduling period with the objective to maximize the system total social surplus over that period. We simulate the clearing of the hourly transmission-constrained *DAM*s by solving the *DCOPF* problem that is used to represent each hourly market. We formulate the offers and the bids into each market based on the realizations used to construct the sample paths of the wind, load and conventional resource available capacity random processes together with the storage scheduler results to determine the bid/offer actions of the units that are not idle. As such, the approach explicitly represents the chronology of time-dependent phenomena and transmission network constraints that influence the deliverability of the energy. The methodology provides a broad range of capabilities and is applicable to a wide array of planning, investment analysis and operational planning problems. Salient characteristics include the ability to allow the comparison of various resource mixes and network configurations and the ability to answer a broad spectrum of *what if* questions.

We have presented the results of some representative case studies to effectively illustrate the synergies among wind and storage resources. Our studies indicate that the deepening penetration of wind resources in systems with integrated storage resources contribute to significantly reducing the *LMP*s and the expected wholesale purchase payments and provide marked improvements in the system reliability. The presence of utility-scale *MWweek* storage units indeed accentuates such benefits, particularly at deeper wind penetrations where it tends to attenuate the "diminishing return" effects of installing more wind capacity. The expected CO_2 emissions depend upon the particular system resource mix. In the case studies presented, the base-loaded units, typically, pollute more than the peaking units and therefore can lead to slight increases of CO_2 emissions as the storage units tend to use charging energy from the base-loaded units so as to displace some of the peaking unit generation. The integration of storage resources exerts strong influence on the congestion patterns, thereby impacting the congestion rents and the *LMP*s. The case study results discussed the impacts that the siting of a storage unit can have on certain nodes and even the entire system performance. However, such matters require detailed assessment on a case-by-case basis as the results are highly system dependent. Furthermore, our studies on the integration of multiple storage units show that it is more beneficial, in general, to implement smaller distributed storage units into the network rather than the installation of a single large storage unit.

Some clear directions of future work include the integration of additional resources, including demand response and solar [12]. A topic of considerable interest is the analysis of the impacts of

renewable resource integration on ramping capability requirements. For this end, a more detailed representation of power system operations is required. Future efforts on the assessment of including such requirements will focus on t he evaluation of the reliability, economic and emission impacts.

References

[1] A. J.Wood and B. F.Wollenberg, Power Generation, Operation and Control, 2nd ed. New York, NY: John Wiley and Sons, Inc., 1996.

[2] H. Baleriaux, E. Jamoulle and Fr. Linard de Guertechin, "Simulation de l'exploitation d'un parc de machines thermiques de production d'electricite couples a des stations de pompage." RevueE, (édition SRBE), Vol. 5, No. 7, pp. 3-24, 1967.

[3] R.R. Booth, "Power System Simulation Model based on Probability Analysis." IEEE Transactions, Vol. PAS-91, pp. 62-69, 1972.

[4] N. Maisonneuve and G. Gross, "A production simulation tool for systems with integrated wind energy resources", *IEEE Transactions on Power Systems*, vol. 26, no. 4, pp. 2285 - 2292, Nov. 2011.

[5] "Markov models for reliability evaluation" (notes for ECE 588 UIUC), http://courses.engr.illinois.edu/ece588/handouts/Lecture3-MarkovModelsforReliabilityEvaluation.pdf.

[6] J.P.C. Kleijnen, *Statistical Techniques in Simulation – Part 1*, Marcel Dekker, Inc., New York, 1974.

[7] B. Stott and E. Hobson, "Power system security control calculations using linear programming, part i", Power Apparatus and Systems, IEEE Transactions on, vol. PAS-97, no. 5, pp. 1713-1720, Sept. 1978.

[8] B. Stott and E. Hobson, "Power system security control calculations using linear programming, part ii", Power Apparatus and Systems, IEEE Transactions on, vol. PAS-97, no. 5, pp. 1721-1731, Sept. 1978.

[9] 118 bus power flow test case [Online] Available: http://www.ee.washington.edu/research/pstca/pf118/pg_tca118bus.htm

[10] Y. Degeilh, J. Descloux and G. Gross; "Simulation of Energy Storage in a System With Integrated Wind Resources", Proceedings of the *17th Power Systems Computation Conference*, Stockholm, Sweden, Aug. 2011.

[11] Z. Zheng; "Impacts of Energy Storage Siting on Power System", Senior Thesis, submitted to the Department of Electrical and Computer Engineering, University of Illinois, Urbana, IL, May 2012.

[12] R. Bhana, "A Production Simulation Tool For Systems With Integrated Photovoltaic Energy Resources," thesis submitted to the Department of Electrical and Computer Engineering in fulfillment of the MS degree requirements, University of Illinois, Urbana, IL, Nov. 2011.

Part 2

Modeling and Simulation to Study the Impact of Storage on the Reliability of Composite Power Systems with Wind Farms

Chanan Singh
Alex Sprintson
Hagkwen Kim, Doctoral Student
Texas A&M University

For information about Part 2, contact

Chanan Singh
Regents and Runyon Professor
Department of ECE
Texas A&M University
3128 TAMU
College Station, Texas 77843-3128
Email: singh@ece.tamu.edu

Power Systems Engineering Research Center

The Power Systems Engineering Research Center (PSERC) is a multi-university Center conducting research on challenges facing the electric power industry and educating the next generation of power engineers. More information about PSERC can be found at the Center's website: http://www.pserc.org.

For additional information, contact:

Power Systems Engineering Research Center
Arizona State University
527 Engineering Research Center
Tempe, Arizona 85287-5706
Phone: 480-965-1643
Fax: 480-965-0745

Notice Concerning Copyright Material

Table of Contents

List of Figures

List of Tables

1. Introduction

Many countries have set targets to include significant share of wind and solar power into their energy portfolios. However, wind power is unstable because of its intermittent and fluctuating characteristics. Storage devices offer substantial benefits to system operations by providing the flexibility to mitigate the effects of variable renewable energy sources and the ability to provide energy- and capacity-based ancillary services. The basic objective of this effort is to develop modeling and simulation methodology to study the impact of storage on the reliability of power systems when wind farms are integrated into the composite system.

To develop realistic models for the composite system, it is important to construct good models for the subsystems. The reliability models of conventional generation have been well developed. However, it was felt that the models for the wind farms are inadequate and lack realism. Accordingly, the first subsection describes the work done to improve the wind farm models and the subsequent sections describe the optimization methods employed and the modeling and simulation methodology to study the effect of storage on the reliability of the composite power system. This includes the optimal storage deployment for managing fluctuation characteristics of wind with sensitivity analysis.

Several studies for illustrating the use of this methodology are also presented. Monte Carlo Simulation [8]-[10] is used for system simulation. It uses next event form of sequential method and the results are compared. The improved wind farm models and the storage are incorporated. To calculate the system reliability we use indices [11]-[12] such as Loss of Load Expectation (LOLE), Expected Energy Not Supplied (EENS. The results from the simulation are analyzed and compared for different scenarios. Wind data used is from National Renewable Energy Laboratory (NREL) [13] and load data is from IEEE Reliability Test System (RTS) [14].

2. Background

Since turbines generate electricity from the entering wind, the wind speed (energy) entering a turbine is higher than that leaving it. During this process, in the area behind a turbine, leeside, turbulent flow occurs. This power loss is called wake effect [1]. Because of this effect, downstream wind turbines generate less power, because of lower wind speed. In general, for a free standing wind turbine, there is no wake effect by other wind turbines. However, when a turbine is located in a relatively close spacing with others, wake effect can have a significant influence on the calculations. As the effect gets stronger, loadability of wind farms decreases. Therefore, it is essential to consider the wake effect and to examine its impact on the overall wind power system reliability and economics for more accurate and reliable wind power calculation. This report shows that wake effect does make an impact on the reliability of a wind farm and quantifies this impact.

A wind farm model [2]-[4] can be divided into two sub-models, a wind speed model and a wind turbine model. For wind speed model, a transition rate method [5] and clustering method [6]-[7] are proposed and compared. The proposed transition rate method considers all transition behaviors between wind speed states from an actual wind speed. And the probability of each wind state can be derived by using the transition rates. On the other hand, the clustering method assigns given wind speed and load to some clusters so that the correlation between them is

reflected in time. Wind turbines are modeled as a two state generating unit, fully available state or out of service state. For each wind speed state, corresponding power generated by turbines is calculated.

3. Proposed Wind Farm Model

Conventional units generate power depending on their failure/repair status. Unlike these units, wind turbines in wind farm generate power, depending on the wind speed as well as their operational status. This is why wind farm is represented by wind speed model and wind turbine model. The output of each wind turbine is determined by combining these two models. This research uses the general wind power curve [15] whose input information is a cut in speed, rated speed, cut out speed, and rate power to determine wind power. And then overall power of wind farm which is added by all wind turbines is supplied to the load at a given time.

Figure 3.1 shows the state space of a wind farm. The circles in the left box represent wind speed states, and the squares in the right box indicate wind turbine states. The arrows between the circles represent transitions between different wind speed states and the arrows between the squares are failure and repair transitions of turbines with specific rates. State Up is properly working state, and state Down is out of service state. The lines between the circle and the squares indicate that for a given wind speed, a turbine could be either up or down. The transition rates between the up and down states could be represented as a function of the wind state as the failure rate may depend on the wind speed. The aggregate state of wind farm is updated with sampling so that the corresponding power is determined during simulation.

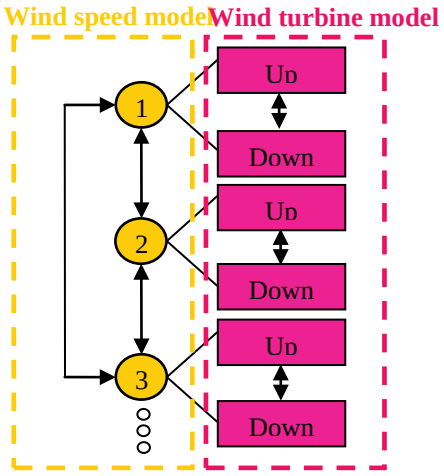

Figure 3.1: Electric Energy Storage Integrated in the Distribution System

3.1 Wind Speed Models

3.1.1 Transition Rate Model

This approach is based on the transition rates among wind states. Transition rate is the ratio of number of state changes and duration stayed in the state before transition. To consider wind speed changes, all transition rates are gleaned from the original wind speed. Using those rates,

the frequency, duration, and probability of all wind states can be derived. And then wind state is generated in series by selecting the lowest transition time. The lowest transition time implies the highest probability of its transition.

3.1.2 Clustering based model

Load and wind speed may have a pattern of variation relative to each other as both values have some relation to the time of the day, season, or weather. In other terms, load and wind speed may be correlated variables. Exact transition method does not capture this correlation as the transition rate matrix contains average rates over the period of study and these are assumed constant. Clustering approach is proposed for such cases. Actual load and wind speed data as functions of time are collected. Each pair of wind speed and the corresponding load constitute one data point. Then using clustering algorithm, all given data points are grouped into several clusters using the nearest centroid sorting based on the Euclidean distance. Clustering is generally categorized as partitional method and hierarchical method [16]-[19]. In this work, partitional clustering is used and compared. It partitions original data into the specific data size holding data characteristics. K-Means (KM) is a simple and fast method. Once the clustering size is determined, it iterates to find the optimal clusters with the closest distance between clusters and points starting from the initially selected clusters. Fuzzy C-Means (FCM) provides additional membership probability of clusters for each point to show fuzziness. These two methods basically depend on the initially randomly selected clusters. So the final clusters can be different every iteration. To solve this issue, global approach can be applied for clustering like Global K-Means (GKM) and Global Fuzzy C-Means (GFCM). And for the faster simulation procedure, Fast Global K-Means (FGKM) and Fast Global Fuzzy C-Means (FGFCM) are also examined to the research. These global or global fast approaches find the optimal clusters by adding a cluster step by step, instead of starting initial guess with preselected clustering size. They are independent of the initial guess so that it is possible to make more accurate and reliable clustering from original data.

As an input to clustering, cluster size should be determined using validity measurement [20]. Data consist of two dimensional observations; wind speed and load, and the size of the data is simulation period, one year in the research. The number of iterations for different clustering approaches is developed and compared in this work, shown by Table 3.1. Where n is the data size, k is the clustering size, and c is the number required to satisfy convergence. As the size of data or cluster becomes bigger, the simulation time of global approach exponentially increases more. And n is much bigger than k in general composite power systems so that fast global approaches like FGKM and FGFCM are efficient to simulate.

Table 3.1: Integration of Clustering

Number of iterations for different clustering approaches	
KM	FCM
$2nkc$	$nk^2c + 2nkc$
GKM	GFCM
$n^2k^2c + n^2kc + nk^2$	$n^2k^3c + 2n^2kc + n^2k^2$
FGKM	FGFCM
$n^2k(k-1) + nk^2c + nkc$	$n^2k^2 + nk^3c + 2nkc$

By using the mean load and the corresponding wind speed in the same cluster and probability of each cluster, it is possible to capture the correlation and make a quantitative reliability analysis. This is because the data in the same cluster represents the similarity amongst data points. Power generated by wind energy can be different for the same wind speed because of the failure and repair characteristics of turbines. So, comparing correlated load with power generated by the corresponding wind speed, loss of load event is determined, and the corresponding reliability indices are also computed.

3.2 Wind Turbine Model

Like conventional turbines, wind turbines are also modeled using Monte Carlo simulation [8]-[10]. Each turbine is assumed to have two generating states; fully available and out of service. From failure/repair rates of turbines, probabilities of two operating states can be calculated. As one of sequential methods, next event approach [21] is applied as the system simulation. Probability distribution function for transition duration time of each turbine is assumed to be exponential. And then the operating state of a turbine and its transition time demonstrates failure/repair behaviors of the turbine.

3.3 Wind Turbine Model

In general, there are three different wake effect models [23]-[27] for the wind, Jensen model, Ainslie (Eddy Viscosity) model, and G.C. Larsen model. The Jensen model is based on wake decreasing constant thrust coefficient which is related to the surface roughness and turbulence intensity. The Ainslie model is based on the differential equations demonstrating the wake velocity field. It includes turbulent mixing of wake and ambient turbulence on wake. The Larsen model comes from the turbulence boundary layer equations which are based on Swain's paper [28]. In this report, Jensen model is used to generate wake speed of downstream wind turbines. This model was first developed by N. O. Jensen in 1983 which is a simple analytical model with a short calculation time. This work adopts the Jensen model for its simplicity. However, any wake model could be used with the overall approach proposed in this research. From the

conventional Jensen model, a newly modified model is developed using wind shade, shear, and cumulative wake effect.

Figure 3.2 shows the basic Jensen model which uses a cylindrical coordinate system in the radial and axial directions. Using this model, wake speed is determined from the given free wind speed.

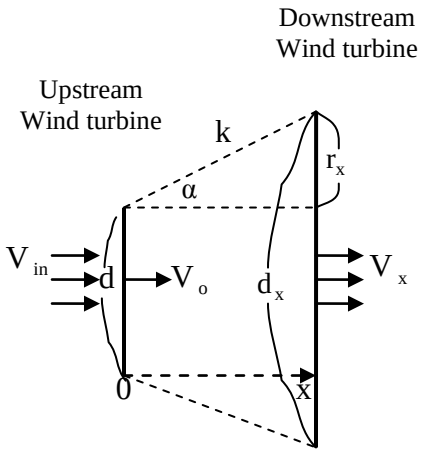

Figure 3.2: Jensen Model Principle

$$V_x = V_{in}[(1-(1-\sqrt{1-C_t})(\frac{d}{d_x})^2] \qquad 3.1$$

Where V_{in} [m/s] is free or incoming wind speed, V_x [m/s] is downstream speed, C_t is thrust coefficient, $d_x[m] = d + 2r_x = d + 2kx$, and k is wake decreasing constant. The thrust coefficient is given,

$$C_t = \frac{F_t}{\rho\pi r^2 V_{in}{}^2} \qquad 3.2$$

Where F_t $[kg * m/s^2]$ is the thrust force, ρ $[kg/m^3]$ is air density, and r [m] is radius of the rotor.

If thrust coefficient is zero, there is no waking, so the speed at an upstream turbine is the same as that at a downstream turbine. If distance x is zero, we can see that the relationship between leeside wind and free wind is derived. In general, k is set to 0.075 for onshore, and to 0.05 for offshore [29] installations. In this work, it is assumed to be 0.075. The leeside speed is given by

$$V_o = V_{in}\sqrt{1-C_t} \qquad 3.3$$

In practice, in a wind farm, free wind speed can be decreased by obstacles around, other neighboring turbines. This is called wind shade effect [23]. By considering this effect, previous model is modified.

$$V_x = V_{in}[(1-(1-\sqrt{1-C_t})(\frac{d}{d_x})^2(\frac{A_s}{A})] \quad 3.4$$

Where $A_s\,[m^2]$ is shade area by the other upstream turbine, and A $[m^2]$ is area of downstream wind turbine. If shade area is zero, there is no interruption by other turbine, so wind speed at upstream is the same that at downstream. If shade area is the same as downstream turbine area, it means that the downstream turbine is immediately behind the upstream turbine resulting in an eclipse phenomenon.

In a wind farm, there are many wind turbines. So, cumulated effect of each turbine should be considered. As a result, using the momentum conservation theorem [30], the equation is modified, as follows.

$$V_x = V_{in}[(1-\sum_{i}^{n}(1-\sqrt{1-C_t})(\frac{d}{d_{xi}})^2(\frac{A_{si}}{A})] \quad 3.5$$

Where n is number of the upstream turbines of a downstream turbine, and $A_{si}\,[m^2]$ is shade area by upstream turbine i.

There is one more consideration to take into account. Atmosphere above 1km is hardly influenced by the friction against the ground. However, in the lower layers, wind speed increases as the height of air goes up. This is called wind shear effect [27]. So if the height of some wind turbines is different, this effect should be also incorporated.

$$V = V_{ref}\frac{\ln(\frac{h}{h_o})}{\ln(\frac{h_{ref}}{h_o})} \quad 3.6$$

Where V_{ref} [m/s] is reference wind speed and h_o [m] is roughness length.

As a result, waked speed is calculated.

$$V_x = V_{in}[(1-\sum_{i}^{n}(1-\sqrt{1-C_t})(\frac{d}{d_{xi}})^2(\frac{A_{si}}{A})]\frac{\ln(\frac{h}{h_o})}{\ln(\frac{h_{ref}}{h_o})} \quad 3.7$$

There is one more thing to consider in the wake effect on wind farm. Wind direction by its nature varies with time. Because of different wind directions, the relationship of upstream and downstream turbines can change over time. So wind direction also has an important impact on wake effect as well as shade effect. In general, there are two ways to express wind direction. One way is to express in terms of degree where exact degree value is measured at specific sampling time. The other is shown by wind rose which indicates wind speed and direction at the same time graphically. For this method, direction is usually recorded by 16 cardinal directions such as S, SW, NE, ESS, and so on in a specific sampling rate.

A wind farm consists of a number of wind turbines which generate power depending on wind speed. A general wind power curve [15] is adopted in this work. At cut in speed, turbines begin generating power and then power increases nonlinearly with the speed. From rated speed to cut out speed, turbine keeps generating rated power, and above cut out speed, turbine is shut down for the equipment safety. To incorporate the wake effect, the power of each turbine is determined by waked speed and not by free wind speed with varying wind direction. The total power of a wind farm is calculated by the sum of the power of all turbines and by their failure/ repair characteristics.

4. Optimization Techniques to Find Minimum Load Curtailment

4.1 Two Phase Method for Linear Programming

At composite level, all transmission constraints are considered for reliability analysis. DC power flow is embedded in the formulation of minimum curtailment of load formulation. In this formulation N is the number of buses, C_k is load curtailments at bus k, g_k is generation at bus k, f_{kj} is real power flow between bus k and j, d_k is load at bus k, g_{lower} is lower limit of generation, g_{upper} is upper limit of generation, f_{lower} is lower limit of power flow, and f_{upper} is upper limit of power flow.

This formulation is solved using linear programming. Simplex method uses the reduced costs of the system problem to get the final optimal solution with iterations. At the beginning, it is required to choose the initial basic feasible solution once the system problem is converted into the standard form.

In general, the initial basic feasible solution may be unavailable from the original problem. As alternative method, artificial variables are added to the problem. There are generally we approaches for using artificial variables [32]; two phase method, and big M method - two phase method is used in this research. Two phase method has two phase levels to optimize a problem. At the phase one level, its objective function is the sum of all artificial variables. If the optimal value is not zero, it does not have any feasible solutions, since artificial variables are added to the original problem. Otherwise, it goes to next level, phase two. If some artificial variables are in basic variables, they are replaced by other non-basic variables. And it iterates the simplex process using the reduced costs to find the final optimal solution to the original problem. Programming code is developed for the algorithm of two phase method using a computer tool Matlab.

$$\text{Objective function} = \min \sum_{k=1}^{N} C_k \tag{4.1}$$

$$C_k + g_k - \sum_{j} f_{kj} = d_k \tag{4.2}$$

$$0 \le C_k \le d_k \tag{4.3}$$

$$g_{lower} \le g_k \le g_{upper} \tag{4.4}$$

$$f_{lower} \leq f_{kj} \leq f_{upper} \quad 4.5$$

4.2 Sensitivity Analysis in the Optimization Problem

The Right Hand Side (RHS) of the power flow problem consists of load, available generation, and power flow capacity of the transmission. It changes over time, since load and generation vary every hour. In addition it can also change by storage deployment, since the upper bound of generation vector with storage increases. So if we run optimization process every time, it is very time consuming. Sensitivity analysis [32]-[33] is used to calculate the final optimal solution to sum of load curtailments in the power system.

By using basic matrix B (coefficient matrix of constraints by basic variables), cost vector C_B (coefficient vector of objective function by basic variables), and newly changed RHS b_{new}, it is determined whether the optimization should be restarted or directly calculated by sensitivity analysis. If C_B times inverse of B is greater or equal to zero, it means that previous basic matrix can hold the problem for feasible availability. So the final optimal solution is directly taken using $Z^* = C_B B^{-1} b_{new}$. Otherwise, optimization should be restarted, since basic matrix is changed by b_{new}.

5. Storage Techniques

5.1 Integration of Storage

Wind power has fluctuating characteristics, since it is dependent on wind speed. So using wind energy alone is hard to satisfy varying load. To mitigate this problem, energy storage can be added on the wind farm. In general, electric energy cannot be stored itself. So it is required to convert into other types of energy like kinetic, potential, or chemical energy and so on. Table 5.1 shows general storage types [34]-[36]. Considering the composite power level, Pumped Hydro Energy Storage (PHES) and Compressed Air Energy Storage (CAES) are used in the research.

Table 5.1: Storage Types

Types	Usage level	Storage	Capacity	Efficiency
Pumped Hydro Energy Storage (PHES)	Composite	Pumping water	1 [GW]	70 [%]
Compressed Air Energy Storage (CAES)		Compressing air	100-300[MW]	80 [%]
Battery Complex	Distribution	Chemical process	20-50 [MW]	90-95 [%]
Flywheels		Spinning flywheel	25-30 [kW]	85-90 [%]

Storage technologies are incorporated on the buses with wind farm. For buses without storage, conventional linear programming is used. For buses with storage, the upper limit of the generation constraint is changed by creating storage vector with charge/discharge rates, where x_k is a storage vector at bus k, which is calculated using energy balance vector, x_{bk} and charge/discharge rates storage. Positive x_{bk} means energy storing mode, and negative x_{bk} means energy generating mode of storage. It represents storable energy amount at bus k. x_{bk} is taken from the difference between generation and load at bus k. Figure 5.1 shows the process of calculation of x_k every time, where i is the sequence of time, and max_cap is the maximum capacity of.

$$g_{lower} \le g_k \le g_{upper} + x_k \qquad 5.1$$

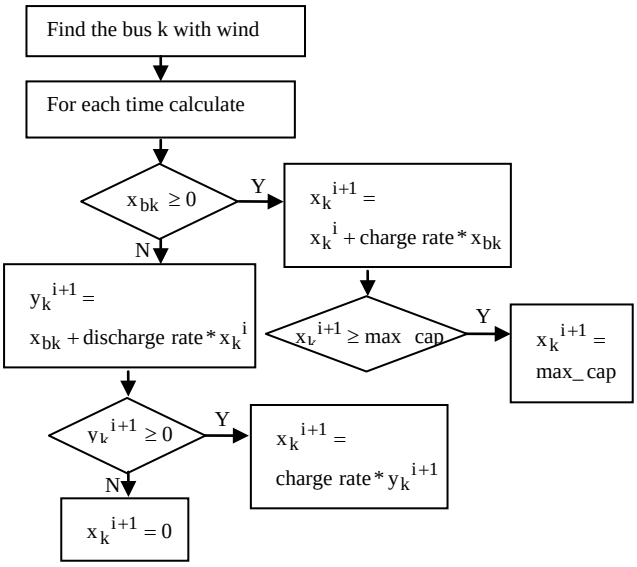

Figure 5.1: Flowchart for Calculation of Storage Vector

5.2 Optimal Storage Placement

One issue is to determine the buses where to place the storage. The placement of storage becomes important because of the transmission constraints. If there were no transmission constraints, then storage could be placed anywhere. Storage bus deployment cases can be a dimensionally complex problem depending on the power system size. For IEEE RTS [14], there are 24 buses. If we choose 3 buses as storage buses with wind farm, the number of possible locations is 3 combinations out of 24, which is 2024. To find the candidates for optimal storage buses, this report introduces an approach based on expected capacity [3].

The upper limit of generation vector with storage consists of maximum available generation vector and storage vector. Available generation depends on the failure/repair process of turbines. Storage vector is determined by the energy balance vector and charge/discharge rates. So once charge/discharge rates are fixed, the upper limit of generation vector with storage is determined by expected capacity of a bus. Where N is the number of available generation states at a bus, C_i is the capacity of state i, P_i is the probability of state i. One possible simple approach seems to be to use a bus with higher expected capacity as a candidate of the optimal storage buses with wind farm. The idea is that if the capacity is high then at low load periods, the excess capacity could be used for charging. Then one could perform simulations on a selected number of candidates to make the final choice.

$$\text{Expected capapcity} = \sum_{i=1}^{N} C_i P_i \qquad 5.2$$

6. Simulation Procedure for Reliability Evaluation

Figure 6.1 shows the simulation procedure of algorithm to find optimal storage deployment using sensitivity analysis with Monte Carlo and clustering. During simulation period, one year, optimal solutions for all clusters are gleaned and the final reliability indices by different storage cases are calculated using the probabilities of clusters. By comparing reliability indices of different storage deployment cases, the final optimal storage bus is determined with wind farm. The coefficient of variance [12] is set to be 5 [%] as convergence criterion for reliability indices.

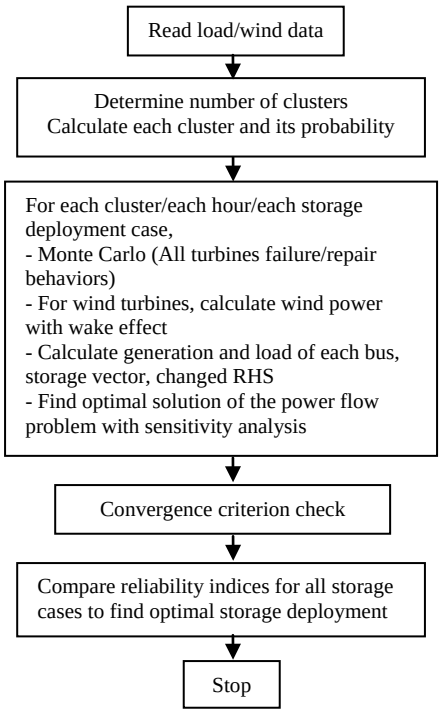

Figure 6.1: System Simulation Procedure

7. Case Studies

Figure 7.1 shows the schematic of the proposed system from viewpoint of a bus. IEEE RTS has 24 buses and 32 conventional generating units showing capacity 3405 [MW]. The annual peak load is 2850 [MW]. Three buses of the system have wind farm and storage. Generation system of IEEE RTS is placed for a swing bus or PV buses. Load is connected at PQ buses. Grid represents the transmission network of the system by the bus admittance matrix. Figure 7.2 shows the layout of wind farm which has 16 identical wind turbines with square by square structure. Here d [m] indicates the diameter of the turbine. Three wind farms are assumed to be installed at different buses. The capacity of each wind farm is 80 [MW], having each wind turbine 5 [MW]. Wind data is from National Renewable Energy Laboratory (NREL) [13]. The number of site area is 10. The wind speed and wind turbine data is shown in Table 7.1.

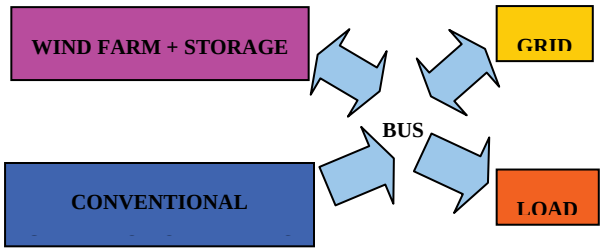

Figure 7.1: System Figure from Viewpoint of a Bus

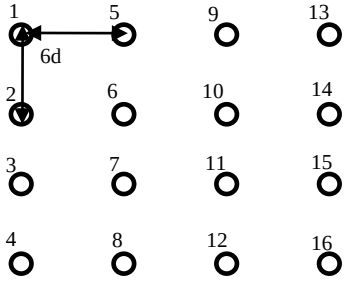

Figure 7.2 Layout of Wind Farm

Table 7.1: Wind Speed and Turbine Data

Wind speed data	
Peak wind speed [m/s]	27.57
Mean wind speed [m/s]	8.20
Standard deviation of wind speed [m/s]	3.19
Wind turbine data	
Cut in speed [m/s]	6
Rated speed [m/s]	11
Cut out speed [m/s]	19
Rated power [MW]	5
Rotor diameter [m]	80
Hub height [m]	70

Table 7.2 shows failure/repair rates of conventional units and wind turbines. Transition rate of wind turbines depends on wind speed [37]. From original wind data, wind speed states are identified in Table 7.3. In the proposed transition rate method for wind speed modeling, all transition rates among wind speed states are required to be calculated.

Figure 7.3 demonstrates the correlation between load data and wind speed. These data are based on average values during a day. The magnitude of average hourly load is scaled down to compare them explicitly. It is observed that power generated from wind speed is small during the peak load time, showing negative correlation. To take into account for the correlation, clustering approach is proposed in the research. For example, Table 7.4 represents the centroid and probability of each cluster using FGFCM. First column of each centroid is mean wind speed, and second one is mean load. From validity measurement, optimal cluster size is chosen to be seven.

Table 7.2: Transition Rates of Operating Turbines

Units	Conventional unit	Wind turbine	
Weather		Normal speed	Extreme speed(>19m/s)
Failure rate[#/yr]	6	6	36
Repair rate[#/yr]	130	130	36

Table 7.3: Identification of Wind Speed States

State	Range [m/s]	Prob.	Freq [#/yr]	Dur [h/#]	Power [MW]
1	0-4	0.0872	321	2.37	0
2	4-5	0.0751	731	0.89	0
3	5-6	0.0996	997	0.87	0
4	6-7	0.1098	1138	0.84	0.43
5	7-8	0.1162	1215	0.83	1.33
6	8-9	0.1199	1202	0.87	2.30
7	9-10	0.1088	1108	0.85	3.33
8	10-11	0.0939	977	0.84	4.43
9	11-12	0.0730	805	0.79	5
10	12-13	0.0487	562	0.75	5
11	13-14	0.0328	347	0.82	5
12	14-15	0.0138	200	0.60	5
13	15-16	0.0082	125	0.57	5
14	16-17	0.0050	89	0.49	5
15	17-18	0.0034	60	0.50	5
16	18-19	0.0017	39	0.37	5
17	19-20	0.0009	20	0.39	0
18	20-21	0.0006	18	0.30	0
19	21-34	0.0011	10	0.99	0

Table 1.4: Clustering Information Using FGFCM

Clusters	Centroids ([m/s],[MW])	Probabilities
1	(8.21,1750.6)	0.1835
2	(9.02,1362.7)	0.1563
3	(7.26,2274.1)	0.1402
4	(8.73,1111.2)	0.1220
5	(7.91,1990.4)	0.1884
6	(7.87,2488.2)	0.0687
7	(8.23,1540.5)	0.1409

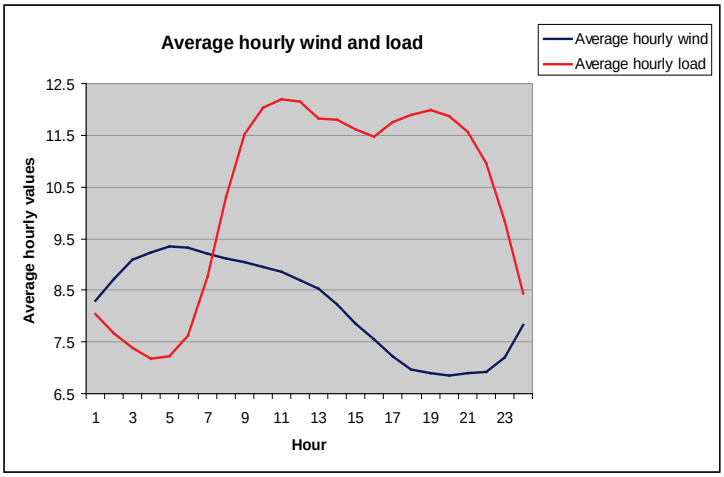

Figure 7.3: Correlation between Load and Wind Speed

To find the changes of wind states for different wake models in details, let us observe a case of south wind direction. When the wind blows from the south, upstream turbines are {4,8,12,16} and downstream turbines are {3,7,11,15},{2,6,10,14}, and {1,5,9,13} from Figure 7.2. Figure 7.4 shows the state changes of downstream turbines. Arrows indicates the change of the state. Red color shows only one state drop, blue dotted ones show two state drops. Wind speed drop by wake effect relatively decreases, as the wind speed grows up. For example, for turbines {1, 5, 9, 13} in Figure 7.4, states from 4 to 11 drop by two states. However, states from 12 to 16 falls only one state. And for high speed beyond state 17, there is no change by wake effect. Turbines {1, 5, 9, 13} show more wake loss than {3, 7, 11, 15}. This is because that for turbines {1, 5, 9, 13} more wake effects are influenced by around upstream turbines as the combined wake effect increases.

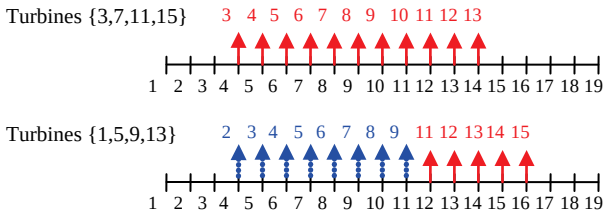

Figure 7.4: State Changes of Turbines

From the proposed power system, 124 slack variables and 3 artificial variables are initialized for optimization in the two phase method. Equations (7.1)-(7.6) show original problem for bus number one in IEEE RTS. Where A_1 is the upper limit of generation at bus one. It changes every hour depending failure/repair behavior of turbines. The upper limit of transmission line connected with bus one is 175 [MW]. To convert into standard form, slack variables are added on the problem in equations (7.7)-(7.11). Where S_i indicates slack variable for i =1, 2, 3, 4, and 5. The variables are non-negative. To have the initial basic matrix with non-negativity of RHS, an artificial variable should be added in equation (7.1). So it is replaced by equation (7.12) where Z_1 is artificial variable. S_i and Z_1 are used for the initial basic variables to make up basic matrix in phase one. After simplex process, if Z_1 is zero, it goes to phase two so that the final solution to the original problem is derived.

can do the numbering manually as below.

$$C_1 + g_1 - f_{12} - f_{13} - f_{15} = d_1 \qquad 7.1$$

$$0 \le C_1 \le d_1 \qquad 7.2$$

$$0 \le g_1 \le A_1 \qquad 7.3$$

$$0 \le f_{12} \le 175 \qquad 7.4$$

$$0 \le f_{13} \le 175 \qquad 7.5$$

$$0 \le f_{15} \le 175 \qquad 7.6$$

$$C_1 + S_1 = d_1 \qquad 7.7$$

$$g_1 + S_2 = A_1 \qquad 7.8$$

$$f_{12} + S_3 = 175 \qquad 7.9$$

$$f_{13} + S_4 = 175 \qquad 7.10$$

$$f_{15} + S_5 = 175 \qquad 7.11$$

$$C_1 + g_1 - f_{12} - f_{13} - f_{15} + Z_1 = d_1 \qquad 7.12$$

Table 7.5 shows the expected capacity of IEEE RTS. A probability of each capacity state is calculated using transition matrix approach [3]. From the TABLE, if we select three buses with storage, there exist two choices for optimal storage deployment; (23, 13, 18) or (23, 13, 21). Using sensitivity analysis to compare reliability indices, the final optimal storage buses can be determined. From the table, it is also possible to choose three more storage buses as candidates of optimal deployment. For example, if we select five storage buses, there is one choice; (23, 13, 18, 21, 22) by expected capacity order.

Table 7.6 compares LOLE [h] by different wind speed models using two phase method and sensitivity analysis. Wind farms are assumed to be installed at bus 3, 17, and 24. Clustering method is more accurate than transition rate method, since it deals with all correlations between load and wind speed. Especially, global or fast global approach of clustering is much closer to original wind data approach by making sure that it is convergent to the global optimum. Instead, it takes longer time than traditional clustering, KM or FCM in Table 7.7. The running time is the duration of clustering process for the optimal cluster size which is determined by validity measurement. Fast global approach accelerates the simulation speed. As the proposed wake model is incorporated on the system, reliability level drops in Table 7.8. As peak load increases, LOLE [h] also goes up.

Table 7.5: Expected Capacity of Bus

Bus	Expected capacity [MW]
1	184.9639
2	184.9639
7	288
13	561.4500
15	207.6000
16	148.8000
18	352
21	352
22	297.0000
23	619.4052

Table 7.6: LOLE[h] by Different Wind Speed Model

LOLE[h]	Exact transition			original		
	26.399			22.90		
	Clustering					
	KM	FCM	GKM	FGKM	GFCM	FGFCM
	25.37	25.91	22.55	23.21	23.00	22.74

Table 7.7: Running Time of Different Clustering Approaches

Time [min]	Clustering					
	KM	FCM	GKM	FGKM	GFCM	FGFCM
	0.012	1.21	73.2	59.53	391.8	65.4

Table 7.8: LOLE[h] without and with Wake Effect

Peak load[MW]	Without wake	With wake
2750	11.3741	14.3104
2850	22.7418	25.6343
2950	38.1095	41.0188

To determine the optimal storage buses, Table 7.9 compares LOLE [h] without and with storage for candidates of optimal bus using FGFCM with wake effect. As you see, for cases without storage, LOLE [h] is almost the same regardless of the location of wind farms. And we know that the final optimal storage buses with wind farms are bus 23, 13, and 18 by observing the changes of LOLE [h]. Table 7.10 shows LOLE [h] for selected optimal storage buses, 23, 13, and 18 by different peak load. For a case with peak load 2850[MW], reliability indices are compared by different storage performances in Figure 7.5 and Figure 7.6. As charge/discharge rates and capacity of storage increases, LOLE [h] tends to decreases. Finally, EENS [MWh/y] becomes greater for higher peak load, shown by Figure 7.7.

Table 7.9: LOLE[h] without and with Storage

Cases	Without storage		With storage	
Wind farm bus	23,13,18	23,13,21	23,13,18	23,13,21
LOLE[h]	25.6535	25.6543	21.8774	22.3725

Table 7.10: LOLE[h] of Optimal Storage

LOLE [h]	
Peak load[MW]	Optimal storage
2750	12.3003
2850	21.8774
2950	36.7522

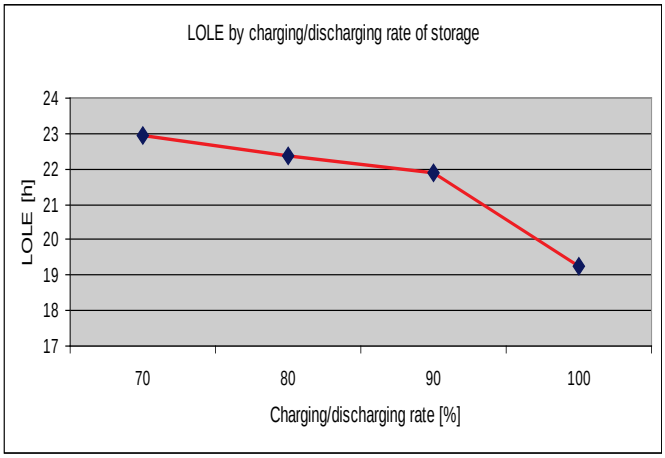

Figure 7.5: LOLE [h] by Different Charge/Discharge Rates

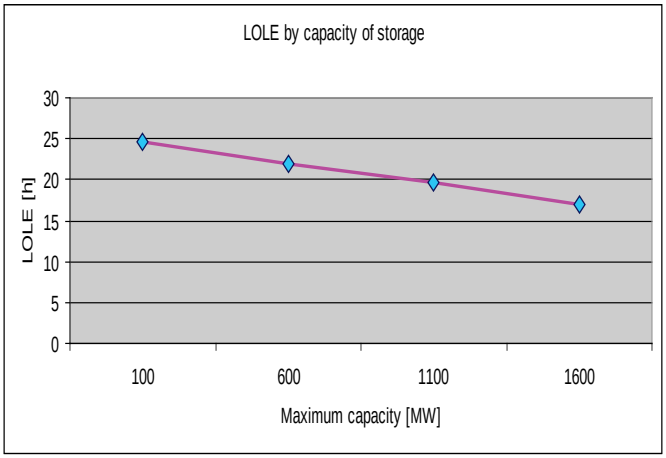

Figure 7.6: LOLE [h] by Different Maximum Capacity

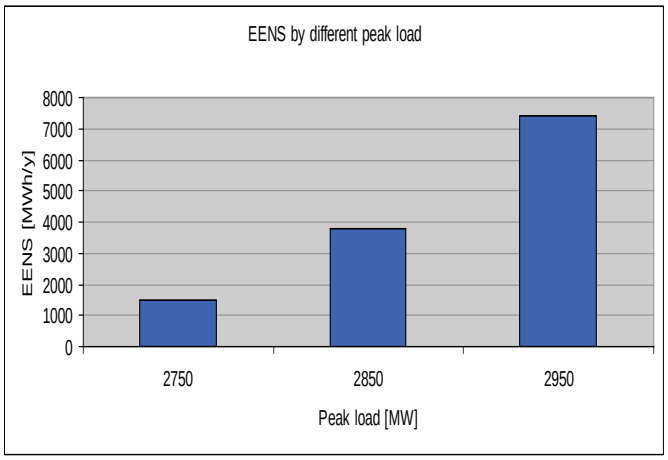

Figure 7.7: EENS [MWh/y] by Different Peak Load

8. Conclusions

Power system is modeled by conventional generating turbines, wind farms, and storage devices. Turbines are based on two generating states; fully available and out of service. To find efficient wind speed modeling, transition rate method and clustering method are applied and compared. Clustering approach is more accurate than transition method, since it can capture the correlation between wind speed and load. It needs mean wind speed, mean load, and probability of each cluster to evaluate reliability in the power system. To find efficient algorithm for partitional clustering, k means, fuzzy c means, global approach, and fast global approach are being compared. As one of the best algorithm, fast global approach is applied on the power systems with wind farms. Optimal storage bus using sensitivity analysis and proposed clustering method will be chosen and compared. From the original N. O. Jensen wake model, newly developed wake model is proposed on wind farm. As wake effect is incorporated into the system, reliability level drops by energy losses.

The flow model embedded in the linear program is DC power flow. To ensure that an initial basic feasible solution is available, artificial variables are added to the original constraints. Two phase method is applied to the system to get reliability indices. For a bus with wind farms, storage is incorporated to regulate the fluctuation of wind power. The upper limit of generation vector at the bus is updated by the storage vector. As storage is added to the system, it is observed that the reliability is improved. Optimization process is needed for every hour of simulation. Using sensitivity analysis, we can reduce simulation running time. Simulation methodology to select the optimal storage buses is developed and applied to the system, using LOLE [h] and EENS [MWh/y] to figure out the system reliability explicitly.

References

[1] Vaughn Nelson, *Wind Energy: Renewable Energy and the Environment*, 1st ed. Boca Raton, FL: CRC Press, 2009.

[2] F.C. Sayas and R.N. Allan, "Generation availability assessment of wind farms," in Proc. IEEE Gene. Trans. Distri. Vol. 143, no. 5, Sep. 1996, pp. 507-518.\

[3] Electrical Power System Reliability, Dr Singh's Homepage, [Online]. Available: http://www.ece.tamu.edu/People/bios/singh/

[4] H. Ascher and H. Feingold, *Repairable systems reliability modeling, inference, misconceptions, and their causes*, 1st ed. New York: Marcel Dekker, Mar. 1984.

[5] C. Singh and R. Billinton, *System reliability modelling and evaluation*, 1st ed. London, U.K.: Hutchinson Educational, Jun. 1977.

[6] C. Singh and Y. Kim, "An efficient technique for reliability analysis of power systems including time dependent sources," IEEE Trans. Power Syst., vol. 3, no. 3, Aug. 1988, pp. 1090-1096.

[7] Siddheswar Ray and Rose H. Turi, "Determination of number of clusters in K-means clustering and application in colour image segmentation," International Conference on Advances in Pattern Recognition and Digital Techniques (ICAPRDT), Dec. 1999, ISBN: 81-7319-347-9, pp 137-143.

[8] B. Bagen, P. Koegel, M. Couillard, K. Stradley, B. Giggee, A. Jensen, J. Iverson, and G.E. Haringa, "Probabilistic resource adequacy assessment of large interconnected systems," *in Probabilistic Methods Applied to Power Systems, IEEE 11th International Conf.* Jun. 2010, pp. 252-258.

[9] C. Singh and J. Mitra, "Monte Carlo Simulation and Intelligent Search methods", IEEE Tutorial on Electric Delivery System Reliability Evaluation (editor: J. Mitra), pp 23–38. IEEE, Piscataway, NJ: 2005.

[10] C. Singh and J. Mitra, "Monte Carlo simulation for reliability analysis of emergency and standby power systems," *in Proc. IEEE Industry Applications Conf. Thirtieth IAS Annu. Meeting*, vol. 3, no. 8–12, Oct. 1995, pp. 2290–2295.

[11] R. Billinton, and R. N. Allan, *Reliability Evaluation of Power Systems*, 2nd ed. New York: Plenum, Jan. 1996.

[12] . Wen, Y. Zheng, and F. Donghan, "A review on reliability assessment for wind power," Renewable and Sustainable Energy Reviews, Vol. 13, no. 9, Dec. 2009, pp.2485-2494.

[13] National Renewable Energy Laboratory (NREL), Western wind resource dataset [Online]. Available: http://wind.nrel.gov/Web_nrel/

[14] Power Systems Engineering Committee, "The IEEE reliability test system," IEEE Trans. Power App. Syst., vol. PAS-14, no. 3, Aug. 1999, pp.1010–1020.

[15] P. Giorsetto and K. F. Utsurogi, "Development of a new procedure for reliability modeling of wind turbine generators," IEEE Trans. Power App. Syst., vol. PAS-102, no. 1, Jan 1983, pp. 134-143.

[16] R. Xu and D. C. Wunsch, *Clustering*, *IEEE Press Series on Computational Intelligence*, John Wiley & Sons Inc., 2009.

[17] J. Valente de Oliveira and W. Pedrycz, *Advances in fuzzy clustering and its applications*, John Wiley & Sons Ltd., 2007.

[18] A. Likas, M. Vlassis, and J. Verbeek, "The global k-means clustering algorithm," Pattern Recognition, vol. 36, pp. 451–461, 2003.

[19] W. Wang, Y. Zhang, Y. Li, and X. Zhang, "The global fuzzy c-means clustering algorithm," in *Proc. of 6th World Congress on Intelligent Control and Automation Conf.*, pp. 3604-3607.

[20] Siddheswar Ray and Rose H. Turi, "Determination of number of clusters in K-means clustering and application in colour image segmentation," *Int. Conf. on Advances in Pattern Recognition and Digital Techniques (ICAPRDT)*, Dec. 1999, ISBN: 81-7319-347-9, pp 137-143.

[21] Hagkwen Kim and Chanan Singh, "Reliability modeling and simulation in power systems with aging characteristics," *IEEE Trans. Power Syst.*, vol. 25, no. 1, Feb. 2010, pp. 21-28.

[22] X. Zhang, and W. Wang, "Wind farm and wake effect modeling for simulation of a studied power system," *IEEE Power Systems Conference and Exposition (PSCE)*, 2009, pp. 1-6.

[23] Wind Farm Wake Effect Model in WAsP8, the Wind Atlas Analysis and Application Program. [Online]. Available: http://www.risoe.dk/vea/storpark/presentations/WAsP8%20Wake-effect%20model.pdf

[24] N.O. Jensen, "A note on wind generator interaction," *RISO National Laboratory*, DK-4000 Roskilde, Denmark, Nov. 1983.

[25] J.F. Ainslie, "Calculating the flowfield in the wake of wind turbines," *Journal of Wind Engineering and Industrial Aerodynamics*, vol. 27, no. 1-3, Jan. 1988, pp. 213-224.

[26] G.C. Larsen, "A simple wake calculation procedure," *RISO National Laboratory*, DK-4000 Roskilde, Denmark, Dec. 1988.

[27] J. F. Manwell, J. G. McGowan, and A. L. Rogers, *Wind Energy Explained: Theory, Design and Application*, 2th ed., United Kingdom: Wiley, 2009.

[28] L.M. Swain, "On the turbulent wake behind a body of revolution," *Proc. of Royal Society of London*, Series A 125, pp.647-659.

[29] D. Zigras, and K. Moennich, "Farm efficiencies in large wind farms," Deutsches Windenergie-Institut (DEWI), Nov. 2006.

[30] "*Conservation of Momentum*," Light and Matter Series. [Online]. Available: http://www.lightandmatter.com/html_books/2cl/ch04/ch04.html

[31] S. Mathew, *Wind Energy: Fundamentals, Resource Analysis and Economics*,1st ed. New York: Springer, 2006.

[32] MokhtarS. Bazaraa, John J. Jarvis, and Hanif D. Sherali, *Linear Programming and Network Flows*, 4th ed. Wiley, Dec. 2009.

[33] Practical Optimization: A Gentle Introduction [Online]. Available: http://www.sce.carleton.ca/faculty/chinneck/po.html

[34] P. Taylor, "Companies race to develop utility-scale power storage," New York Times, Sep. 2009.

[35] D. Rastler, "New demand for energy storage: electric perspectives," vol. 33, no. 5, pp. 30–47, Sep. /Oct. 2008.

[36] C. Vartanian, "The coming convergence, renewables, smart grid and storage," IEEE Energy 2030, Nov. 2008.

[37] J. A. Carter, B. Johnson, R.W. Sherwin, Rade-Makers, and L.W.M.M. "Failure modes and effects analysis for the AOC 15/50 wind turbine," *Proc. of the AWEA Wind power Conf.*, 1993, pp. 175-182.

Part 3

Integration of Electric Energy Storage at the Distribution Level with Renewable Energy Resources

Chanan Singh
Yixing Xu, Doctoral Student
Texas A&M University

For information about this project, contact

Chanan Singh
Regents and Runyon Professor
Department of ECE
Texas A&M University
3128 TAMU
College Station, Texas 77843-3128
Email: singh@ece.tamu.edu

Power Systems Engineering Research Center

The Power Systems Engineering Research Center (PSERC) is a multi-university Center conducting research on challenges facing the electric power industry and educating the next generation of power engineers. More information about PSERC can be found at the Center's website: http://www.pserc.org.

For additional information, contact:

Power Systems Engineering Research Center
Arizona State University
527 Engineering Research Center
Tempe, Arizona 85287-5706
Phone: 480-965-1643
Fax: 480-965-0745

Notice Concerning Copyright Material

Table of Contents

Table of Contents (continued)

List of Figures

List of Tables

1. Introduction

1.1 Background

The goal of this part of part is to investigate the reliability and economic impact of energy storage and renewable energy integration at the distribution level. The reliability and economy evaluation framework is presented. Novel operation strategies of energy storage and renewable energy are proposed. The methodology for optimizing the energy storage sizing and operation strategy in order to achieve optimal reliability and economy level is developed.

Section 2 investigates the scheduling and operation in distribution systems with energy storage. The major benefits of electric energy storage include electric energy time-shift, power supply capacity, and transmission congestion relief [3]. The types and amount of benefits of EES depend on how it is operated. The problem of scheduling and operation for a distribution system with energy storage focuses on how a load aggregator who participates in the day-ahead market and the real-time balancing market should utilize the energy storage to schedule its energy purchase in day-ahead market and operate in real-time market. The objective is to save energy purchasing cost in the market environment. By applying a Model Predictive Control-based approach, the potential to better manage the energy cost of a load aggregator with EES in a market mechanism consisting of day-ahead market and real-time balancing market is explored. As the price and load forecasts are crucial for this operation strategy, the impact of the forecast uncertainties is investigated.

Section 3 discusses the adequacy and economy analysis of distribution systems with energy storage and renewable energy. Reliability impact and economic benefits are tightly related. Especially with the operational flexibility of EES, different EES operation strategies could bring different sets of reliability impact and economic benefits. A novel Model Predictive Control (MPC)-based operation strategy for distribution system load aggregator is proposed to improve the economy of system by minimizing energy purchasing cost in power market with the utilization of price, load, and renewable energy forecasts. An islanding operation with power supplies from RER and EES is implemented to enhance distribution system reliability. In order to accurately assess the reliability and economic impact brought by proposed operation strategies, an assessment framework based on sequential Monte Carlo simulation approach is presented.

Section 4 discusses the multi-objective approach to design of energy storage in distribution Systems. The objective of energy storage is to help build a more reliable and efficient smart grid. Energy storage can help achieve many goals. Among these goals, we focus on two of the most important objectives which are reliability and economy. Majority of research done on energy storage design problems mainly considers the impact of energy storage capacity and power rate. The impact of energy storage operation strategy is ignored or not considered as a major factor. We demonstrate the significant impact of energy storage operation strategy on reliability level and economic benefits. A modified particle swarm optimization approach is proposed for the designing the problem of energy storage in distribution systems, where not only the energy storage capacity and power rate are determined but also the energy storage operation strategy.

Each major section is made almost independent for the convenience of the reader. In achieving this there is some repletion of the material but this will help the reader in navigating this part.

2. Optimal Scheduling and Operation of Load Aggregator with Electric Energy Storage in Power Markets

2.1 Introduction

Electric power systems are operated on the basis of real-time balancing of supply and demand without large-scale electric energy storage (EES) capabilities. With the objective of transformation towards a more reliable, secure, and efficient smart grid, and with the recent rapid development of EES technologies, feasible applications of EES in power systems have started to be investigated [1]-[2]. This section models the EES as operated by a load aggregator that participates in the day-ahead market and the real-time balancing market. The focus is on the energy cost savings.

Among the research efforts towards energy cost savings by utilizing storage, authors in [4] discusses the optimal demand-side response to electricity spot prices for storage-type customers (e.g. municipal water plants); Reference [5] reports on an experiment on the real-time pricing based control of thermal storage to save cost; Research in [6] investigates the economics of sodium sulfur batteries for the application of energy arbitrage in New York state's electricity market. Besides operating storage on the demand side, Researchers in [7] discusses the potential of using storage to increase profit of wind power in the day-ahead market and balancing market. Research work reported in [8] proposed a Model Predictive Control (MPC)-based method to solve the dispatch problem with intermittent resources using the short-term wind power and load forecasts. Several forecasting techniques for predicting short term electricity price [9]-[13] and load [14]-[16] are presented. Good short-term (e.g. within 24 hours) price and load forecasts are available. In this work, by applying a MPC-based method, the potential of taking advantage of these forecast technologies to better manage the energy cost of a load aggregator with EES in a market mechanism consists of day-ahead market and real-time balancing market is explored. In the presented MPC-based approach, the most updated price and load forecast information is integrated in the decision making process.

2.2 Energy Cost Saving with Energy Storage in Distribution Systems

2.2.1 Distribution Systems with Energy Storage

The load aggregator provides power to its customers (i.e. load) in a distribution network. The demand is assumed to be price inelastic. It also operates an EES located within the same distribution network. The topology of the system is simplified as in Figure 2.1 The distributed loads are modeled into one lumped load. Load in each period, $L(k)$, is price inelastic. The charging $C(k)$ and discharging $D(k)$ operations of the EES are determined by the load aggregator. The summation of the load and the EES power charging and discharging is the imported power $U(k)$ from the power market, delivered from the external grid. The load aggregator's objective is to minimize its energy cost by optimally scheduling the imported power in the day-ahead market and determining the imported power during operation in the real-time balancing market.

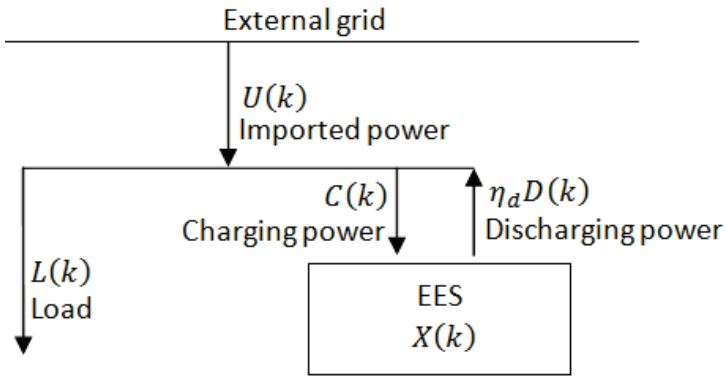

Figure 2.1: Electric energy storage integrated in the distribution system.

2.2.2 Day-ahead and Real-time Power Markets Model

The power markets are simplified as the following day-ahead market model and real-time balancing market model. The market models are similar to the models in [7].

In the day-ahead market, the load aggregator submits its offers to import power to meet its demands for each period in the next day. After the closure of the day-ahead market, system operator will determine which offers are accepted and work out the market clearing price for each period of the next day. All the load aggregator's offers are assumed to be cleared by the market and its bidding is assumed not affecting the market clearing price. In the day-ahead market, the energy cost for each period in the next day is

2.1 $$U_{sch}(k) \cdot P(k)$$

where $U_{sch}(k)$ is the amount of power scheduled to be imported in the day-ahead market for the period k in the next day, $P(k)$ is the actual day-ahead market clearing price for the period k in the next day. The total energy cost for a day is the sum of energy cost of each period in the day.

The amount of imported power scheduled by load aggregator is based on their prediction of the load and price, and EES characteristics in each period of the next day. The details of how the load aggregator optimally schedules its imported power are presented in Section 2.3.1 .

As the prediction is not perfect, during the real time operation, based on the actual load and price, load aggregator might decide to adjust its actual imported power to minimize energy cost while meeting the actual load. The discrepancies between day-ahead scheduled imported power and actual imported power are settled in the real-time balancing market. The balancing cost for each period is:

2.2 $$[(U_{actual}(k) - U_{sch}(k)] \cdot P_{balancing}(k)$$

where $U_{actual}(k)$ is the actual imported power in period k during real-time operation, $P_{balancing}(k)$ is the imbalance cost due to upregulation or downregulation of generators. The balancing cost for a day is the sum of the cost for each period in the day. The real-time balancing market is simplified by introducing two penalty factors p_{up} and p_{down} for upregulation and downreglation. The imbalance cost in period k is expressed as the penalty factor times the day-ahead market price for

the same period *k*

2.3 $$P_{balancing}(k) = \begin{cases} p_{up} \cdot P(k), \text{ if } U_{actual}(k) > U_{sch}(k) \\ p_{down} \cdot P(k), \text{ if } U_{actual}(k) > U_{sch}(k) \end{cases}$$

where $p_{up} \geq 1$ and $p_{down} \leq 1$.

The imbalance $U_{actual}(k) - U_{sch}(k)$ is based on the scheduled imported power in the day-ahead market, actual price and load, real-time forecasted price and load in the future periods, and EES characteristics. The details of how the load aggregator optimally determines the actual imported power during real-time operation is presented in section 2.3.2. The total energy cost is the sum of the day-ahead cost plus the real-time balancing cost. This is the objective function load aggregator tries to minimize.

2.2.3 Imported Power Model

The load is assumed to be price inelastic which needs to be met all the time. However, the charging and discharging behavior of the EES are fully controllable within its physical limits. Both load and EES are in the same distribution system, thus load and the charging and discharging behavior of the EES are combined together as the imported power for the load aggregator. The imported power is elastic to some extent because of the flexibility of the EES charging and discharging operation. Load aggregator is assumed to be net power importer. Thus,

2.4 $$U_{actual}(k) \geq 0$$

2.5 $$U_{sch}(k) \geq 0$$

2.2.4 Electric Energy Storage Model

EES is modeled by its energy storage capacity, charging power limit, discharging power limit, charging efficiency, discharging efficiency, available periods, initial storage level and final storage level. The storage level has to be equal or below its capacity. The values of charging and discharging power have to be within their limits. Power loss during discharging and charging operations are considered in its charging and discharging efficiencies. The storage is only available for operation during the specified available periods. Most of the EES technologies such as sodium sulfur batteries and flywheels are stationary and could be operated all the time after installation. However some EES such as PHEVs are not stationary, and are only available for operation during some specific periods (e.g. from 8AM to 6PM when plugged in charging stations). The operation of EES needs to meet the initial and final storage level constraints. For example, the energy stored in PHEVs' batteries must be higher than certain level before leaving charging station. The storage level at the end of each period is determined by the previous period storage level and the charging and discharging operation during this period, it is expressed as:

2.6 $$X(k) = X(k-1) + \eta_c \cdot C(k) - D(k)$$

where *C(k)* is the power charged to EES, *D(k)* is the power discharged from EES, *X(k)* is the energy storage level at the end of period *k*. All three variables needs to be within their operation limits, expressed as:

2.7 $$0 \le C(k) \le C_{Max}(k)$$

2.8 $$0 \le D(k) \le D_{Max}(k)$$

2.9 $$X_{Min}(k) \le X(k) \le X_{Max}(k)$$

When the EES is not available, $C_{max}(k)$, $D_{max}(k)$, $X_{min}(k)$ and $X_{max}(k)$ are all zeros.

2.3 Scheduling and Operation with Energy Storage

2.3.1 Optimal Scheduling in the Day-ahead Market

In the day-ahead market, the objective of the load aggregator is to schedule the imported power for each period in the next day at the least cost. As the day-ahead market clearing price *P(k)* is unknown before submitting its offers, and the actual load *L(k)* during real-time operation is also uncertain, day-ahead predicted price $\hat{P}(k)$ and load $\hat{L}(k)$ are used for day-ahead scheduling. There are several forecasting techniques for predicting electricity price and load. The focus here is on how to use the predicted price and load for optimal scheduling instead of how to predict them. The objective function of the day-ahead market optimal scheduling problem can be formulated as a linear programming problem which minimizes the energy cost in the day-ahead market based on price and load forecast:

2.10 $$Min. \sum_{k=1}^{K} U_{sch}(k) \cdot \hat{P}(k)$$

Subject to the constraints (2.5)-(2.9), and

2.11 $$U_{sch}(k) = \hat{L}(k) + C(k) - \eta_c D(k)$$

where *K* is the total number of periods in the next day. After submitting its schedule to the system operator, the market clearing price is worked out. The actual energy cost in day-ahead market can be calculated as:

2.12 $$\sum_{k=1}^{K} U_{sch}(k) \cdot P(k)$$

The forecasted day-ahead market price and load play an important role in the minimizing the total energy cost. If it can be perfectly forecasted, the load aggregator could optimally operate its EES to take advantage of the low prices periods by importing more power and storing it while reducing the imported power during the high price periods by supporting the load with the stored energy.

2.3.2 Optimal Operation in the Real-time Balancing Market

Day-ahead forecasted price and load are not perfectly accurate, the discrepancies of scheduled imported power in the day-ahead market and actual imported power during operation are settled in the real-time balancing market. A MPC-based method is proposed to determine the optimal real-time operation.

The basic approach of MPC is that a finite–horizon optimization problem determining the series of optimal control operations is solved before each control step, but only the first control operation is implemented. A predictive model is used to estimate the state space trajectory over the prediction horizon, with the initial state being the actual state of the system. After implementing the first control operation, the system updates the actual state of the system and the future states using the predictive model. Then the optimal control routine is repeated to determine the next step's optimal operation. This method of receding-horizon strategy has been successfully applied in the real world, such as in chemical process industry. Applying the above MPC-based approach, balancing cost minimization problem with uncertain price and load at period i can be implemented as follows

1) Obtain the actual load and price in the current period *i*.
2) Select a receding optimization horizon *N* periods (e.g. 24 hours). Use a load and price forecast model to obtain the most updated load and price forecast for the future periods from *i+1* to *i+N*.
3) Solve the balancing cost minimization problem, which is a linear programming problem, formulated as:

$$\begin{aligned} &Min.\ [U_{actual}(i) - U_{sch}(i)] \cdot P_{balancing}(i) + \\ &\sum_{k=i+1}^{i+N} [U_{actual}(k) - U_{sch}(k)] \cdot \hat{P}_{balancing}(k) \end{aligned} \tag{2.13}$$

$$\text{s.t. } (4), (6) - (9),$$
$$\text{For } (4), (6) - (9),\ k = i, i+1, \cdots, i+N,$$
$$U_{actual}(i) = L(i) + C(i) - \eta_c D(i),$$
$$U_{actual}(k) = \hat{L}(k) + C(k) - \eta_c D(k), k = i+1, \cdots, i+N$$

The first part $(U_{actual}(i) - U_{Sch}(i)] \cdot P_{balancing}(i)$ $[U_{actual}(i) - U_{sch}(i)] \cdot P_{balancing}(i)$ is the balancing cost of the current period *i*, its actual load *L(i)* and actual imbalance cost $P_{balancing}(k)$ is known. The second part $\sum_{k=i+1}^{i+N} [U_{actual}(k) - U_{sch}(k)] \cdot \hat{P}_{balancing}(k)$ is the balancing cost of the following periods *i+1* to *i+N*. Its load $\hat{L}(k)$ $\hat{L}(k)$ and price $\hat{P}_{balancing}(k)$ are real-time forecasted values. The solution of this optimization problem gives an optimal operation schedule for the periods from *i* to *i+N*.

4) Implement the first period operation of the above solution, which is the period *i* to determine how the EES should be operated and the actual imported power $U_{actual}(i)$.

5) Update the EES storage level state, move to the next period, then repeat the algorithm from step 1.

The actual imbalance cost is simplified as the day-ahead price multiplied by a penalty factor. Thus both actual imbalance cost $P_{balancing}(k)$ and forecasted imbalance cost $\hat{P}_{balancing}(k)$ are expressed as:

$$\begin{aligned} & P_{balancing}(k) = \hat{P}_{balancing}(k) \\ & = \begin{cases} p_{up} \cdot P(k), \ if \ U_{actual}(k) > U_{sch}(k) \\ p_{down} \cdot P(k), \ if \ U_{actual}(k) > U_{sch}(k) \end{cases}, \\ & k = i, i+1, \cdots, i+N, \end{aligned} \tag{2.14}$$

The short-term (e.g. next 2-3 hours) forecast is more accurate than the relatively longer term (e.g. 23-24 hours) forecast. Thus, by using this MPC-based method, the most updated price and load forecast could be effectively integrated into the operation decision making process to minimize the balancing cost.

2.4 Case Studies

2.4.1 Case I: Stationary Energy Storage

In this case, the proposed method is applied to a load aggregator with a stationary EES. Both the day-ahead scheduling periods and real-time receding optimization horizon are 24 hours. Each hour is considered as a period.

The forecasted and actual day-ahead market clearing price is shown in Figure 2.2. The penalty factors $p_{up}=1.2$ and $p_{down}=0.8$. The day-ahead forecasted load and actual load during real-time operation are shown in Figure 2.3. The actual load curve has the peak load at 10MW.

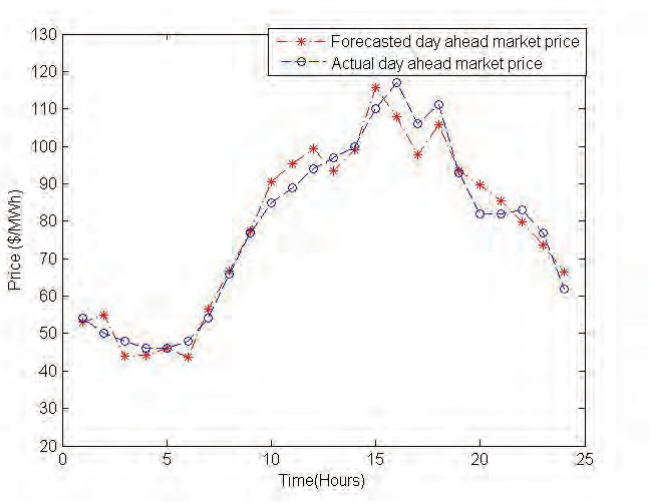

Figure 2.2: The forecasted and actual day-ahead market clearing price.

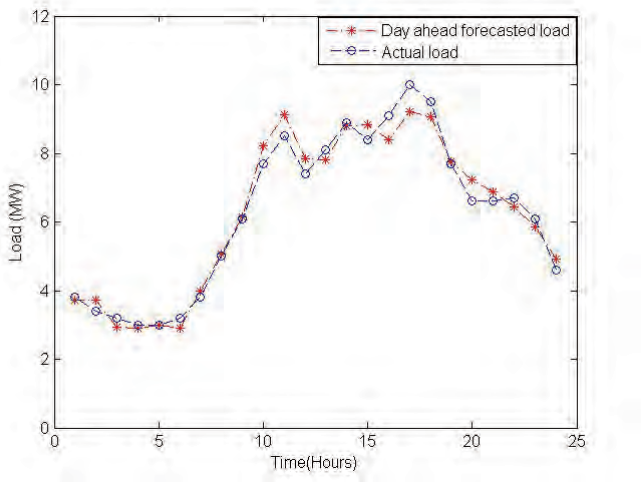

Figure 2.3: Day-ahead forecasted load and actual load.

The parameters of the EES are shown in Table 2.1 "Initial storage level" means the storage level at the beginning of 0AM. "Final storage level" means the storage level at the end of 11PM.

Table 2.1: Energy Storage Parameters

Capacity(MWh)	10
Charging Power Limit(MW)	1
Discharging Power Limit(MW)	1
Charging Efficiency	0.95
Discharging Efficiency	0.95
Available Periods	24/7
Initial storage level(MWh)	3
Final storage level(MWh)	3

The energy costs of the following scenarios are simulated and compared:

1) Load aggregator does not have EES. It schedules its import power in the day-ahead market based on perfect load and price forecast.
2) Load aggregator operates EES. It uses the proposed method to schedule its imported power in the day-ahead market based on perfect load and price forecast.
3) Load aggregator does not have EES. It schedules its imported power in the day-ahead market based on not perfect day-ahead load and price forecast. The discrepancies during real-time operation are settled in balancing market.
4) Load aggregator operates EES. It uses the proposed method to schedule its imported power in the day-ahead market and operate in the real-time balancing market based on not perfect day-ahead and real-time load and price forecast.

The day-ahead and real-time forecast uncertainties in scenario 3 and 4 are set to be equal. The simulation results are shown in Table 2.2

Table 2.2: Case I Cost Comparison

	Scenario 1 No EES/ Perfect forecast	**Scenario 2 EES/ Perfect forecast**	**Scenario 3 No EES/ Not perfect forecast**	**Scenario 4 EES/ Not perfect forecast**
Day-ahead market cost($)	12958	12605	13280	12943
Real-time balancing market cost($)	0	0	-187	-275
Total cost($)	12958	12605	13093	12668

The results in Table 2.2 show the cost savings the optimal scheduling and operation methods can bring, and the importance of the forecast accuracy. The negative cost in the real-time balancing market means the load aggregator over estimated the load in the day-ahead market, surplus power is sold during real-time operation. By comparing the cost difference caused by imperfect forecast, it also suggests that the proposed method is more robust to forecast uncertainty.

Figure 2.4 shows the difference of the day-ahead scheduled imported power between scenario 1 and 2. Generally, more energy is imported during the low price periods and less energy is imported in the high price periods. As the load correlates with price to some extent, the imported power curve is leveled to some extent.

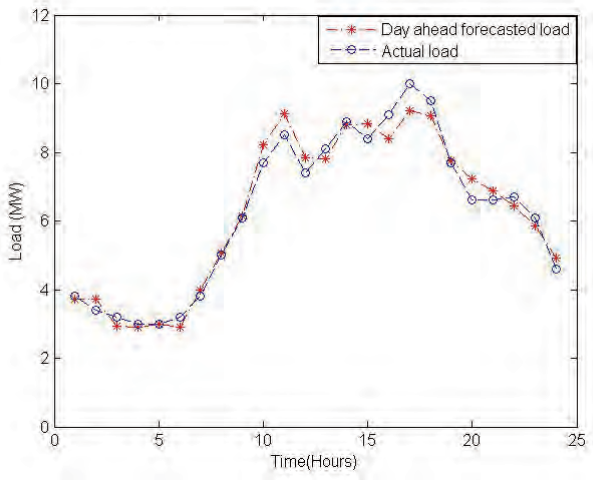

Figure 2.4: Day-ahead scheduled imported power comparison.

Figure 2.6 shows the day-ahead scheduled storage level variation based on the perfect forecasted day-ahead market price of scenario 2. EES is generally charged during the low price periods and discharged during high price periods.

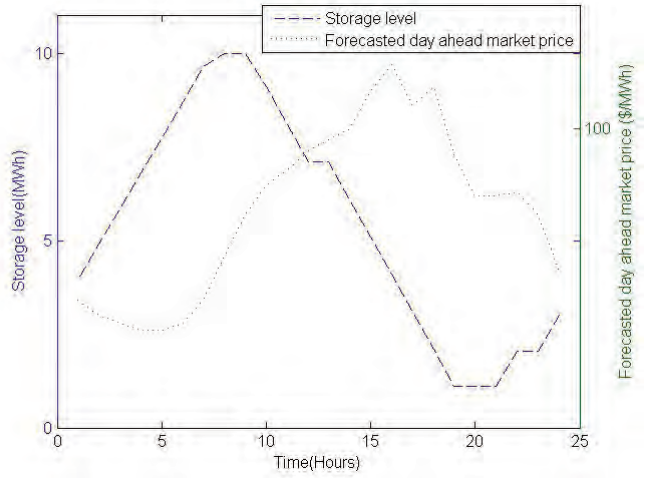

Figure 2.5: Day-ahead scheduled storage level variation based on the forecasted day-ahead market price of scenario 2.

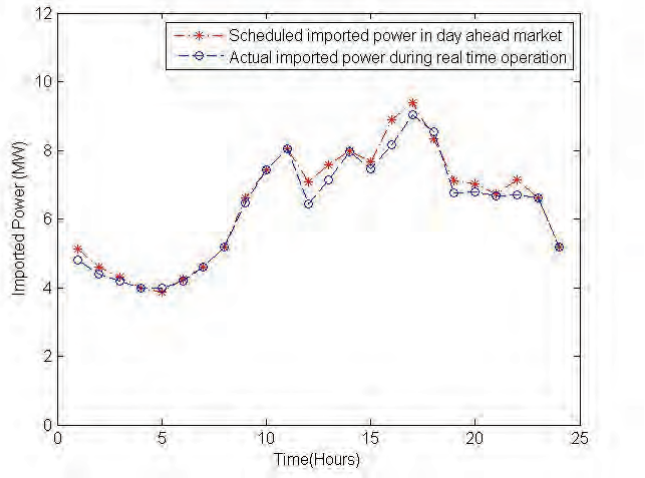

Figure 2.6: The comparison of scheduled imported power in day-ahead market and actual imported power during real-time operation in scenario 4.

Figure 2.6 shows the difference of the scheduled and actual imported power of scenario 4. The optimal real-time operations do not necessarily follow the day-ahead schedule.

2.4.2 Case II: Mobile Energy Storage

In case II, V2G (vehicle to grid) capable PHEVs' batteries are utilized as the EES which can be charged and discharged according to control signals from the load aggregator. The PHEVs are assumed to be plugged in the charging stations located in the load aggregator's distribution network where other commercial activities also reside. Load aggregator is assumed to have certain contracts with the PHEVs parked in the charging stations which allow it to operate the PHEVs' batteries when they are plugged in. The topology of the distribution network could be simplified as in Figure 2.1. All the individual PHEVs are combined and modeled as one EES.

The load aggregator can operate the batteries as they wish, but need to ensure that before the PHEVs leave the charging station, the stored energy has to be above certain required level. The proposed methods are applied to help load aggregator optimally operate these PHEVs' batteries to minimize its energy cost. The PHEV battery parameters used in the simulation are shown in Table 2.3. While we recognize that studying the inherent uncertainty of PHEVs' availability at any given time is an important future research direction, here in this work we assume that 50 PHEVs are available for operation from 8AM to 6PM in the simulation day.

Table 2.3: PHEV Battery Parameters

Capacity(kWh)	5.2
Charging Power Limit(kW)	2
Discharging Power Limit(kW)	2
Charging Efficiency	0.95
Discharging Efficiency	0.95
Availabile Periods	8AM to 6PM
Initial storage level(kWh)	1
Final storage level(kWh)	5

A load curve of an aggregation of commercial activities is used. A price curve with large variation is used to show the volatile behavior of the electricity price in downtown load centers. The load without PHEVs and price curves are shown in Figure 7.

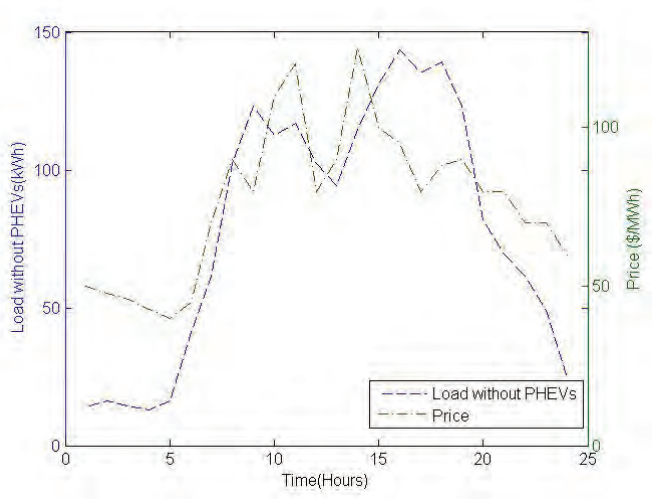

Figure 2.7: Load without PHEVs and price curves.

The costs of the following two scenarios are compared:

- Perfect day-ahead price and load forecast is assumed. The PHEVs are immediately charged when plugged in until reaching the required storage level. Load aggregator does not utilize the PHEVs' batteries to reduce its energy cost.

- Perfect day-ahead price and load forecast is assumed. The load aggregator uses the proposed method to optimally schedule the imported power in the day-ahead market and operate the PHEVs' batteries to reduce its energy cost while ensuring the required energy storage level before PHEVs' leaving charging stations.

Figure 8 compares the imported power of scenario 1, scenario 2 and the load curve without PHEVs. In scenario 1, the imported power jumped up from 8am to 1pm, because the PHEVs are being charged during those periods. In scenario 2, PHEVs' charging and discharging operations are determined by load aggregator to manage its energy cost. Figure 9 shows the storage level variation in scenario 1 and scenario 2. In scenario 1, the storage level climbs up to the required level and stays there for the rest of the available periods. In scenario 2, the batteries are generally charged when the price is low and discharged to support the load when the price is high. The results in Table 4 show the cost savings by optimal scheduling the imported power and operating the PHEVs' batteries

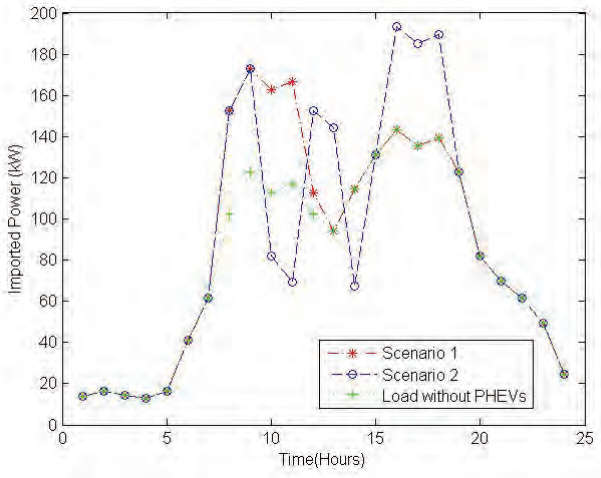

Figure 2.8: Load Imported power comparison between scenario 1 and scenario 2 with load curve without PHEVs.

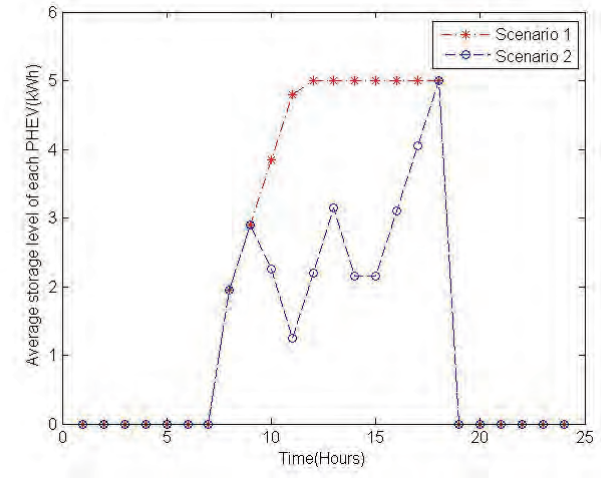

Figure 2.9: Average storage level of each PHEV in Scenario 1 and Scenario 2

The cost comparison is shown in Table 2.4.

Table 2.4: Case II Cost Comparison

	Scenario 1 Charging immediately/ Perfect forecast	**Scenario 2 Optimal charging and discharging/ Perfect forecast**
Day-ahead market cost($)	189.12	183.43

In the day-ahead market, a load aggregator can use the proposed method to schedule the imported power in each period of the next day with day-ahead forecasted price and load. During real-time operation, the discrepancies caused by the forecast errors are compensated in the real-time balancing market. The load aggregator can use the proposed MPC-based method to optimally determine its actual imported power in balancing market and EES operations during real-time operation. The proposed MPC-based method integrates the most updated price and load forecast data over a receding horizon to achieve the optimal operation.

2.5 Summary

In competitive power markets, with increasing penetration of variable renewable energy resources such as wind power, electricity price becomes more uncertain. In distribution systems, adoption of renewable distributed generation technologies adds another dimension of uncertainty in load forecast. Facing these higher price and load uncertainties, it becomes more challenging for load aggregators to manage their electricity cost. Within this context, a Model Predictive Control (MPC)-based scheduling and operation strategy is proposed for the load aggregator with electric energy storage (EES) to manage electricity cost in day-ahead and real-time power markets with different levels of price and load uncertainties. Price and load forecasts are actively integrated into the scheduling and operation decision making process to determine the optimal operation. Two other strategies are also discussed and studied for comparison. Case studies demonstrate better performance of the proposed MPC-based strategy compared to the other two strategies facing different levels of price and load uncertainties. The MPC-based strategy is also shown to be robust with the increase of price and load uncertainties. The benefit of energy arbitrage with MPC-based strategy is also illustrated. With this MPC-based strategy, load aggregators schedule purchase power in the day-ahead market with day-ahead price and load forecasts. Then during real-time operation, real-time price and load forecasts are updated constantly in each period. By utilizing these forecasts, load aggregator optimally adjusts its operations to reduce real-time electricity cost.

3. Adequacy and Economy Analysis of Distribution Systems Integrated with Electric Energy Storage and Renewable Energy Resources

3.1 Introduction

Although the potential benefits of RER are significant, many major challenges need to be conquered first. One of the major challenges is the reliability impact caused by intermittent RER

such as wind power. This problem could be ignored earlier because the integrated RER were only a very small percentage (e.g., 3%) of the total generation. The intermittent property of RER does not have a notable reliability impact on systems which are mainly supported by conventional fossil fuel generations. With expected greater penetration of RER (e.g., 20% wind power), their reliability impact can no longer be ignored. A comprehensive reliability analysis considering the impact of high RER penetration is required.

An efficient method of reliability analysis of electric power systems with time-dependent sources, such as photovoltaic and wind generation is presented in [20], in which the reliability impact of fluctuating characteristics of unconventional generation units is studied. Reference [21] investigates the reliability effects on a composite generation and transmission system associated with the addition of large-scale wind energy conversion systems using the state sampling Monte Carlo simulation technique, where the wind speed correlation is considered. The work in [22] presents a reliability analysis framework which includes both the deterministic and probabilistic approaches for bulk power system adequacy and security assessment when wind power is added. Considerable work has been done on RER integration in transmission systems. Reliability impact of RER integrated in distribution systems is also studied by researchers. In [23], the authors investigate the system reliability benefits of adding wind turbine generation as an alternative supply in a rural distribution system. In [19], both Monte Carlo simulation and analytical methods are used to assess distribution system adequacy including wind-based distribution generation units, with implementation of the islanding mode of operation in the assessment.

With a rapid development of Electric Energy Storage (EES) technologies, and their operational flexibility, interest in integrating both RER and EES into power systems to improve systems reliability and economy has been growing. A reliability cost/worth evaluation method that can incorporate the impact of wind energy and EES utilization in electric power systems is presented in [18]. Research in [24] evaluates system reliability considering wind and hydro power coordination, where hydro facilities with energy storage capability are utilized to alleviate the impact of wind power fluctuations and also improve the system adequacy. A methodology for the operation of a hybrid plant with wind power and hydrogen storage to maximize economic benefits (i.e., maximizing profits) in a market environment is presented in [7].

Previous reported work has been on either the reliability impact of RER and EES integration, or on economic benefits of the integration. However, reliability impact and economic benefits are tightly related. Especially with the operational flexibility of EES, different EES operation strategies could bring different sets of reliability impact and economic benefits.

In this section, a novel Model Predictive Control (MPC)-based operation strategy for distribution system load aggregator is proposed to improve the economy of system by minimizing energy purchasing cost in power market with the utilization of price, load, and renewable energy forecasts. An islanding operation with power supplies from RER and EES is implemented to enhance distribution system reliability. In order to accurately assess the reliability and economic impact brought by proposed operation strategies, an assessment framework based on sequential Monte Carlo simulation approach is presented.

3.2 Distribution System Integrated with Energy Storage and Renewable Energy

A distribution system integrated with distributed RER (e.g., wind-based distributed generation) and EES is shown in Figure 3.1. Load aggregator of a distribution system participates in the wholesale power markets to purchase electric energy to serve its customers in the distribution system. Meanwhile, load aggregator is also assumed to operate the RER and EES integrated in its served distribution system. Renewable energy generation can be controlled by curtailing available renewable energy output. EES devices are operated by determining the charging/discharging operations. It is assumed that electric energy price is determined by the markets and load is determined by customers, which is inelastic to price. The objective of the load aggregator is to serve its customers with reliable power supply while minimizing the electric energy purchasing cost in power markets. The goals are to propose novel operation strategies to enhance reliability and economy, and present a comprehensive framework for assessing both reliability and economy.

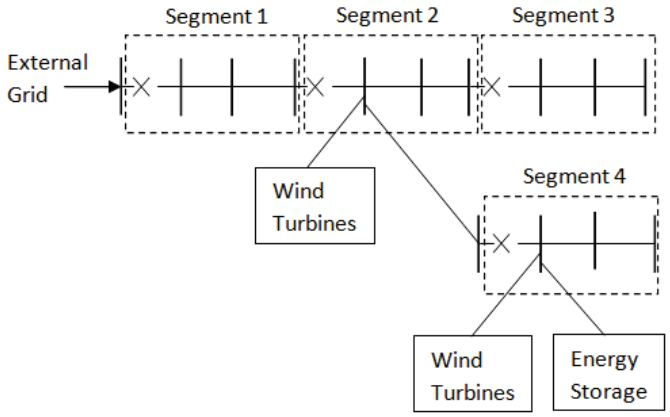

Figure 3.1: Schematic diagram of a radial distribution system integrated with wind turbines and electric energy storage.

As most distribution systems are operated radial, the focus here is considering radial distribution system with RER and EES integrated. Figure 3.1 shows an example of a radial distribution system with RER and EES integrated, where "X" sign represents protective devices such as circuit breakers and reclosers. The following assumptions are used in the study of the system. Only the active power is considered. Voltage levels are assumed to be properly regulated. This assumption is normally acceptable in adequacy analysis for planning purposes. If the impact of voltage cannot be ignored, a more detailed distribution system AC power flow could be used instead. Power output from RER is considered constant within a period.

3.3 Operation Strategies

3.3.1 Modes of Operation

A distribution system consists of components such as wires, circuit breakers and reclosers. A group of components can be modeled as one segment if the entry component is a protective device such as a switch or a recloser and the entry protective device is the only protective device of this segment. In this way, the distribution system is modeled by segments instead of

components. The rationale behind this segment modeling is that if a component failure occurs downstream of a protective device and within its protection zone, the protection zone will be isolated and all the customers in that protection zone will lose power supply. Even if there are other power sources such as RER or EES integrated into this segment, once a component failure occurs within this segment, the power supply from all energy resources is cut off. For example, in Figure 3.1, the components of the distribution system are grouped into 4 segments according to the location of protective devices. If a component failure occurs in segment 2, the protective devices isolate this segment, external grid power cannot be supplied to this segment, the power supply from wind turbines is also cut off, the load demand in this segment cannot be met and a loss of load event occurs.

In a radial distribution system without distributed generation (DG) such as RER, if a component failure occurs within a segment, the segment is isolated and grid power cannot be supplied to the load within this segment and the segments downstream. However, when DG or EES is integrated, if a component failure occurs within a segment, the segment is still isolated but the downstream segments can utilize power from DG or EES integrated to support their load. In this case, the loss of load event might be avoided if there is enough power from these alternate energy resources. Following the previous example, when segment 2 is isolated, as there is no DG or EES integrated in segment 3, there is no power supply for its load. Instead, power from wind turbines and EES can be used to supply the load within segment 4.

To summarize the above discussion, when there is a failure within a segment, all the power supply for this segment is cut off. When there is no failure within a segment, there are two modes of operation, grid connected mode and islanding mode. In grid connected mode, the transformers connecting transmission system and distribution are up, the external grid is capable of delivering sufficient energy. Thus grid power can be supplied to this radial distribution system and no failure occurs within any upstream segment. Thus the power from external grid can go through all the upstream segments and reach the studied segment. In islanding mode, at least one failure occurs in upstream segments, or the transformers are down, or the external grid is unable to deliver sufficient energy to this distribution system caused by outage. Thus power from external grid cannot be supplied to the segment under study. Power from the DG and EES integrated in this segment is utilized to support the load. The identification of operation modes is not limited for radial system. Operation mode of segment in non-radial system can also be identified through more complicated evaluation considering the distribution system topology.

3.3.2 Operations in Grid Connected Mode and Islanding Mode

EES operation strategies affect the reliability and economic performance of a distribution system. This part presents the proposed operation strategies in different operating modes.
Operation Strategy in Grid Connected Mode: In grid connected mode, the power from external grid, RER and EES can all be utilized to serve the load. The objective of the load aggregator is to minimize its energy purchasing cost in power market while meeting the demand. The allocating of power supplies is crucial in determining the energy purchasing cost.

With more and more accurate methods developed for load forecasting, renewable energy forecasting, and energy price forecasting, EES can utilize these forecasts to reduce the energy purchasing cost. A Model Predictive Control (MPC)-based operation strategy is proposed to minimize the energy purchasing cost by optimally coordinating the energy purchase from the

power market, EES charging/discharging operation, and utilization of RER. In the MPC-based operation strategy, short term forecasts of load, available renewable energy and energy price, are utilized to determine the operation. Power market modeling and EES modeling are introduced first before further describing of the proposed operation strategy.

The power market here is simplified as a real time power market model. During each market period (e.g. an hour), load aggregator determines how much energy it needs to purchase from the market, then submits its offer to get that needed amount of energy. The market clearing mechanism determines the energy price for each period. Load aggregator is assumed to be a price taker whose transactions do not affect the clearing price determined by the market. The energy purchasing cost for N periods starting from period $i+1$ is

$$\sum_{k=i+1}^{i+N} U(k) \cdot P(k) \tag{3.1}$$

With the proposed operation strategy, no specific EES technology is addressed. Rather the EES unit is modeled by its operation limits which include EES maximum and minimum state of charge level, charging/discharging power limit, charging/discharging efficiency. The energy storage state of charge level at any time has to be within its minimum and maximum range. This range is considered as the effective capacity. The charging and discharging rates have to be within the power limits. Power losses during charging/discharging operations are considered in its charging/discharging efficiencies. The state of charge at the end of each period is determined by the previous period state of charge level and the charging/discharging operation during this period, it is expressed as

$$SOC(k) = SOC(k-1) + \eta_c \cdot C(k) - D(k) \tag{3.2}$$

All EES operation variables are within their operation limits.
The basic approach of MPC is that a finite–horizon optimization problem determining the series of optimal control operations is solved before each control step, but only the first control operation is implemented. After implementing the first control step, the system updates the actual state of the system and the future states using a predictive model. Then the control routine is repeated to determine the next step's operation. Applying the above MPC approach, energy purchasing cost minimization problem with forecasted, load, available renewable energy and price at period i can be implemented as follows:

1) Obtain the actual load, available renewable energy and price in the current period i.
2) Select a receding optimization horizon of N periods (e.g. 24 hours). Use load, renewable energy and price forecast models to obtain the most updated load, renewable energy and price forecasts for the next N periods, from period $i+1$ to $i+N$.
3) Solve the optimization problem, formulated as follows.

Objective: Minimizing energy purchasing cost from period i to $i+N$

$$Min.\ U(i) \cdot P(i) + \sum_{k=i+1}^{i+N} U_f(k) \cdot P_f(k) \tag{3.3}$$

The first part $U(i) \cdot P(i)$ is the energy purchasing cost of the current period *i*. The second part $\sum_{k=i+1}^{i+N} U_f(k) \cdot P_f(k)$ is the predicted total energy purchasing cost of the following periods from *i+1* to *i+N*. $U(i)$ and $U_f(k)$ are the decision variables to be solved.

Constraints:

EES operation constraints:

$$0 \le C(k) \le C_{Max} \tag{3.4}$$

$$0 \le D(k) \le D_{Max} \tag{3.5}$$

$$SOC_{Min} \le SOC(k) \le SOC_{Max} \tag{3.6}$$

where $k=i,i+1,\ldots,i+N$. The charging and discharging operations of EES are to be solved. The maximum charging and discharging rates are constant. As one hour is considered as one period, the charging energy equal to $C(k)$ multiplied by 1 hour. For convenience $C(k)$ is used interchangeably as charging rate and energy charged in one hour. $D(k)$ is treated in the same way.

Available renewable energy constraints:

$$0 \le R(i) \le R_{Max}(i) \tag{3.7}$$

$$0 \le R_f(k) \le R_{f,Max}(k) \tag{3.8}$$

where $k = i+1,\ldots, i+N$. The utilized renewable energy is equal to or less than the available renewable energy. Extra energy not utilized is dumped in ways such as adjusting the wind turbines' blade pitch, so wind turbines do not generate the maximum power they can in that period. Utilized renewable energy for current period and future period are to be solved.

Power balance constraints:

$$U(i) + R(i) = L(i) + C(i) - \eta_d D(i) \tag{3.9}$$

$$U_f(k) + R_f(k) = L_f(k) + C(k) - \eta_d D(k) \tag{3.10}$$

where $k = i+1,\ldots,i+N$. Load, available renewable energy, and price in current period *i* are the actual values and known. While load, available renewable energy, and price in future periods are predicted using forecast models, thus are given parameters for the optimization problem. The solution of this optimization problem gives an optimal operation schedule for EES charging/discharging operation, energy purchase and renewable energy utilization from period *i* to *i+N*.

4) Implement the first period's operation of the solved operation schedule, which is the current period i.
5) Update the EES state of charge level, move to the next period, and repeat the algorithm from step 1.

The solved operation schedule is optimal with respect to the given forecast. The accuracy of forecast will affect the optimality of the solution because of the difference between the forecast and the actual values. We have assumed the forecast to be perfect but if information on characteristics of forecast uncertainty were available, it could be incorporated in the determination of the schedule. The short-term (e.g. next 2-3 hours) forecast is more accurate than the relatively longer term (e.g., 23-24 hours) forecast. By using this MPC-based operation strategy, load, renewable energy and price forecasts are updated according to the newest information after each operation step. Then the most updated forecasts could be effectively integrated into the operation decision making process to minimize the energy purchasing cost. By taking into consideration what the future load, renewable energy and price will be, better operation for current period can be determined. 24 hours is chosen as the optimization horizon considering the 24 hours cycling period of load variation, renewable energy variation and energy price variation. Because of the increasing forecast uncertainty into future periods, different choice of optimization horizon such as 12 hours, could lead to different operation schedule. More detailed information about the forecast uncertainty could be used to determine the optimal optimization horizon.

The integration of RER and EES itself could reduce energy purchasing cost. However, the proposed MPC approach optimally determines from which power sources (RER, EES or external grid) to get power supplies to support the load, how much energy should be supplied by each selected power source, and chronological operations such as whether the renewable energy generated in this period should be used up now or stored for future use to avoid high energy price, and at which period EES should be discharged in order to release more storage capacity for storing lower priced energy in the coming periods. These operation decisions provided by the MPC approach could reduce energy purchasing cost even more than simply integrating RER and EES. The proposed MPC operation strategy reduces the energy purchasing cost by better coordinating the power supply from different power sources and energy usage along the time line.

Operation Strategy in Islanding Mode: In islanding mode, avoiding and minimizing load curtailment is the objective. The available renewable energy is first utilized to serve the load. If it is not enough to cover the load, the energy stored in EES is discharged to avoid or minimize load curtailment. Only when the load demand is met, and there is renewable energy surplus, the extra energy is stored in EES for future usage without violating EES operation limits. The extra energy which cannot be stored in EES is then dumped.

3.4 Reliability and Economy Assessment Framework

The proposed reliability and economy assessment framework is based on Sequential Monte Carlo Simulation. During operation, EES sometimes serves as generation providing power to the load and sometimes it is charged acting as a load. Current EES state of charge level at a point in time is determined by the previous operations. The utilization of energy from EES in the current period is determined by both its current state of charge level and planed utilization in the future. Because of these unique chronological characteristics of EES, its impact on system reliability and economy is best captured using sequential Monte Carlo method, in which its specific operation strategies are integrated. The assessment flowchart is shown in Figure 3.2 Details of the assessment framework are presented as follows.

3.4.1 Distribution System Reliability Analysis

In adequacy analysis, a power system is considered to be operating in either success state or failure state. A system is considered operating in success state when it has enough generation capacity to serve the load. When generation capacity is not sufficient to meet the load demand and loss of load occurs, the system is in failure state. The probabilities and durations associated with the system residing in success and failure states and energy not served during failure states are the adequacy indices for reliability analysis.

For a distribution system modeled in terms of segments, a modified reliability analysis is presented to evaluate the reliability of the system in more details. In the modified analysis, besides evaluating the reliability of the distribution system, each segment of the distribution system is also evaluated. The determination of segment state is explained later. After the states of the segments are determined, the system state is then determined as following: the system is in success state if all the segments are in success state; the system is in failure state if any segment is in failure state. By performing the modified reliability analysis, reliability indices for each segment and the whole system can be obtained. The different reliability levels of segments caused by network topology, RER and EES can be evaluated.

3.4.2 Segment State Determination and Operation

In the assessment framework, time horizon is divided into periods (hourly). Once the component simulation is done, up or down state of each component in the distribution system is determined. Information of distribution system topology is needed with the component state information to determine segment operation mode. Then the success or failure state of each segment could be evaluated considering their operation mode.

Under grid connected mode, the load is compared with the total power supply which consists of the available power from external grid, RER and EES. If the total power supply is not sufficient for the load, the system is identified as in failure state. If the total power supply can serve the load, it is in success state. After evaluating the segment state, MPC-based operation strategy is implemented using the most updated system state, and load, renewable energy, price forecasts. EES state of charge is then updated accordingly after each operation.

Under islanding mode, the load is compared with the total power supply which only consists of RER and EES. The system is in failure state if the total power supply cannot serve the load. If the power supply can cover the load, it is in success state. With the state determination finished, islanding mode operation is implemented. EES state of charge is then updated accordingly.

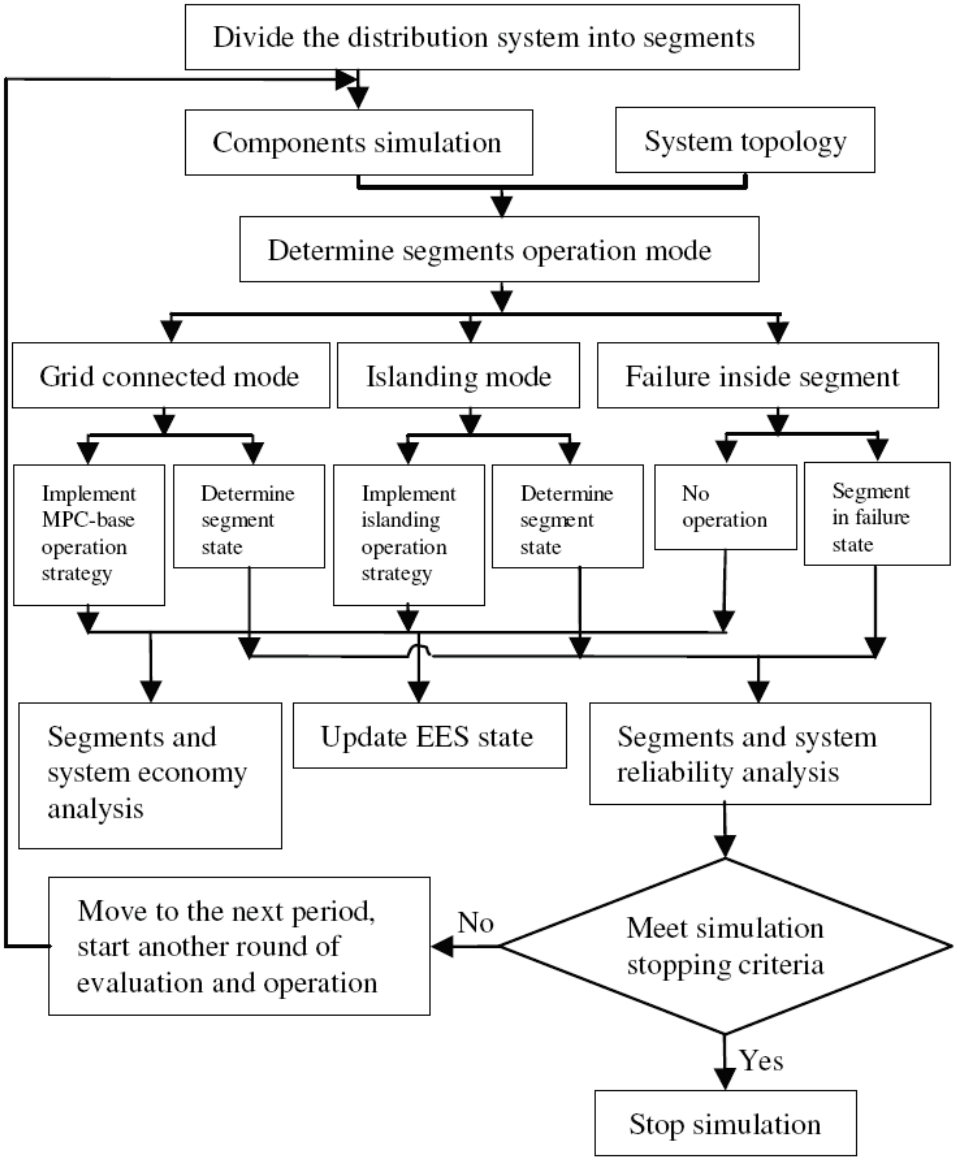

Figure 3.2: Proposed reliability and economy assessment framework flowchart.

If there is a failure within a segment, this segment is in failure state. No operation is performed until the failure is removed.

After state determination and operation for the current period, the process moves to the next period and starts another round of state determination and operation. Simulation stops when the specified maximum number of simulation years is reached or the probability of system in failure state converges. Considering there is generation integrated in the distribution system and the objective of comparing the available generation with the load, adequacy analysis indices, Loss of Load Expectation (LOLE) and Expected Energy Not Served (EENS) are calculated as the reliability indices. Other common distribution system indices, such as SAIFI and SAIDI, could also be calculated if needed.

3.4.3 Distribution System Economy Analysis

Annual energy purchasing cost and customer interruption cost are used as the economic indices. Hourly energy purchasing cost is calculated according to the actual operation. Then annual energy purchasing cost is the sum of hourly energy costs in a year. We focus on the cost during operation. Thus the investment cost of RER and EES are not included in the economic indices, but it can be included if desired. If the optimal capacity of RER and sizing of EES are to be solved, the investment cost should be considered.

Customer interruption cost is the cost of damage to customers caused by the power delivery interruption. When a service interruption occurs, the normal activities of customers in the distribution system could be affected and bear certain interruption cost. According to the nature of their activities, customers are grouped into 7 sectors, large user, industrial, commercial, agriculture, residential, government and institution, and office and buildings. Postal surveys have been conducted to estimate the customer interruption cost [25]. The survey data has been analyzed to provide Sector Customer Damage Function (SCDF). Customer damage cost is related to the type of customer and the duration of the interruption. As only limited interruption cost data is available, logarithmic interpolation and linear extrapolation can be used to calculate the cost within and outside the provided cost data. Composite Customer Damage functions (CCDF) are used to evaluate the interruption cost of mix types of customers. SCDF is used to construct CCDF using following equation

$$CCDF = \sum_{i=1}^{n} k_i SCDF_i \tag{3.11}$$

where k_i is the per unit energy consumption of customer sector *i*, $SCDF_i$ is the sector customer damage function of customer *i*, *n* is the number of customer sectors. SCDF gives the customer damage cost for each sector, while CCDF gives the total customer damage cost for a mix of customer types.

For an unreliable system, its annual energy purchasing cost might be low. But it does not mean this system is more economically efficient. It is because larger amount of energy could not be purchased and delivered to the distribution system due to frequent and long duration service interruptions. By evaluating the customer interruption cost at the same time, a more complete picture of the system economy can be obtained.

3.5 Case Studies

A modified practical radial distribution system integrated with wind turbines and EES, as shown in Figure 3.3, is studied. A step-down transformer is connecting the external grid and the distribution system. The components of the distribution system are grouped into two segments. Wind turbines and EES are integrated in segment 2 at node 28. The integration node could be determined by the network topology and the capability of handling required power injection. Node 28 is assumed to be able to accommodate the power injection. Other suitable nodes could also be chosen. If the transformer has a fault or external grid fails to deliver sufficient energy because of outage, power could not be delivered to the distribution system. Thus in this reliability analysis, the transformer and external grid are considered as one component, with Mean Time To Failure (MTTF) of 1440 hours and Mean Time To Repair (MTTR) of 6 hours.

A series of cases are studied to investigate the reliability and economic impacts from integration of EES and wind turbines. Table 8 shows the studied 12 sets of EES effective capacity and power limit. The charging/discharging round efficiency is set to be 90%. EES is assumed to be perfectly reliable.

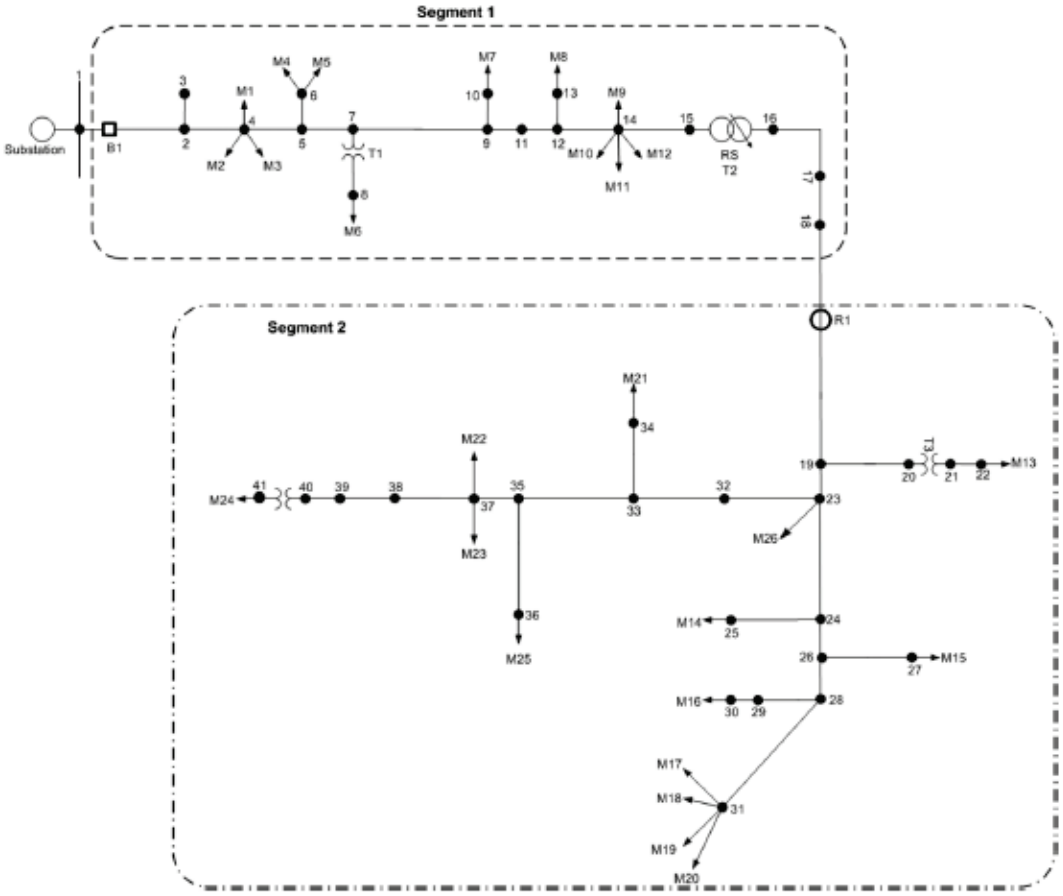

Figure 3.3: Proposed Modified practical radial distribution system with wind turbines and EES integrated in segment 2.

Table 3.1: Electric Energy Storage Parameters in Case Studies

Capacity (MWh)	Power limit (MW)	Capacity (MWh)	Power limit (MW)	Capacity (MWh)	Power limit (MW)
5	1	10	1	15	1
5	2	10	2	15	2
5	2.5	10	2.5	15	2.5
5	5	10	5	15	5

Six sets of Wind Turbine Generation (WTG) capacities are studied. They are 1MW, 2MW, 4MW, 6MW, 8MW and 12MW. Historical wind power output data is used [26]. 1MW capacity wind turbine's MTTF is 720hrs and the MTTR is 30hrs. Other WTG capacities are obtained by

utilizing multiple 1MW wind turbines. The reliability indices for other capacities are also calculated accordingly.

A case is formed by matching an EES unit, which includes its capacity and power limit characteristics, with a WTG capacity. Thus 72 (12×6=72) cases are formed and studied. A base case with no EES and WTG is also studied for comparison. In each case study, LOLE, EENS, energy purchasing cost, customer interruption cost of each segment and the system are obtained.

When implementing the proposed MPC-based operation strategy, forecast tools are needed to obtain the price, load, and wind power forecasts. The actual forecasts are not perfect. The effect of inaccurate forecasts is investigated in research work [27].

The peak load of the distribution system is 8MW. IEEE-RTS load profile is used as the chronological load profile. Segment 1 and segment 2 each share 50% of the total system load. The MTTF of both segments is 1440 hours and the MTTR is 1 hour. The hourly energy price profile used in the case study is shown in Table 9. Customer interruption cost of three customer mixes representing high commercial activities, high industry activities and high residential activities respectively are studied. The percentages of each customer sector for the three mixes are shown in Table 10.

Table 3.2: Electric Energy Price

Hour	1	2	3	4	5	6	7	8	9	10	11	12
Price ($/MWh)	50	48	46	43	40	45	70	90	80	110	120	80
Hour	13	14	15	16	17	18	19	20	21	22	23	24
Price($/MWh)	90	125	100	95	80	88	90	80	80	70	70	60

Table 3.3: Customer Sector Percentage For Each Customer Mix

	Commercial (%)	Industry (%)	Residential (%)
High Commercial Mix	80	10	10
High Industry Mix	10	80	10
High Residential Mix	10	10	80

Table 3.4: Base Case Economy Indices (Million $/Year)

	Segment 1 Customer Damage Cost	Segment 2 Customer Damage Cost	System Customer Damage Cost	Energy Purchasing Cost
High Commercial Mix	0.761	1.262	2.023	3.435
High Industrial Mix	0.584	0.990	1.574	
High Residential Mix	0.268	0.439	0.707	

Base case without EES and WTG, and seventy-two cases with different matching of EES and WTG capacity were studied. For reasons of space limitations, only selected results are presented here. Base case results are shown in Table 3.3 and Table 3.4.

In Table 3.4, the LOLE for the system is exactly the same as LOLE for segment 2. It is caused by this particular distribution system configuration, where segment 2 is in series with segment 1 and downstream. For other configurations, LOLE are not necessarily the same for both system and one segment. Selected results of system with EES and WTG are shown in Table 13. The results demonstrate the reliability and economic improvement brought by the EES and WTG integration, and the proposed operation strategies. They also provide insights on how EES capacity, power limit and WTG capacity affect reliability and economy. These results could also be helpful in determining the proper EES capacity, power limit and WTG capacity to achieve desired reliability level and economy benefit.

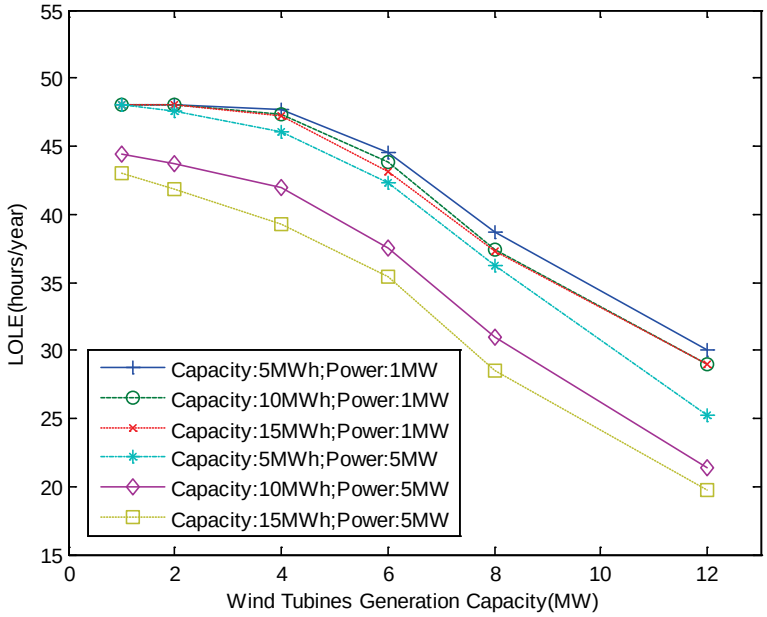

Figure 3.4: System LOLE when EES power limit is 1MW and 5MW.

Results show that increasing EES capacity, power limit, or WTG capacity can all enhance reliability, save energy cost and reduce customer interruption cost. However, the impact each factor has on reliability and economy depends on the situation. It can be observed from Figure 3.4 that only when EES power limit increases to a higher level (5MW), the increase in EES capacity can effectively improve system LOLE. That is because when power limit is low (1MW), it becomes the bottle neck preventing sufficient power discharged to support the load even when there is abundant energy stored. The potential of large EES capacity is not utilized. Meanwhile, with the EES power limit of 5MW, the LOLE improvement tends to saturate when increasing EES capacity from 10MWh to 15 MWh compared with the increase from 5MWh to 10 MWh. This means with EES capacity of 10MWh and power limit of 5MW, a large portion of loss of load events could be avoided. Only a small additional portion of more rare and sever loss of load events would be eliminated with the additional 5MWh EES capacity. When the LOLE improvement will reach saturation with the increase of EES capacity is affected by the specific load level and segments failure rate. The proper matching of EES capacity and power limit is very important in the effectiveness of reliability improvement.

Table 3.5: Reliability Indices of System with EES and WTG

Electric Energy Storage		WTG Capacity (MW)		LOLE (hrs/yr)	EENS (MWh/yr)
Energy Capacity (MWh)	Power (MW)				
5	1	1	Segment 1	42.71	73.95
			Segment 2	48.06	120.56
			System	48.06	194.51
5	1	4	Segment 1	42.30	57.92
			Segment 2	46.14	91.86
			System	47.65	149.78
5	2.5	1	Segment 1	42.67	73.22
			Segment 2	46.59	116.57
			System	48.02	189.79
5	2.5	4	Segment 1	40.78	57.53
			Segment 2	43.05	89.50
			System	46.13	147.02
10	1	1	Segment 1	42.71	70.59
			Segment 2	48.06	114.92
			System	48.06	185.51
10	1	4	Segment 1	41.94	54.68
			Segment 2	45.46	86.45
			System	47.29	141.13
10	5	1	Segment 1	39.10	67.94
			Segment 2	40.63	105.19
			System	44.45	173.13
10	5	4	Segment 1	36.57	52.68
			Segment 2	37.44	80.49
			System	41.92	133.17

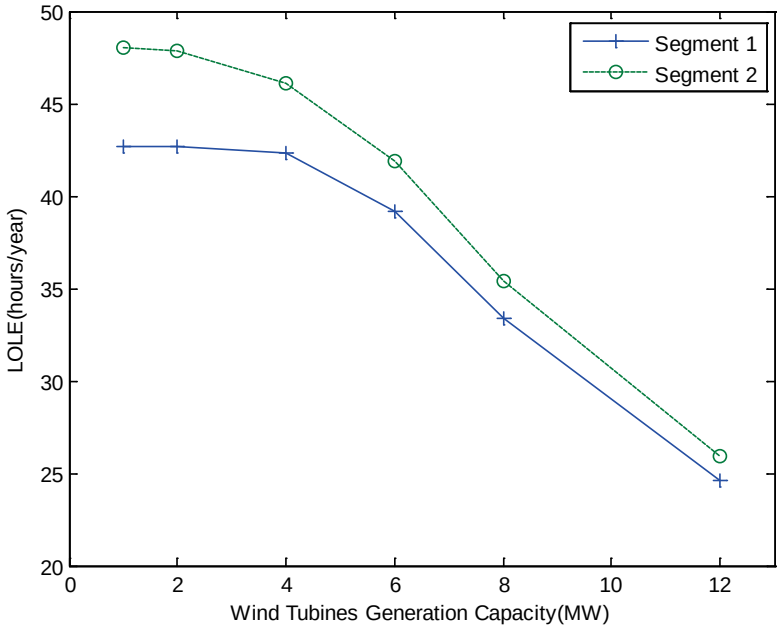

Figure 3.5: Segment 1 and Segment 2 LOLE when fixing EES capacity at 5MWh and power limit at 1MW.

Reliability improvement for both segments is shown in Figure 3.5. With the increase of WTG capacity, reliability level of segment 2 is improved much faster than segment 1 when increasing WTG capacity to 6MW. After increasing WTG capacity over 6MW, the reliability of segment 2 is still improving faster but not as significant as when the WTG capacity below 6MW. This result implies the possibility of reliability differentiation by integrating proper size of WTG and EES into the segments which need reliability improvement. Figure 3.6 shows the energy purchasing cost with EES capacity of 5MWh and 15MWh. The energy cost with EES having 15MWh capacity and 1MW power limit is higher than that with EES having 5MWh capacity and 2MW power limit. This phenomenon implies the importance of proper matching of EES capacity and power limit in order to achieve desired economic benefits. Customer interruption cost for high commercial mix system with EES capacity of 15MWh is shown in Figure 3.7. There is a sharp interruption cost reduction when increasing EES power limit from 1MW to 2MW.

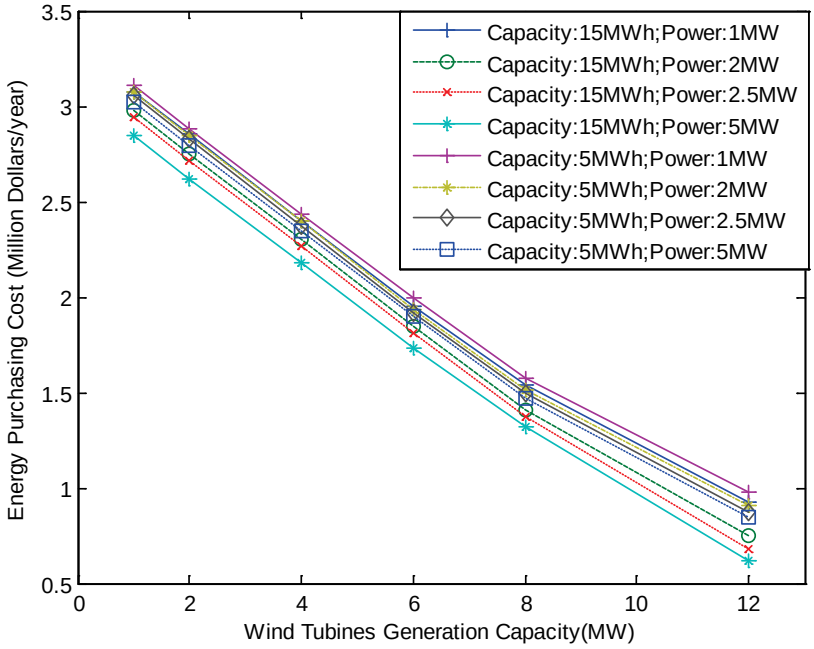

Figure 3.6: Energy purchasing cost when EES capacity is 15MWh and 5MWh.

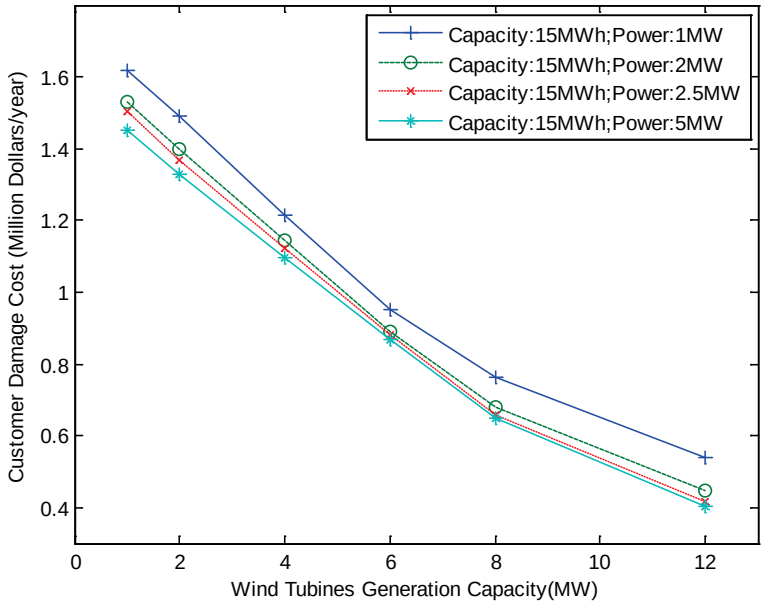

Figure 3.7: System customer interruption cost for high commercial mix system when fixing EES capacity at 15WMh.

However, the reduction is very limited when increasing power limit beyond 2MW. This result suggests the nonlinear and saturation effect when utilizing EES to improve system economy.

3.6 Summary

The integration of Renewable Energy Resources (RER) into an existing distribution system is an important topic in dealing with energy challenge the world is facing. With rapid development of Electric Energy Storage (EES) technologies, there is a growing interest in integrating both EES and RER into power systems to improve their reliability and economy. The adequacy and economy of distribution systems integrated with both EES and RER are assessed. A novel Model Predictive Control (MPC)-based operation strategy is presented to minimize distribution system energy purchasing cost by coordinating multiple power supplies from EES, RER and external grid. An islanding operation is implemented to improve the distribution system reliability and reduce customer interruption cost. A reliability and economy assessment framework based on sequential Monte Carlo method integrated with the MPC-based operation and islanding operation is proposed. Case studies are conducted to demonstrate the reliability and economy improvement by implementing the proposed operation strategies together with integration of EES and RER, and also investigate how EES capacity, power limit, and wind turbine generation capacity affect system reliability and economy.

4. Multi-Objective Design of Energy Storage in Distribution Systems Based on Modified Particle Swarm Optimization

4.1 Introduction

The major benefits of energy storage include electric energy time-shift, frequency regulation and transmission congestion relief. Energy storage can help achieve many goals. Here, we focus on the objectives of reliability and economy. Some researchers have investigated the effect of energy storage on improving reliability. Researchers in [28] explore the feasibility of installation of battery storage plant to enhance power system reliability and security. A reliability cost/worth evaluation method that can incorporate the impacts of wind energy and energy storage utilization in electric power systems is presented in [27].

Among the research efforts towards achieving higher economic benefits by utilizing energy storage, [4] discusses the optimal demand-side response to electricity spot prices for storage-type customers. Authors in [5] reports on an experiment on the real-time pricing based control of thermal storage to save cost.

The energy storage sizing problems are also being investigated. Reference [17] describes an analytical approach to evaluate reliability improvement by using energy storage as a backup storage and determine the size of the storage, which includes the capacity and power rate, to meet a specified reliability target.

Reliability impact and economic benefits are tightly related when considering energy storage integration [29]. Especially with the operational flexibility of energy storage, different operation strategies could bring different reliability impact and economic benefits. For load aggregator of distribution system integrated with energy storage, it is important to know the reliability and economy impact of the implemented energy storage operation strategies. Then proper energy storage operation strategies can be chosen and implemented to achieve desired reliability and economy improvement goals.

However majority of research done on energy storage design problems mainly consider the impact of energy storage capacity and power rate. The impact of energy storage operation strategy is ignored or not considered as a major factor. This work demonstrates the significant impact of energy storage operation strategy on reliability level and economic benefits. A modified particle swarm optimization approach is proposed for the designing the problem of energy storage in distribution systems, where not only the energy storage capacity and power rate are determined but also the energy storage operation strategy.

4.2 System Description

4.2.1 Energy Storage Integrated in Distribution System

In a market environment, the load aggregator purchases electric energy from wholesale market and delivers the purchased electric energy to its customers in the distribution system. The objective of the load aggregator is to serve its customers reliably and economically.

With the integration of energy storage devices in the distribution system, they could be utilized to improve distribution system reliability and economy. As most distribution systems are radial, the focus here is on considering such distribution systems. However, the proposed method can be also applied to other distribution systems with different configurations Figure 4.1 shows an example of a radial distribution system integrated with energy storage, where "X" represents protective devices such as circuit breakers and reclosers. The transformers and all the generation and transmission systems are represented as the external grid, through which the electric energy is delivered to the distribution system.

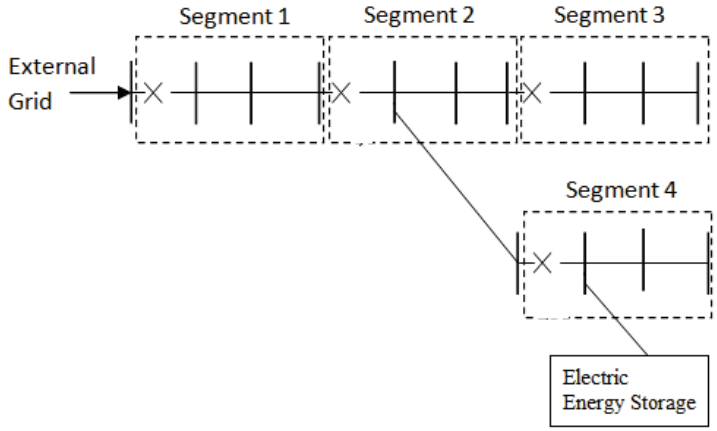

Figure 4.1: A radial distribution system integrated with energy storage.

4.2.2 Modes of Operation

In a radial distribution system without distributed generation (DG) or energy storage, if a component failure occurs within a segment, the segment is isolated. Grid power cannot be supplied to the load within this segment and the segments downstream. The load demand in all these segments cannot be met. However, when DG or energy storage are integrated, if a component failure occurs within a segment, the segment is still isolated but the downstream segments can utilize power supply from integrated DG or energy storage to support its load. In

this case, the loss of load event might be avoided if there is enough power from these energy resources. In Figure 4.1,when segment 2 fails and is isolated, as there is no DG or energy storage integrated in segment 3, there is no power supply for its load. Instead, power from energy storage can be used to supply the load within segment 4.

To summarize the above discussion, when there is a failure within a segment, all the power supply for this segment is cut off. When there is no failure within a segment, there are two modes of operation, grid connected mode and islanding mode. In the grid connected mode, if the external grid is in success state grid power can be supplied to this radial distribution system and there is no failure within any upstream segment. Thus the grid power can go through all the upstream segments and reach the studied segment. In the islanding mode, at least one failure occurs in upstream segments or the external grid is in failure state. Thus grid power cannot be supplied to the segment under study. If there are no DGs and energy storage integrated in the studied segment, load in this segment cannot be met. If there are DGs and energy storage is integrated in the studied segment, power from DGs and energy storage is utilized to support its load. Loss of load might be avoided or loss of energy is minimized.

4.3 Energy Storage Operation Strategies

The operation of energy storage is very flexible and behaves very different from either generation or load. Energy storage can be flexibly operated to act as generation, load or simply standby according to the needs of load aggregator. How energy storage is operated has a major impact on distribution system reliability level and economic benefits. In this chapter, a standby backup operation strategy, a Model Predictive Control (MPC)-base operation strategy and a hybrid operation strategy are presented. Approach for the reliability and economy improvement evaluation of these operation strategies is discussed.

4.3.1 Standby Backup Operation Strategy

One commonly used operation strategy is utilizing energy storage as a standby backup energy resource. The standby backup operation strategy is implemented as follows. In the islanding mode, power from external grid cannot reach the studied segment. Energy storage integrated in this segment is discharged to sustain the service in this segment. The objective is to avoid a loss of load event or minimize the unserved energy within its operation constraints including energy storage capacity limits and power rate limits. When the system is restored and the segment is back to the grid connected mode, energy storage is being charged until it reaches its energy storage upper limit and then it is in standby to prepare for the next failure.

4.3.2 MPC-based Operation Strategy

The presented MPC-based operation strategy minimizes the energy purchasing cost. This operation strategy is implemented in grid connected mode. With this strategy, short term forecasts of energy price and load are utilized to determine the optimal operation schedule. Power market modeling and energy storage modeling are briefly introduced first before further description of the MPC-based operation strategy.

The power market is simplified as a real time power market model. However, this strategy can

also be implemented in other market structures. During each market period (e.g. an hour), load aggregator determine how much energy it needs to purchase from power market, then submits its offer to get that amount of energy. The market clearing mechanism determines the energy price for each period. Load aggregator is assumed to be a price taker who cannot affect the clearing price determined by the market. The energy cost for period *k* is

$$U(k) \cdot P(k) \tag{4.1}$$

where *U(k)* is the amount of energy purchased in power market in period *k*, *P(k)* is the market clearing price in period *k*. Assume load aggregator can only purchase energy, we have

$$U(k) \geq 0 \tag{4.2}$$

The total energy cost for the period *i* and the following *N* periods is

$$\sum_{k=i}^{i+N} U(k) \cdot P(k) \tag{4.3}$$

The energy storage unit is modeled as a set of parameters and operation limits. Energy storage is modeled by its energy storage capacity, charging power limit, discharging power limit, charging efficiency, discharging efficiency. The energy storage state of charge (SOC) at the end of each period is determined by the previous period SOC and the charging/discharging operation during current period, it is expressed as

$$SOC(k) = SOC(k-1) + \eta_c \cdot C(k) - D(k) \tag{4.4}$$

where *C(k)* is the power charged to energy storage, *D(k)* is the power discharged from energy storage, *SOC(k)* is the SOC at the end of period *k*, η_c is the charging efficiency. All three variables need to be within their operation limits, expressed as

$$0 \leq C(k) \leq C_{Max} \tag{4.5}$$

$$0 \leq D(k) \leq D_{Max} \tag{4.6}$$

$$SOC_{Min}(k) \leq SOC(k) \leq SOC_{Max}(k) \tag{4.7}$$

The basic approach of MPC is that a finite–horizon optimization problem determining the series of optimal control operations is solved before each control step, but only the first control operation is implemented. A predictive model is used to estimate the state space trajectory over the prediction horizon, with the initial state being the actual state of the system. After implementing the first operation, the system updates the actual state of the system and the future states using the predictive model. Then the optimal control routine is repeated to determine optimal operation for the next step. Applying the above MPC-based approach, energy cost minimization problem at period i can be implemented as follows

1) Obtain the actual load and price in the current period *i*.
2) Select a receding optimization horizon *N* periods (e.g. 24 hours). Use load and price forecast tools to obtain the most updated load and price forecasts for the future periods from *i+1* to *i+N*.
3) Solve the energy purchasing cost minimization problem, which is a linear programming problem, formulated as:

4.8 $$Min.\, U(i)\cdot P(i) + \sum_{k=i+1}^{i+N} U(k)\cdot \hat{P}\,(k)$$

$$\text{s.t.}\,(2),(4),(5)\text{-}(7),\ k = i, i+1, \cdots, i+N,$$

4.9 $$U(i) = L(i) + C(i) - \eta_d D(i),$$

4.10 $$U(k) = \hat{L}(k) + C(k) - \eta_d D(k), k = i+1, \cdots, i+N$$

The first part $U(i)\cdot P(i)$ is the energy cost in the current period *i*. Its actual load *L(i)* and energy price $P_{balancing}(i)$*P(k)* are known. The second part $\sum_{k=i+1}^{i+N} U(k)\cdot \hat{P}(k)$ is the total energy cost of the following periods from *i+1* to *i+N*. Its load $\hat{L}(k)$ $\hat{L}(k)$and energy price $\hat{P}\,(k)$ $\hat{P}_{balancing}(k)$are forecasted values. The solution of this optimization problem gives an optimal operation schedule for energy storage from periods *i* to *i+N*.

4) Implement the first period's operation of the above solution, which is the period i to determine how the energy storage should be operated and the amount of energy U (i) needs to be purchased.
5) Update the energy storage level state, move to the next period, and then repeat the algorithm from step 1.

Several forecasting techniques for predicting short term electricity price and load have been presented by researchers. Good short-term (e.g. within 24 hours) price and load forecasts are available. The very short-term (e.g. next 2-3 hours) forecast is more accurate than the relatively longer term (e.g. 23-24 hours) forecast. Thus, by using this MPC-based method, after each control step, the price and load forecast are updated according to the newest forecast. Then the most updated and accurate price and load forecast could be effectively integrated into the operation to minimize the energy purchasing cost.

The proposed MPC-based control method is implemented in grid connected operation mode. Then in the islanding mode, the energy storage is operated to sustain the service in this segment to avoid a loss of load event or minimize the unserved energy within operation limits.

4.3.3 Hybrid Operation Strategy

The standby backup operation strategy can significantly improve reliability level, as the energy storage generally holds maximum amount of energy to support the load when an islanding

occurs. The loss of load events and unserved energy can be effectively reduced. The MPC-based operation strategy can significantly improve the economic benefits by reducing energy purchasing cost, as energy storage is actively utilized to store energy when the energy price is low and to discharge energy when the energy price is high. The basic idea of the hybrid operation strategy is conceptually dividing the energy storage device storage capacity into two portions. One portion of the energy storage is implemented with the standby backup operation strategy, while the other portion is implemented with the MPC-based operation strategy. The standby backup portion maintains a certain specified energy storage level to prepare for the failure event, which helps improve reliability. The MPC-based portion is taking the advantage of the energy storage operation flexibility to minimize energy cost, which contributes to the economic benefits. With a certain energy storage capacity, if the standby backup portion, expressed as *B%*, increases, the MPC-based portion, *(100%−B%)*, decreases. Accordingly, the reliability of the system is further improved but the economic benefit is reduced, and vice versa. Through this operation strategy, a flexible tradeoff between reliability and economic improvements is achieved. The feasible range for *B%* is from *0%* to *100%*. When *B%* equals to *0%*, it is a pure MPC-based operation strategy; when *B%* equals to *100%*, it is a pure standby backup operation strategy; when *B%* is in between, it is a hybrid operation strategy mixed with the MPC-based and the standby back operation strategy. Thus *B%* could be used as a parameter representing which energy storage operation strategy is implemented. This operation strategy parameter is as important as the other energy storage parameters such as energy storage capacity and power rate when it comes to the impact on distribution system reliability and economy.

4.3.4 Reliability and Economy Evaluation

With a given set of energy storage parameters including operation strategy parameter, energy storage capacity and power limit, etc, its impact on distribution system reliability and economy could be evaluated.

In reliability evaluation, a power system is considered to be operating in either success state or failure state. A system is considered operating in success state when it has enough generation to serve the load. When there is not sufficient generation to meet the load demand, and loss of load occurs, the system is in failure state. Loss of Load Expectation (LOLE) and Expected Energy not Served (EENS) are chosen as the reliability indices. In economy evaluation, the annual energy purchasing cost for load aggregator is used as the economy index.

In order to capture the inter-temporal characteristic of energy storage which has a key impact on distribution system reliability and economy, Sequential Monte Carlo Simulation is used for reliability and economy evaluation.

4.4 Problem Formulation

The objective of the energy storage design is to simultaneously optimize multiple objectives including reliability and economy by choosing the optimal energy storage parameters subject to the constraints for a specific distribution system. In this work, the design variables of energy storage include not only the energy storage capacity and power, but also the operation strategy, which is a major contribution of this research work. Other design variables such as charging/discharging efficiency could also be included.

4.4.1 Energy Storage Design Objectives

Objective 1: Reliability

One of the purposes of utilizing energy storage is to improve distribution system reliability. Reliability indices such as LOLE and EENS could be used to measure the reliability performance. These reliability indices are provided through the previously discussed reliability and economy evaluation using Sequential Monte Carlo Simulation.

Objective 2: Cost

The improvement of reliability normally comes with higher economic cost. Here, two sources of cost are considered. One is the annual energy purchasing cost, and the other is the annual energy storage cost. Annual energy purchasing cost is obtained through the reliability and economy evaluation. Annual energy storage cost is computed as the sum of the annual operation and maintenance cost, annualized total capital cost, and annualized replacement cost[30].

The annual operation and maintenance cost, OMC, is

$$OMC = OM_f \cdot C_{Max} \tag{4.11}$$

where OM_f is the annual operation and maintenance cost per kW.
The total capital cost for energy storage, TCC, consists of three components: the total (power) cost of power electronic rectifiers/inverters, the total (energy) cost for storage units, and the cost for the balance of plant.

The total cost for the power electronics, PCS, is

$$PCS = PCSU \cdot C_{Max} \tag{4.12}$$

where PCSU is the cost for power electronics per kW.

The total cost of storage units, SUC, is

$$SUC = SUCU \cdot SOC_{max} \tag{4.13}$$

where SUCU is the storage unit cost per kWh.

The total cost for the balance of plant, BOP, is

$$BOP = BOPU \cdot SOC_{max} \tag{4.14}$$

where BOPU is the cost for the balance of plant per kWh.

The TCC is calculated as

4.15 $$TCC = PCS + SUC + BOP$$

The annualized capital cost, AC, is

4.16 $$AC = TCC \cdot CRF$$

where CRF is capital recovery factor, expressed as

4.17 $$CRF = \frac{i_r(1+i_r)^y}{(1+i_r)^y - 1}$$

where i_r is the annual interest, y is the lifetime of energy storage (year).

The annualized energy storage replacement cost, ARC, is

4.18 $$AEC = OMC + AC + ARC$$

4.4.2 Energy Storage Design Constraints

A set of technical and operational constraints need to be satisfied when considering energy storage design.

Energy storage technology constraints: Due the current energy storage technologies development, the choices of available energy storage are limited. Normally, for a specific energy storage technology, such as Sodium Sulfur battery, there are limits on how large the capacity and power rate can be built. The design choices of energy capacity and power rate should be within the feasible range.

Power flow and other operational constraints: During operation, power flow should be balanced. Energy storage operations should be within the operational limits. These constraints are implemented in the reliability and economy evaluation process. Energy storage operation strategy, which is represented by the operation strategy parameter, *B%*, is within the range from 0% to 100%.

4.5 Solution Approach: Modified Particle Swarm Optimization Approach

Particle Swarm Optimization (PSO) is a population-based stochastic optimization procedure originated from the ideas of swarm intelligence and field of evolutionary computation. It is being used in diverse optimization problems including power systems optimization, such as economic dispatch [31].

In this work, a constrained multi-objective particle swarm optimization approach is proposed to solve the energy storage design problem. Unlike single objective optimization, the optimal solutions of the multi-objective optimization are a set of non-denominated solutions. These solutions form a Pareto front which provides flexible choice of tradeoff among multiple objectives for decision maker.

The decision variables include energy storage capacity, power rate, and operation strategy. The solution candidate can be represented as

$$x_i = [x_{i_1}, x_{i_2}, x_{i_3}] \tag{4.19}$$

where $x_{i_1}, x_{i_2}, x_{i_3}$ represents energy storage capacity, power rate, and operation strategy parameter respectively. i is the number of the particle. i_1, i_2, i_3 represents the 1st, 2nd, and 3rd design variables of the *ith* particle. Each design variable is constrained within its design limit.

4.5.1 Optimization Procedure

The modified multi-objective particle swarm optimization procedure is implemented as follows:

1) Determine the design variables constraints, which include the upper and lower bound of energy storage capacity, power rate, and operation strategy parameter.
2) Initialize the first population of particles and their velocity by random generation within design variables constraints.
3) Evaluation the predetermined objective values (i.e. reliability and economy) for each particle in the population.
4) Select the personal best, *pbest*, through the personal best selection procedure described later.
5) Select the global best, *gbest*, through the global best selection procedure described later.
6) Update the member velocity *v* of each individual particle

$$\begin{aligned} v_{i_d}(t+1) = {} & w v_{i_d}(t) + c_1 r_1 [pbest_{i_d} - x_{i_d}(t)] \\ & + c_2 r_2 [gbest_d - x_{i_d}(t)], \\ & i = 1, \cdots, N;\ d = 1,2,3 \end{aligned} \tag{4.20}$$

The parameters ω, c_1, and c_2 ($0 < \omega < 1.2$, $0 < c_1 < 2$, $0 < c_2 < 2$) are user-supplied coefficients. r_1 and r_2 ($0 < r_1 < 1$, $0 < r_2 < 1$) are random values regenerated for each velocity update. $v_{id}(t)$ is the velocity of the *dth* design variable of the *ith* particle at time *t*. $pbest_{id}$ is the *dth* design variable of the *ith* particle's personal best solution. $gbest_d$ is the *dth* design variable of the global best solution. N is the total number of particles. d is the number of design variables.

7) Update the member position (design variable) of each particle

$$\begin{aligned} x_{i_d}(t+1) = {} & x_{i_d}(t) + v_{i_d}(t+1), \\ & i = 1, \cdots, N;\ d = 1,2,3 \end{aligned} \tag{4.21}$$

8) Add turbulence factor into the current position.

$$x_{i_d}(t+1) = x_{i_d}(t+1) + R_T \cdot x_{i_d}(t+1), \quad i = 1,\cdots,N;\ d = 1,2,3 \tag{4.22}$$

where R_T is a random value as the turbulence factor used to enhance the solution diversity.

9) Check the feasibility of the design variables for each particle. If the design variables are out of the boundaries, the design variables are corrected to the nearest boundary values.

10) Increase the iteration by one. Stop the optimization and output Pareto front if the stopping criterion is reached (e.g. maximum number of iterations). Or go to step 3) to start another round of iteration.

4.5.2 Personal Best and Global Best

In step 4, personal best solution of a particle needs to be selected. This personal best selection procedure is implemented as follows. For each particle, there is a memory space for storing only one personal best solution. Thus N particles correspond to N personal best solutions. In the first iteration, each personal best memory is empty and then is filled in with the corresponding particle from the first population. After the first iteration, the personal best memory is not empty. Each personal best is then compared with the newly updated particle. If the newly updated particle is not dominated by the personal best in the memory, the newly updated particle replaces the personal best in the memory. And then used as the *pbest* for updating velocity.

In step 5, global best solution of the population needs to be selected. The procedure is as follows. First, an initial size of the global best solutions archive is determined. This global best archive is used to store all the non-dominated solutions from the population. For each iteration, the personal best solution for each particle is added to the global best archive if any of the following criterions is met: 1) The archive is empty; 2) The personal best is not dominated by any solution in the archive. After adding all the personal best solutions meeting the previous criterions, the solutions in the global best archive is checked to eliminate any solution which is dominated by any other solution. This process is to maintain that all the solutions in the global best archive are non-dominated. The initial size of the global best archive is increased if more qualified solutions are to be added. After updating the global best archive, a solution in the archive is randomly selected as the *gbest* for updating velocity. When the iteration process is stopped, the solutions in the global best archive are outputted to provide the Pareto front for decision makers.

4.6 Case Studies

The proposed methodology is applied to the energy storage design problem in a modified practical distribution system, shown in Figure 34, where energy storage is integrated in segment 2. The objectives considered in this case study are ENNS as the reliability index, and the total annual cost as the economy index, which is the sum of the annual energy purchasing cost and energy storage cost. IEEE-RTS load profile is applied. Electric energy price profile is shown in Table 3.2. The price and load forecasts are assumed to be perfect. The impact of the imperfect forecasts is studied in [27]. The energy storage design constraints and parameters, distribution system parameters, and particle swarm optimization parameters are listed in

Table 4.1.

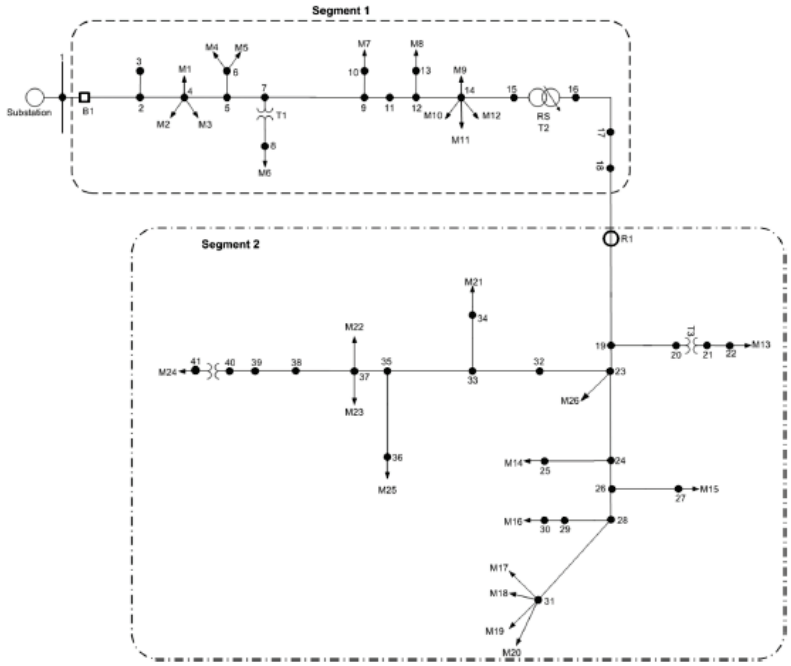

Figure 4.2: Modified practical radial distribution system with energy storage integrated in segment 2

Table 4.1: Case Study Parameters[32] [33]

Energy storage capacity	0 to 30MWh
Energy storage power rate	0 to 4MW
Energy storage operation parameter	0% to 100%
Energy storage efficiency	90%
Energy storage technology	Sodium Sulfur
Energy storage unit cost for power electronics ($/kW)	1000
Energy storage unit cost for storage units ($/kWh)	500
Energy storage fixed O&M cost ($/kW)	20
Energy storage unit cost for balance of plant ($/kWh)	0
Energy storage financing interest rate	5%
Energy storage Lifetime (year)	5
Energy storage replacement times of lifetime	0
Distribution system peak load (MW)	8
External supply: Mean Time To Failure (MTTF) (hours):	1440
External supply: Mean Time To Repair (MTTR) (hours):	8
Segment 1: Mean Time To Failure (MTTF) (hours):	720
Segment 1: Mean Time To Repair (MTTR) (hours):	4
Segment 1: Shared load percentage	50%
Segment 2: Mean Time To Failure (MTTF) (hours):	720
Segment 2: Mean Time To Repair (MTTR) (hours):	4
Segment 2: Shared load percentage	50%
PSO: ω	1
PSO: c_1, c_2	1,1
PSO: R_t	[-0.02,0.02]
PSO: Number of Particles	25
PSO: Maximum number of iterations	100

After implementing the proposed approach on the studied system, the Pareto front is generated and displayed in Figure 4.3.

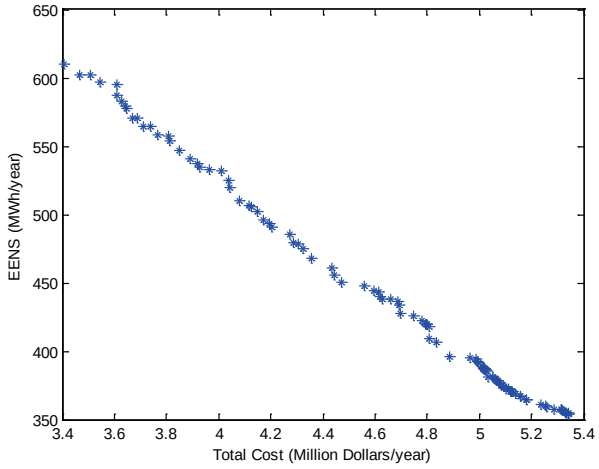

Figure 4.3: Pareto front with the tradeoff between EENS and total annual cost.

With the Pareto front, the decision makers could have the knowledge of what level of reliability improvement and economic benefits can be achieved through energy storage optimal design. After the desired level of reliability and cost are determined, corresponding energy storage

capacity and power sizing, and operation strategy can be determined. Depending on the specific energy storage technology considered, if the energy storage capacities and power rates are only available at discrete level, the nearest discrete level of capacity and power could be chosen as the feasible design. A list of design examples is presented in Table 4.2. Design #1 to #10 are Pareto optimal designs selected from solutions shown in Figure 4.3. Design #11 is a dominated design for comparison.

Table 4.2: Energy Storage Design Solution Examples

	Objectives		Energy Storage Design		
#	EENS (MWh/yr)	Cost (M$/yr)	Capacity (MWh)	Power (MW)	Operation Parameter
1	610	3.41	0.00	0.00	-
2	547	3.85	5.71	1.92	73%
3	541	3.89	7.99	1.85	45%
4	394	4.99	30.00	4.00	48%
5	377	5.08	30.00	4.00	69%
6	365	5.18	30.00	4.00	86%
7	354	5.34	30.00	4.00	100%
8	570	3.69	4.64	1.06	43%
9	565	3.71	4.52	0.89	87%
10	434	4.69	20.21	2.54	100%
11	437	4.89	30	4.00	10%

As shown in Table 4.2, one possible design (#1) is simply not having energy storage. In this way, cost is low due to no investment in energy storage, but the reliability is suffering. Design #2 and #3 give similar reliability and cost tradeoff, however the designs are quite different. Design #3 has a much higher energy storage capacity. While design #2 has a much higher operation parameter, which means a larger portion of energy storage is operated with standby backup strategy. This result illustrates the importance of the matching of the energy storage design variables. Design #4, #5, #6, and #7 all choose the same highest energy storage capacity (30MWh) and power (4MW). However, the operation strategies are very different. The same energy storage operated with different strategies leads to very different reliability level and economic benefits. The energy storage capacity and power of Design #8 are higher than those of Design #9. Accordingly, the annual energy storage cost of Design #8 is higher than that of #9, which is part of the total cost. However, this does not necessarily mean the total cost of Design #8 is higher than Design #9. Design #8 utilizes a lower portion with standby backup operation strategy and a higher portion with MPC-based operation strategy, which reduces the energy purchasing cost. Because of the different operation strategies implemented, the total cost of Design #8 with more expensive energy storage is actually less than the total cost of Design #9. Design #11 is not a Pareto optimal design. Compared to Design #10, which is a Pareto optimal design, design #11 has a better energy storage capacity and power. But because #10 has a better matching of energy storage and operation strategy, both EENS and cost are less than those with design #11. These observations demonstrate the importance of operation strategy consideration when designing energy storage.

4.7 Summary

The objectives of the movement toward the smart grid include making the power systems more reliable and economically efficient. The rapid development of the large scale energy storage technology, such as sodium sulfur batteries, makes it an excellent candidate in achieving the goals of the smart grid. This chapter presented a modified multi-objective particle swarm optimization approach to solve the energy storage design problem in distribution systems. A Pareto front is provided by the proposed approach for decision makers to determine the desired tradeoff between multiple objectives. Within the energy storage design variables, not only the conventionally considered energy storage capacity and power rate are included, but also the energy storage operation strategy. Three energy storage operation strategies are presented and their impacts on reliability and economy are illustrated. A case study is performed to demonstrate the effectiveness of the proposed approach. Insights based on the case study results are discussed.

In this chapter, three energy storage operation strategies, which are standby backup strategy, MPC-based strategy and hybrid strategy, are presented. A parameter is proposed to represent the energy storage operation strategy in energy storage design process. The importance of energy storage operation strategy in reliability improvement and economic benefits is demonstrated. A modified multi-objective particle swarm optimization approach is proposed to solve the energy storage design problem which not only includes energy storage capacity and power rate, but also the operation strategy. The case study results demonstrate the effectiveness of the proposed approach in providing a Pareto front of the multi-objective optimization problem. Insights on the importance of the proper matching of the energy storage design variables and the impact of energy storage operation strategy are illustrated.

5. Conclusions

With the recent rapid development of energy storage technologies, expected large penetration of renewable energy, and the movement toward a more reliable and efficient smart grid, many technical challenges need to be solved. This part of the report focuses on the operation strategies, evaluation methods and optimization framework related to the integration of energy storage and renewable energy which could be utilized to make the electric grid more reliable and efficient. Several important topics in this research arena are investigated.

- In the past, electric power systems have been basically operated on the basis of real-time balancing of supply and demand. With relatively more affordable large scale energy storage devices available, the conventional operation strategies should be revisited. In a market environment, a distribution system load aggregator with energy storage devices needs to understand how to optimally operate them. In Section 2, a method for determining the optimal scheduling and operation of a load aggregator with energy storage in power markets is presented. Load aggregators could use this method to minimize its energy purchasing cost in power markets. This method takes in the price and load forecasts as its input to determine what should be the optimal operation in the current period. With real-time updated forecasts, its operations are also adjusted to be optimal.

- The renewable energy penetration is increasing with the expectation to reach more than 20% of the total generation. Energy storage could be utilized to facilitate the integration of renewable energy. A novel Model Predictive Control (MPC) based operation strategy is proposed to optimally coordinate the power supplies from renewable energy, energy storage and external grid in order to minimize energy purchasing cost. A reliability and economy evaluation framework integrated with the proposed operation strategies is also presented. Case studies demonstrate the relative benefits of the proposed operation strategies and also provide insights on how energy storage capacity, power limit and wind turbine generation capacity impact reliability and economy.
- Utility scale energy storage devices are still a high cost investment. During the planning stage of energy storage installation and expansion, an optimization framework needs to be developed to determine the sizing of energy storage and its value to the power systems. A modified multi-objective particle swarm optimization approach is proposed to solve the energy storage design problem which not only includes energy storage capacity and power rate, but also the operation strategy. The case study results demonstrate the effectiveness of the proposed approach in providing a Pareto front of the multi-objective optimization problem. Insights on the importance of the proper matching of the energy storage design variables and the impact of energy storage operation strategy are illustrated.

The proposed MPC-based operation strategy and hybrid operation strategy utilize renewable energy forecast, electric energy price forecast, and load forecast. The accuracy of these forecasts is important to the effectiveness of these strategies. With the development of the more accurate forecast techniques and algorithms, these operation strategies could be more beneficial to the power systems. Meanwhile, large scale stochastic optimization methods could be utilized to deal with the forecast uncertainties. The proposed energy storage sizing and operation strategy optimization framework needs to perform reliability and economy evaluation based on Monte Carlo Simulation. More efficient and accurate reliability and economy evaluation methods could in turn improve the efficiency of the optimization process. In order to cover the high investment cost, more revenue streams and benefits besides energy purchasing cost savings and reliability improvement needs to be investigated. The possible applications include frequency regulation, spinning reserve and transmission congestion relief, etc. These applications could be included in the proposed multi-objective particle swarm optimization framework to evaluate the investment and determine the energy storage sizing and operation strategy. With the understanding of the reliability impact on the transmission systems brought by the energy storage and renewable energy integrated in the distribution systems, system operators could more efficiently plan for the future demand growth with the utilization of these resources.

References

[1] US DOE Electricity Advisory Committee, "Bottling Electricity: Storage as a Strategic Tool for Managing Variability and Capacity Concerns in the Modern Grid," US DOE Electricity Advisory Committee, Dec. 2008.

[2] US DOE Electricity Advisory Committee, "Smart Grid: Enabler of the New Energy Economy," US DOE Electricity Advisory Committee, Dec. 2008.

[3] J. Eyer and G. Corey, "Energy Storage for the Electricity Grid: Benefits and Market Potential Assessment Guide", Sandia National Laboratories, Albuquerque, NM and Livermore, CA, Feb. 2010.

[4] B. Daryanian, R. E. Bohn, and R. D. Tabors, "Optimal Demand-Side Response to Electricity Spot Prices for Storage-Type Customers", Power Engineering Review, IEEE, vol. 9, no. 8, pp. 36-36, 1989.

[5] B. Daryanian, R. E. Bohn, and R. D. Tabors, "An experiment in real time pricing for control of electric thermal storage systems", IEEE Trans. Power Syst., vol. 6, no. 4, pp. 1356-1365, Nov. 1991.

[6] R. Walawalkar, J. Apt, and R. Mancini, "Economics of electric energy storage for energy arbitrage and regulation in New York", Energy Policy, vol. 35, no. 4, pp. 2558-2568, Apr. 2007.

[7] M. Korpas and A. T. Holen, "Operation planning of hydrogen storage connected to wind power operating in a power market", IEEE Trans. Energy Conversion, vol. 21, no. 3, pp. 742-749, Sept. 2006.

[8] L. Xie and M. D. Ilic, "Model predictive economic/environmental dispatch of power systems with intermittent resources", Proc. IEEE PES General Meeting, pp.1-6, Jul. 2009.

[9] J. Zhang and C. Cheng, "Day-ahead electricity price forecasting using artificial intelligence", Proc. Electric Power Conference, Oct. 2008.

[10] N. Amjady and F. Keynia, "Day-Ahead Price Forecasting of Electricity Markets by Mutual Information Technique and Cascaded Neuro-Evolutionary Algorithm", IEEE Trans. Power Syst., vol. 24, no. 1, pp. 306-318, 2009.

[11] A. M. Gonzalez, A. M. S. Roque, and J. Garcia-Gonzalez, "Modeling and forecasting electricity prices with input/output hidden Markov models", IEEE Trans. Power Syst., vol. 20, no. 1, pp. 13-24, 2005.

[12] T. Niimura, "Forecasting techniques for deregulated electricity market prices", Proc. PES General Meeting, 2006.

[13] F. J. Nogales, J. Contreras, A. J. Conejo, and R. Espinola, "Forecasting Next-Day Electricity Prices by Time Series Models", IEEE Power Engineering Review, vol. 22, no. 3, pp. 58-58, 2002.

[14] Z. H. Osman, M. L. Awad, and T. K. Mahmoud, "Neural network based approach for short-term load forecasting", Proc. Power Systems Conference and Exposition, 2009.

[15] K. Y. Lee, Y. T. Cha, and J. H. Park, "Short-term load forecasting using an artificial neural network", IEEE Trans. Power Syst., vol. 7, no. 1, pp. 124-132, 1992.

[16] J. W. Taylor and R. Buizza, "Neural network load forecasting with weather ensemble predictions", IEEE Trans. Power Syst., vol. 17, no. 3, pp. 626-632, 2002.

[17] J. Mitra, "Reliability-Based Sizing of Backup Storage", IEEE Trans. Power Syst., vol. 25, no. 2, pp. 1198-1199, 2010.

[18] B. Bagen and R. Billinton, "Reliability Cost/Worth Associated With Wind Energy and Energy Storage Utilization in Electric Power Systems", Proc. Probabilistic Methods Applied to Power Systems, 2008.

[19] Y. M. Atwa, E. F. El-Saadany, and A. C. Guise, "Supply Adequacy Assessment of Distribution System Including Wind-Based DG During Different Modes of

[20] C. Singh and Y. Kim, "An efficient technique for reliability analysis of power systems including time dependent sources", IEEE Trans. Power Syst., vol. 3, no. 3, pp. 1090-1096, 1988

[21] R. Billinton, G. Yi, and R. Karki, "Composite System Adequacy Assessment Incorporating Large-Scale Wind Energy Conversion Systems Considering Wind Speed Correlation", IEEE Trans. Power Syst., vol. 24, no. 3, pp. 1375-1382, 2009.

[22] F. Vallee, J. Lobry, and O. Deblecker, "System Reliability Assessment Method for Wind Power Integration", IEEE Trans. Power Syst., vol. 23, no. 3, pp. 1288-1297, 2008.

[23] P. Wang and R. Billinton, "Reliability Benefit Analysis of Adding WTG in a Distribution System", IEEE Power Engineering Review, vol. 21, no. 5, pp. 62-62, 2001.

[24] R. Karki, H. Po, and R. Billinton, "Reliability Evaluation Considering Wind and Hydro Power Coordination", IEEE Trans. Power Syst., vol. 25, no. 2, pp. 685-693, 2010.

[25] R. Billinton and R. N. Allan, “Reliability evaluation of power systems”, 2nd ed. New York: Plenum Press, 1996.

[26] North American Electric Reliability Corporation. (2009, Apr.). Accommodating High Levels of Variable Generation. [Online]. Available: http://www.nerc.com/files/IVGTF_Report_041609.pdf

[27] Y. Xu, L. Xie, and C. Singh, "Optimal scheduling and operation of load aggregators with electric energy storage facing price and demand uncertainties," Proc. North American Power Symposium, Boston, 2011.

[28] W. R. Lachs and D. Sutanto, "Battery storage plant within large load centres", IEEE Trans. Power Syst., vol. 7, no. 2, pp. 762-767, 1992.

[29] Y. Xu; C. Singh, "Distribution systems reliability and economic improvement with different electric energy storage operation strategies," Proc. PES General Meeting, 2011.

[30] P., Poonpun, W. Jewell, "Analysis of the Cost per Kilowatt Hour to Store Electricity," IEEE Trans. Energy Conversion, vol.23, no.2, pp.529-534, Jun. 2008

[31] L. Wang, C. Singh, "Balancing risk and cost in fuzzy economic dispatch including wind power penetration based on particle swarm optimization," Electric Power Systems Research, Volume 78, Issue 8, pp. 1361-1368, Aug. 2008.

[32] S. M. Schoenung and W. V. Hassenzahl, “Long- vs. short-term energy storage technologies analysis: A life-cycle cost study,” Sandia Natl. Lab., Albuquerque, NM, Sandia Rep. SAND2003-2783, 2003.

[33] Energy Information Administration (2006). Annual energy outlook 2006 with projection to 2030. [Online]. Available: http://www.eia.doe.gov/oiaf/aeo/

Part 4

Algorithms for Decentralized Control of Distributed Storage Resources

Alejandro Dominguez-Garcia
Stanton Cady, Masters Student
University of Illinois at Urbana-Champaign

For information about Part 4, contact

Alejandro Dominguez-Garcia
Department of Electrical and Computer Engineering
1406 W. Green Street
Urbana, IL 61801
Phone: 217 333-0394
Email: aledan@illinois.edu

Power Systems Engineering Research Center

The Power Systems Engineering Research Center (PSERC) is a multi-university Center conducting research on challenges facing the electric power industry and educating the next generation of power engineers. More information about PSERC can be found at the Center's website: http://www.pserc.org.

For additional information, contact:

Power Systems Engineering Research Center
Arizona State University
527 Engineering Research Center
Tempe, Arizona 85287-5706
Phone: 480-965-1643
Fax: 480-965-0745

Notice Concerning Copyright Material

Table of Contents

List of Figures

Chapter 1

Introduction

It has been acknowledged that distributed energy resources (DERs) have the potential to provide ancillary services to power systems at the distribution level [1], [2], [3]. One example is using inverter-interfaced DERs, e.g., photovoltaic (PV) systems or motor drives with active rectifier inputs, to provide reactive power support. Although the primary function of these power electronics-based systems is to provide active power, many of them are capable of producing reactive power if appropriately controlled [4]. Another example is utilizing distributed storage resources (DSRs) such as plug-in hybrid electric vehicles (PHEV) or uninterruptible power supplies (UPS) to control active power for up and down regulation. Such resources could provide energy peak-shaving during hours of high demand and load leveling when demand is low [5], or could be utilized to provide frequency regulation.

Generally speaking, in order for DERs to provide these ancillary services to electric grids, however, appropriate control and coordination mechanisms need to be developed. One potential control architecture relies on a centralized strategy in which each DER is coordinated through direct communication with a central decision maker. An alternative approach is to remove the central decision maker and coordinate the DERs in a distributed fashion. Using the latter control architecture to solve the *resource coordination* problem as it applies to the control of distributed storage resources will be the primary focus of this report. Specifically, we develop and implement several algorithms that solve the problem.

Specifically, given a set of DSRs that are each capable of providing energy over a given period of time, the objective of the resource coordination problem is to utilize a communication network to allow these components to exchange information with neighboring DSRs in order to collectively provide a certain amount of energy that is known by a leader. It is assumed that the leading DSR can only communicate with a limited number of other devices in the system and may not necessarily be aware of the total number of DSRs available. Furthermore, the leader does not provide any energy, but rather initiates a request for energy by dividing the total energy demand equally among all neighboring components; however, a leading component is not required, as a variation of the initialization procedure could be used in which any DSR could initiate the request for energy. To address component limitations, upper and lower bounds on the amount of energy each component can provide over some period of time are considered when solving the resource coordination problem in order to find a feasible solution.

In the experimental setup described in this report, each DSR is outfitted with a wireless

transceiver to create a communication network that can be thought of as a stationary, yet unplanned, ad-hoc network. An iterative process is used to exchange information among DSRs such that they collectively meet the demand for energy. At the end of the iterative process, the power output of each DSR is computed based upon the result of the algorithm and the capacity constraints of the respective DSR.

The intention of this report is to develop and demonstrate distributed algorithms that are suitable for coordinating DSRs without the need for a centralized controller. Specifically, the purpose of this work is to document the development and application of a hardware testbed that implements the algorithms proposed in [6], [7], [8]. The remainder of this report is organized as follows.

Chapter 2 begins by providing a model to describe the communication between DSRs and provides a precise problem definition. Next, a distributed algorithm is formulated that serves to iteratively disperse energy demand among a set of DSRs with no limits on the amount of energy they can provide. The *unconstrained algorithm* is extended to account for upper and lower capacity constraints, and it is shown how the result of this algorithm can be used by each DSR to independently determine when the collective capacity of the system has been reached. The *constrained algorithm* is then adapted to create the *robust algorithm* which converges despite imperfect communication links.

Chapter 3 discusses the development of a hardware testbed created to implement the algorithms presented in Chapter 2. The testbed is based upon Arduino Mega microcontroller boards equipped with XBee modules executing software that realizes each of the proposed distributed algorithms.

Chapter 4 presents results which demonstrate the convergence of each algorithm running on the hardware testbed. To conclude, we illustrate a case in which the constrained algorithm is adapted to evenly split demand among all DSRs and demonstrate the ability for each node to independently determine feasibility.

Chapter 5 provides some concluding remarks and discusses future work.

Chapter 2

Algorithm Formulation

In this chapter we formulate three algorithms that are suitable for controlling a set of distributed storage resources (DSRs) without relying on a centralized controller. We begin by developing a model to represent the communication network linking resources that will be used to facilitate analysis and development of the algorithms. Next, we formulate and analyze the convergence of an unconstrained algorithm. We then extend the unconstrained algorithm to account for individual capacity constraints. Finally, the constrained algorithm is adapted to be more resilient to imperfect communication links.

2.1 Communication Model

Let $\mathcal{G}$ be a directed graph describing the communication network in system of DSRs capable of exchanging packetized information via wireless links. Define $\mathcal{V} := V(\mathcal{G})$ to be the set of vertices with each vertex corresponding to a DSR and $\mathcal{E} := E(\mathcal{G})$ to be the set of directed edges with each edge corresponding to a communication link between a pair of DSRs. The exchange of information between two DSRs i and j need not be bidirectional; thus, the ordered pair $(i, j) \in \mathcal{E}$ if and only if DSR i can receive information from DSR j. For each DSR $i \in \mathcal{V}$, we define the set of DSRs from which i can receive information to be the in-neighborhood of i, i.e., $\mathcal{N}_i^- := \{j \in \mathcal{V} : (i, j) \in \mathcal{E}\}$. Similarly, we define the out-neighborhood of i to be the set of DSRs that can receive information from i, i.e., $\mathcal{N}_i^+ := \{j \in \mathcal{V} : (j, i) \in \mathcal{E}\}$, and we denote the cardinality of the out-neighborhood by $\mathcal{D}_i^+ := |\mathcal{N}_i^+|$. We allow all vertices to have self loops, i.e., $(i, i) \in \mathcal{E},\ \forall i \in \mathcal{V}$; thus, each DSR is included in both its own in- and out-neighborhood. For the algorithms formulated in the following sections, it is assumed that the graph $\mathcal{G}$ is strongly connected; that is, for each ordered pair of vertices i, j there is a path from i to j [9].

2.2 Problem Definition

Consider a set of $n+1$ DSRs as described by the aforementioned communication model, i.e., $|\mathcal{V}| = n + 1$, and assume that there exists one leader that knows the total system energy demand, ρ_d^r, over a given period of time Δ, where $r = 1, 2, \ldots$ indexes the interval over which the energy demand is specified. Let x_i^r be the energy provided by DSR i over period

Δ at interval r, where the leader node is indexed by 0 and provides no energy, i.e., $x_0^r = 0$, and define $\rho^r := \sum_{i=1}^n x_i^r$ to be the total energy output of the set of DSRs during the same period and interval. Furthermore, define $l := \mathcal{D}_0^+$ to be the out-degree of the leading DSR, with $l \geq 2$ since $\mathcal{G}$ is strongly connected. Given a demand for energy ρ_d^r during interval r, the objective of this work is to design and implement a set of algorithms which serve to coordinate a set of DSRs such that they collectively meet the demand for energy without a centralized controller. In particular, the algorithms should serve to drive the collective energy output of the DSRs to meet the energy demand, i.e., $\rho^r \to \rho_d^r$. Throughout the remainder of this chapter, we develop three algorithms that can used to implement the above-described objective.

2.3 Unconstrained Algorithm

The case when each DSR has an unlimited amount of energy available is considered first. Despite being unrealistic, the formulation of an unconstrained algorithm will provide the basis for developing an algorithm that can account for individual DSR limitations.

Without constraints, a trivial method for meeting the demand for energy is to have each DSR in the out-neighborhood of the leader adjust its energy output during interval r to be $\frac{\rho_d^r}{l}$ while the remaining $n - l$ DSRs provide no energy. For the case when the capacity of each DSR is limited, however, this method would be infeasible if the energy demand lies outside the collective bounds of the l DSRs in the out-neighborhood of the leader. In order to provide a more adaptable solution, a distributed iterative algorithm is formulated which, after m iterations, divides the total demand among all n DSRs.

2.3.1 Algorithm Description

Each DSR participating in the distributed algorithm maintains an internal state variable that is updated at each iteration. Let $k = 0, 1, \ldots$, index the iterations, and let $\pi_i[k]$ be the value of the internal state variable of DSR i at round k, where $\pi_i[0] = \rho_d^r/l$ if i is in the out-neighborhood of the leader, and $\pi_i[0] = 0$ otherwise. For convenience, we define $\theta[k] := \sum_{i=1}^n \pi_i[k],\ \forall k$.

One method that can be used to distribute the energy demand throughout the system is to have each DSR update its state at each iteration to be a linear combination of its current state and the states of the DSRs in its in-neighborhood. That is, DSR i updates the value of its state variable to be

$$\pi_i[k+1] = p_{ii}\pi_i[k] + \sum_{\substack{j \in \mathcal{N}_i^- \\ i \neq j}} p_{ij}\pi_j[k], \tag{2.1}$$

where p_{ii} is the *self-weight* of DSR i and p_{ij} is *outgoing-weight* of DSR j, $\forall i \in \mathcal{V}$, and $\forall j \in \mathcal{N}_i^-, j \neq i$. After performing m iterations DSR i adjusts its output to be $x_i^r = \pi_i[m]$ and, for the algorithm to be effective, the energy provided during interval r should meet the demand, that is, $\rho^r = \rho_d^r$.

After some analysis, we will see that a carefully chosen set of weights will take advantage of the distributed nature of the system while ensuring that the algorithm meets the aforementioned objective. To find appropriate weights, we first write (2.1) in matrix form as

$$\begin{aligned} \pi[k+1] &= P\pi[k], \\ \pi[0] &= \pi_0, \end{aligned} \tag{2.2}$$

where $\pi_0 = \left[\pi_1[0], \pi_2[0], \ldots, \pi_i[0], \ldots, \pi_n[0]\right]^{\mathrm{T}}$, with $\pi_i[0] = \rho_d^r/l$ if the leader is an in-neighbor of i and $\pi_i[0] = 0$ otherwise, and the matrix P is of the form

$$P = \begin{bmatrix} p_{11} & p_{12} & \cdots & p_{1i} & \cdots & p_{1n} \\ p_{21} & p_{22} & \cdots & p_{2i} & \cdots & p_{2n} \\ \vdots & \vdots & \ddots & \vdots & & \vdots \\ p_{i1} & p_{i2} & \cdots & p_{ii} & \cdots & p_{in} \\ \vdots & \vdots & & \vdots & \ddots & \vdots \\ p_{n1} & p_{n2} & \cdots & p_{ni} & \cdots & p_{nn} \end{bmatrix}, \tag{2.3}$$

where $p_{ij} = 0$ if and only if $(i, j) \notin \mathcal{E}$.

In a distributed system where individual components have only local knowledge of the network, component i is limited to choosing its self-weight, p_{ii}, $\forall i \in \mathcal{V}$, and outgoing-weights, p_{ji}, $\forall j \in \mathcal{N}_i^+, j \neq i$, which correspond to the columns of P. Furthermore, since the initial states of algorithm (2.1) are chosen such that $\theta[0] = \rho_d^r$, and since the objective is for the demand to be distributed among all n DSRs after m iterations, i.e., $\theta[m] = \rho_d^r$, it is sufficient for each DSR to choose weights such that the sum of internal states remains constant throughout the iterative process. If the weights are chosen in such a way that the matrix P is column stochastic, i.e., each entry is nonnegative and the columns sum to one, we will see that the sum of the entries of the vector $\pi[k]$ will remain constant for all k.

A simple choice that maintains column stochasticity of P is for each DSR to set its self- and outgoing-weights to be the reciprocal of its out-degree, i.e., $p_{ii} = p_{ji} = \frac{1}{\mathcal{D}_i^+}$, $\forall i \in \mathcal{V}$ and $\forall j \in \mathcal{N}_i^+, j \neq i$. Thus DSR i will update its state according to

$$\pi_i[k+1] = \sum_{j \in \mathcal{N}_i^-} \frac{1}{\mathcal{D}_j^+} \pi_j[k], \tag{2.4}$$

and adjust its output to be $x_i^r = \pi_i[m]$ after performing m iterations. Given this choice of weights, it should be noted that the algorithm in (2.4) does not necessarily split the total generation energy evenly.

2.3.2 Convergence Analysis

By rewriting the algorithm in (2.4) in matrix form according to (2.2), we use the characteristics of the matrix P to prove that $\theta[k]$ remains constant at every iteration k. Furthermore, we prove that the algorithm ensures the overall energy demand is met, i.e., $\theta[m] = \rho_d^r$, and that the solution obtained is unique.

In addition to being column stochastic by design, P is also primitive since the underlying connectivity graph is assumed to be strongly connected and at least one of its diagonal entries is nonzero [10]. Given a column stochastic primitive matrix, the Perron-Frobenius theorem for nonnegative matrices (see, e.g., [10]) states that the matrix will have a unique eigenvalue with largest modulus at $\lambda_1 = 1$.

Let v and w be the right and left eigenvectors of P associated with λ_1, respectively, normalized such that $v^{\mathrm{T}}w = 1$. Given that P is column stochastic, all the entries of the vector w must be equal. Without loss of generality, let w be the vector of all ones, i.e., $w = \left[1, 1, \ldots, 1\right]^{\mathrm{T}}$, and given that $v^{\mathrm{T}}w = 1$, the entries of v must sum to one. Define $\pi^r = \left[\pi_1^r, \pi_2^r, \ldots, \pi_i^r, \ldots, \pi_n^r\right]^{\mathrm{T}}$, where π_i^r is the steady-state solution of (2.4) for the r^{th} interval. Then by the Perron-Frobenius theorem, we have that $\lim_{k\to\infty} P^k = vw^{\mathrm{T}}$ and the vector of steady-state solutions is given by

$$\pi^r = vw^{\mathrm{T}}\pi_0 = \left(\sum_{i=1}^{n} \pi_i[0]\right) v. \tag{2.5}$$

Since the entries of v are nonnegative and add up to one and $\sum_{i=1}^{n} \pi_i[0] = \rho_d^r$, it follows that the entries of the steady-state solution are nonnegative and sum to ρ_d^r. Although this proof implies that an infinite number of iterations are required to reach the steady-state solution, experimental results have shown that a finite number of iterations are adequate for convergence to a sufficiently accurate solution, thus the proposed algorithm can be used as a practical method for distributively allocating DSRs [6].

2.4 Constrained Algorithm

Any physically realizable network comprised of DSRs will necessarily have limits on energy capacity. Upper bounds on capacity are the most familiar—a battery is only capable of providing power for a finite period of time—but it may also be necessary to enforce lower bounds due to operational or device limitations. Thus, to develop an algorithm that is useful in practical systems, the unconstrained algorithm in (2.4) is extended to account for both constraints.

2.4.1 Algorithm Description

Let $\underline{x}_i^r$ and $\overline{x}_i^r$ for $i = 1, 2, \ldots, n$, be the minimum and maximum energy DSR i can provide during interval r and define the corresponding capacity vectors as

$$\underline{x}^r = \left[\underline{x}_1^r, \underline{x}_2^r, \ldots, \underline{x}_n^r\right]^{\mathrm{T}}, \tag{2.6}$$

$$\overline{x}^r = \left[\overline{x}_1^r, \overline{x}_2^r, \ldots, \overline{x}_n^r\right]^{\mathrm{T}}, \tag{2.7}$$

respectively. Define the collective lower and upper capacity limits of the DSRs during interval r to be $\underline{\chi}^r = \sum_{i=1}^{n} \underline{x}_i^r$, and $\overline{\chi}^r = \sum_{i=1}^{n} \overline{x}_i^r$. As in the unconstrained case, the total amount of energy demand in the system during interval r is ρ_d^r and the total output of the DSRs during the same period is $\rho^r = \sum_{i=1}^{n} x_i^r$. It is assumed that the collective capacity of the

DSRs is sufficient to meet demand, i.e., $\underline{\chi}^r \leq \rho_d^r \leq \overline{\chi}^r$, and that power rating of each DSR is adequate to provide the demanded energy during period Δ, i.e., $\underline{p}_i \leq x_i^r/\Delta \leq \overline{p}_i$, where $\underline{p}_i$ and $\overline{p}_i$ are the minimum and maximum power ratings of DSR i, respectively.

Instead of maintaining a single state variable, DSRs participating in the constrained distributed algorithm maintain two variables, each with different initial conditions that are linear combinations of the capacity constraints. Let $\mu_i[k]$ and $\sigma_i[k]$ be the state variables maintained by DSR i at iteration k, where $\mu_i[0] = \rho_d^r/l - \underline{x}_i^r$ if the leader is an in-neighbor of i and $\mu_i[0] = -\underline{x}_i^r$ otherwise, and $\sigma_i[0] = \overline{x}_i^r - \underline{x}_i^r,\ \forall i \in \mathcal{V}$. The algorithm given in (2.4) is used to update the state variables of DSR i as

$$\mu_i[k+1] = \sum_{j \in \mathcal{N}_i^-} \frac{1}{\mathcal{D}_j^+} \mu_j[k], \tag{2.8}$$

$$\sigma_i[k+1] = \sum_{j \in \mathcal{N}_i^-} \frac{1}{\mathcal{D}_j^+} \sigma_j[k]. \tag{2.9}$$

After m iterations, DSR i computes its output for interval r to be

$$x_i^r = \underline{x}_i^r + \frac{\mu_i[m]}{\sigma_i[m]}(\overline{x}_i^r - \underline{x}_i^r), \tag{2.10}$$

and we have that $\rho^r = \rho_d^r$ and $\underline{x}_i^r \leq x_i^r \leq \overline{x}_i^r,\ \forall i \in \mathcal{V}$.

2.4.2 Convergence Analysis

To prove that the constrained algorithm coordinates the DSRs to meet the overall demand without violating individual constraints, we first rewrite (2.8) and (2.9) in matrix form as

$$\begin{aligned} \mu[k+1] &= P\mu_0, \\ \sigma[k+1] &= P\sigma_0, \end{aligned} \tag{2.11}$$

with P as defined in the formulation of the unconstrained algorithm and where the initial vectors μ_0 and σ_0 are given as

$$\begin{aligned} \mu_0 &= \left[\mu_1[0], \mu_2[0], \ldots, \mu_i[0], \ldots, \mu_n[0]\right]^{\mathrm{T}}, \\ \sigma_0 &= \left[\sigma_1[0], \sigma_2[0], \ldots, \sigma_i[0], \ldots, \sigma_n[0]\right]^{\mathrm{T}}, \end{aligned} \tag{2.12}$$

with $\mu_i[0]$ and $\sigma_i[0]$ as defined above.

From the proof of the unconstrained algorithm, it follows that the steady-state solutions of the iterations in (2.11) are given by

$$\begin{aligned} \mu^{ss} = vw^{\mathrm{T}}\mu_0 &= \left(\sum_{i=1}^{n} (\pi_i[0] - \underline{x}_i^r)\right) v \\ &= \left(\rho_d^r - \sum_{i=1}^{n} \underline{x}_i^r\right) v, \\ \sigma^{ss} = vw^{\mathrm{T}}\sigma_0 &= \left(\sum_{i=1}^{n} (\overline{x}_i^r - \underline{x}_i^r)\right) v, \end{aligned} \tag{2.13}$$

where $\pi_i[0] = \rho_d^r/l$ if the leader is an in-neighbor of i and $\pi_i[0] = 0$ otherwise. Combining (2.10) and (2.13), the output of DSR i is given as

$$\begin{aligned} x_i^r &= \lim_{k\to\infty}\left(\underline{x}_i^r + \frac{\mu_i[k]}{\sigma_i[k]}(\overline{x}_i^r - \underline{x}_i^r)\right) \\ &= \underline{x}_i^r + \frac{\mu_i^r}{\sigma_i^r}(\overline{x}_i^r - \underline{x}_i^r), \end{aligned} \tag{2.14}$$

where the ratio of the steady-state solutions for interval r is defined to be

$$\alpha_i^r := \frac{\mu_i^r}{\sigma_i^r} = \frac{\rho_d^r - \sum_{i=1}^n \underline{x}_i^r}{\sum_{i=1}^n (\overline{x}_i^r - \underline{x}_i^r)}. \tag{2.15}$$

After the algorithm has converged, $\alpha_i^r \in [0,1],\ \forall i \in \mathcal{V}$, if the overall energy demand can be met by the system, i.e., $\underline{\chi}^r \leq \rho_d^r \leq \overline{\chi}^r$. Thus, if the value of $\alpha_i^r \notin [0,1]$, DSR i can determine that the collective capacity of the system is insufficient to meet demand during interval r.

Similar to the proof of the unconstrained algorithm, this proof implies that an infinite number of iterations are required to converge to the steady-state solution. The results presented in the next section, however, illustrate that convergence to a sufficiently accurate solution can be reached for a small network of DSRs in as few as 10 iterations.

2.5 Robust Algorithm with Constraints

Throughout the derivation of the previous two algorithms, it was implicitly assumed that the communication links used to exchange information between DSRs were completely reliable. In an uncontrolled environment, however, conditions such as temperature and humidity as well as obstructions between DSRs can negatively affect link availability. To provide an algorithm that can be useful in systems subject to such non-idealities, the constrained algorithm is extended to be resilient to packet loss.

2.5.1 Communication Model Modifications

Before the algorithm described by (2.8) and (2.9) can be made more robust, the graph modeling the exchange of information between DSRs needs to be modified to account for the possibility that communication links may not be available at every iteration. In this case, the graph is a function of the iteration index k, and is denoted $\mathcal{G}[k]$, where $\mathcal{V} = V(\mathcal{G}[k])$ is independent of k, and $\mathcal{E}[k] = E(\mathcal{G}[k])$ is the set of edges where $(i,j) \in \mathcal{E}[k]$ if DSR i can receive information from DSR j at iteration k. It is assumed that $\mathcal{E}[k] \subseteq \mathcal{E}$, $\forall k \geq 0$, where $\mathcal{E}$ is the set of available edges given completely reliable communication links. Furthermore, it is assumed that each DSR determines the size of its out-neighborhood during an initialization procedure that is perfectly reliable.

If the packets used to exchange information for the distributed algorithm are broadcasted and no acknowledgments are sent, each DSR assumes that all transmitted information is successfully delivered to the intended receiving DSR(s). However, if DSR i attempts to send its weighted values to DSR j at iteration k and $(j,i) \notin \mathcal{E}[k]$, this assumption is invalid

and the information intended for DSR j is lost. In order to mitigate the effects of packet loss without increasing the number of packets exchanged at each iteration, we modify the distributed algorithm with constraints to allow the DSRs to collectively meet the overall demand regardless of communication link availability.

2.5.2 Algorithm Description

One method that can be used to recover information lost due to dropped packets is for each DSR to broadcast the sum of its weighted values up to and including the current iteration k as proposed in [8]. In the case where no packets are lost, the weighted values received from the in-neighbors of a DSR can be inferred at each iteration k, and the proposed method is effectively the same as the constrained algorithm presented above. If packets are lost, however, the algorithm seamlessly recovers any lost information.

At each iteration k, DSR i broadcasts two values that are linear combinations of its internal state maintained throughout the iterative process. Let $y_i[k]$ and $z_i[k]$ be the values of the internal states maintained by DSR i at iteration k and let $\mu_i[k]$ and $\sigma_i[k]$ be the values broadcasted to all out-neighbors of DSR i at iteration k. The value of $\mu_i[k]$ is simply the sum of $y_i[k]/\mathcal{D}_i^+$ since the iterative process began and is given as

$$\mu_i[k] = \mu_i[k-1] + \frac{1}{\mathcal{D}_i^+} y_i[k] = \sum_{s=0}^{k} \frac{1}{\mathcal{D}_i^+} y_i[s]. \tag{2.16}$$

Similarly, the value of $\sigma_i[k]$ is the sum of $z_i[k]/\mathcal{D}_i^+$ up to and including the current iteration k and is given as

$$\sigma_i[k] = \sigma_i[k-1] + \frac{1}{\mathcal{D}_i^+} z_i[k] = \sum_{s=0}^{k} \frac{1}{\mathcal{D}_i^+} z_i[s]. \tag{2.17}$$

At each iteration, DSR i will update the value of its state variables as

$$\begin{aligned} y_i[k+1] &= \frac{1}{\mathcal{D}_i^+} y_i[k] + \sum_{\substack{j \in \mathcal{N}_i^- \\ i \neq j}} (\nu_{ij}[k] - \nu_{ij}[k-1]), \\ z_i[k+1] &= \frac{1}{\mathcal{D}_i^+} z_i[k] + \sum_{\substack{j \in \mathcal{N}_i^- \\ i \neq j}} (\tau_{ij}[k] - \tau_{ij}[k-1]), \end{aligned} \tag{2.18}$$

where the values of $\nu_{ij}[k]$ and $\tau_{ij}[k]$ depend on the successful receipt of a packet from DSR j during iteration k and are given as

$$\begin{aligned} \nu_{ij}[k] &= \begin{cases} \mu_j[k], & \text{if } (i,j) \in \mathcal{E}[k], \\ \nu_{ij}[k-1], & \text{if } (i,j) \notin \mathcal{E}[k], \end{cases} \\ \tau_{ij}[k] &= \begin{cases} \sigma_j[k], & \text{if } (i,j) \in \mathcal{E}[k], \\ \tau_{ij}[k-1], & \text{if } (i,j) \notin \mathcal{E}[k]. \end{cases} \end{aligned} \tag{2.19}$$

The initial values of the state variables are $y_i[0] = \rho_d^r - \underline{x}_i^r$ if i is an out-neighbor of the leader and $y_i[0] = -\underline{x}_i^r$ otherwise, and $z_i[0] = \overline{x}_i^r - \underline{x}_i^r > 0$, $\forall i \in \mathcal{V}$; whereas the initial conditions for the broadcasted values are set to $\mu_i[0] = y_i[0]/\mathcal{D}_i^+$ and $\sigma_i[0] = z_i[0]/\mathcal{D}_i^+$. After m iterations, for large m, DSR i computes its output as

$$x_i^r = \underline{x}_i^r + \frac{y_i[m]}{z_i[m]}(\overline{x}_i^r - \underline{x}_i^r), \tag{2.20}$$

and we have that $\rho^r = \rho_d^r$ and $\underline{x}_i^r \leq x_i^r \leq \overline{x}_i^r$, $\forall i \in \mathcal{V}$ (for a proof see [8]). Similar to the basic algorithm with constraints, we define the ratio of the values of the internal states after m iterations as found by DSR i to be

$$\alpha_i^r := \frac{y_i[m]}{z_i[m]}. \tag{2.21}$$

Thus, DSRs participating in the robust algorithm with constraints can independently determine if the collective capacity of the system is sufficient to meet the overall energy demand if $\alpha_i^r \geq 0$ and $\alpha_i^r \leq 1$

In order to compute the values in (2.19), each DSR needs to keep the most recent set of values received from the DSRs in its in-neighborhood and thus needs to know the source of all packets received. To accommodate this, each DSR creates a list of addresses corresponding to the DSRs in its in-neighborhood during initialization that will remain unchanged throughout the iterative process. Furthermore, when DSR i broadcasts its values $\mu_i[k]$ and $\sigma_i[k]$, it also includes its address in the packet.

Chapter 3

Hardware Implementation

This chapter describes a hardware testbed created to implement the algorithms formulated in the previous chapter. The testbed is centered around nodes with embedded processors capable of wirelessly exchanging information with other nearby nodes. The nodes are designed to be independent of the DSRs, enabling the testbed to be portable to various applications. Throughout the remainder of the chapter, the hardware chosen is described while the software used to implement the algorithms is explained.

3.1 Communication Hardware Platform

In this section, we describe the hardware chosen to create the testbed and provide a brief overview of the software used to exchange information between devices and to implement the algorithms.

3.1.1 Node Hardware

The hardware testbed is based around Arduino, an open-source electronics prototyping platform. Arduino was chosen for its flexibility and ease of use as well as for the numerous software libraries and extension circuit boards, called shields, that are available [11].

Each node in the testbed contains an Arduino Mega 2560 [12] microcontroller (μC) board which is based on the AVR ATmega2560 [13]. The Arduino board, shown in Fig. 3.1a, provides access to the digital I/O and analog input ports on the μC and contains a USB connection for flashing and powering the device. The ATmega2560 μC has 256 kB of flash memory and a clock speed of 16 MHz as well as four universal asynchronous receiver/transmitter (UART) ports that enable it to communicate with several devices independently.

In order to enable the nodes to exchange information wirelessly, each Arduino Mega is connected to a MaxStream XB24-DMCIT-250 revB XBee module [14] via a SparkFun Electronics XBee shield [15]. The XBee shield, shown in Fig. 3.1b, serves as an interface between the Arduino board and the XBee module while providing the requisite 3.3 V power supply via a voltage regulator. Furthermore, each shield is modified to allow the Arduino board to communicate with a computer via USB and the XBee independently. The XBee, shown in Fig. 3.1c, is an embedded RF module operating at 2.4 GHz that utilizes a built-in chip

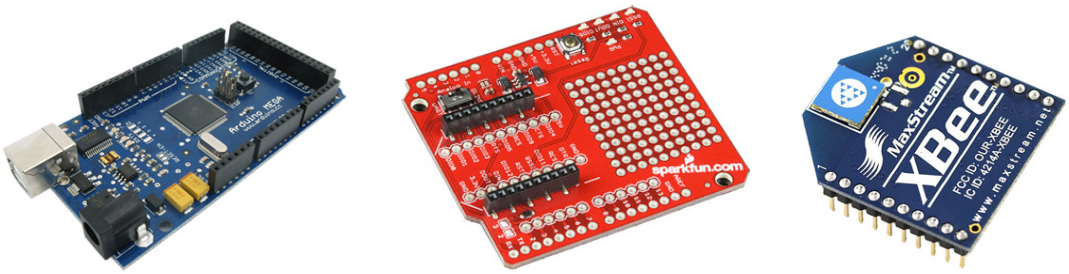

(a) Arduino Mega 2560 (b) SparkFun XBee Shield (c) MaxStream XBee Module

Figure 3.1: Hardware

antenna and requires only a single connection to the μC via one of the UART ports.

3.1.2 Software Setup

To facilitate the exchange of values for the distributed algorithms, each XBee module is put into API mode (AP=2 with escapes), and the three-layered communication protocol stack shown in Fig. 3.2 is implemented. The lowest layer of the stack is based on the ZigBee (IEEE 802.15.4) protocol [16], and is contained entirely on the XBee modules. The middle layer consists of a modified version of the xbee-arduino API [17]. The modifications allow wired communication between the nodes and a computer to continue uninterrupted while the nodes exchange information wirelessly. Additionally, the API was altered to enable incoming and outgoing messages to be time-stamped immediately upon receipt and just before being sent to increase the accuracy of the time synchronization mechanism discussed in the next section. The header of the top layer contains information about the distributed algorithm being used while the payload holds the values exchanged during the iterative process.

All of the software created for implementing the distributed algorithms on the nodes is written in C++. Furthermore, an object-oriented approach is taken where possible to encourage code reuse and to simplify the initialization of the algorithms. The Arduino software environment is used to program the μCs and for monitoring the serial port to gather data.

3.2 Distributed Algorithm Implementation

In order to take advantage of the wireless medium used for communication among nodes, all of the packets used to exchange values are broadcasted; that is, packets are not addressed to a particular node. Furthermore, to minimize network traffic, no acknowledgements are sent upon successful receipt of packets. To create a partially connected network despite the close proximity of the nodes during testing, each μC is programmed to only accept messages received from nodes in its in-neighborhood. In a more realistic setup, however, the testbed could be adapted to allow the availability of links between nodes to be based upon signal strength.

Throughout the formulation of the algorithms in the previous chapter, we assumed that all

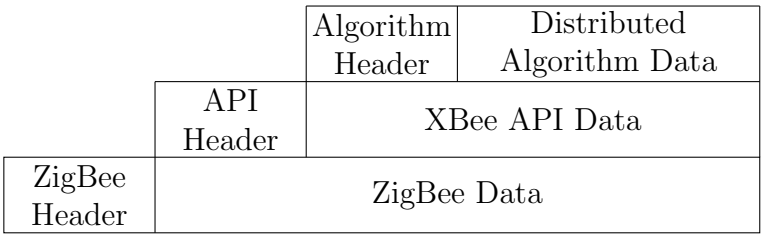

Figure 3.2: Communication protocol stack

participating DSRs update the value of their state variables in unison; i.e., DSR i updates its state at iteration k at the same time DSR j updates its state, $\forall i, j \in \mathcal{V}$. Without a common time reference and with no acknowledgements, however, it is possible for the DSRs to update their states at different times which could cause the DSRs to converge to the wrong solution or possibly diverge. Thus, to ensure convergence to the correct solution, all nodes are synchronized to a common reference before initializing the distributed algorithm.

The synchronization mechanism used in the hardware testbed is based on the hierarchy referencing time synchronization (HRTS) protocol proposed in [18]. This protocol requires very little overhead and is capable of synchronizing the clocks of several nodes to the clock of a reference node using only three packets. As mentioned previously, given the close proximity of the nodes during testing, the graph representing the communication structure in the network is completely connected; thus, in order to simplify the process, no communication restrictions are placed on the nodes during synchronization.

To initiate the time synchronization process, the reference node (e.g. the leader node) broadcasts a `sync_begin` packet at time t_1, specifying a target node from its out-neighborhood chosen randomly. The target node then responds using a unicast packet that contains the time the `sync_begin` packet was received, t_2, and the time the response packet was sent, t_3. All other nodes interested in synchronizing to the reference node record the local time at which the `sync_begin` packet was received, t_2', but do not respond. At time t_4, the reference node receives the response packet from the target node and thus owns all of the timestamps required to determine the offset between its local clock and the local clock of the target node. Assuming negligible propagation delay, the reference node computes the offset as

$$d = \frac{(t_2 - t_1) - (t_4 - t_3)}{2} \tag{3.1}$$

and broadcasts it in a final packet also containing t_2. At this point, the target node can complete the synchronization process by adjusting its clock to be $T = t + d$, where t is the local clock reading before synchronization. The timestamp t_2 included in the final packet from the reference node is used by all other nodes to estimate the offset between their local clocks and the local clock of the target node as $d' = t_2 - t_2'$. Using this estimate, the remaining nodes can now adjust their clocks to be $T = t + d + d'$, where t is the local clock of the respective node before synchronization. In the testbed, rather than adjust the clocks of synchronized nodes, a function extending the low-level clock `timer0_millis` is used which adds the offset found using HRTS to the local time, providing a clock that is common throughout the network.

Procedure 1: General distributed algorithm

Input: iteration period, number of iterations, initial command, *(optional)* constraints
Output: new resource command

```
begin
    generate random transmit time;
    foreach iteration do
        begin timer;
        while timer < iteration period do
            look for incoming packet;
            if packet available then
                if sender ∈ in-neighborhood then
                    store incoming value(s);
            if transmit time = time elapsed then
                broadcast current value(s);
        compute next value;
    compute final command;
```

As mentioned above, the computation of the clock offset between nodes in the HRTS protocol assumes there is negligible communication delay. Thus packets exchanged during the synchronization process should be time stamped at the lowest possible protocol layer to reduce error resulting from data propagating up the protocol stack. In the testbed, however, the bottom layer of the stack cannot be modified, so all time stamps are generated at the middle protocol layer. Given this configuration, the delay present in the system results in a worst case clock error on the order of 10 ms. To mitigate the effects of this error on the distributed algorithms, the nodes are restricted from transmitting data for a period of time which exceeds the clock error during the beginning and end of each iteration.

After synchronizing the clocks of all of the nodes in the network, the distributed algorithm begins. The number of iterations, m, and the period of each iteration is known by all of the nodes *a priori* to ensure that synchronism is maintained throughout the iterative process. The function in Procedure 1 outlines the basic routine executed at each node participating in the distributed algorithm. The required arguments of this function are the initial value, the iteration period and the number of iterations to be performed while resource constraints can be passed as optional arguments. Although the ZigBee protocol seeks to minimize packet collisions at the lowest layer of the protocol stack, the nodes attempt to avoid collisions by broadcasting their values at randomly chosen times within the iteration period.

Chapter 4

Experimental Results

In this chapter, experimental results generated from the unconstrained, constrained and robust algorithms as implemented on the hardware testbed are presented. Throughout this chapter, the inputs and outputs of the algorithms are in units of per unit energy. Furthermore, the terms node and DSR are used interchangeably.

4.1 Unconstrained Algorithm

The hardware testbed is used to implement the unconstrained algorithm on the 4-node network with leader depicted by the graph in Fig. 4.1. For this experiment, the leader node is indexed by 0 and the energy demand is $\rho_d^r = 1$. The leader is an in-neighbor of DSRs 1 and 2, thus, $\pi_1[0], \pi_2[0] = \rho_d^r/l = \frac{1}{2}$, $\pi_3[0], \pi_4[0] = 0$ and the nodes update their values according to algorithm (2.4) as

$$\begin{aligned}
\pi_1[k+1] &= \frac{1}{3}(\pi_1[k] + \pi_2[k] + \pi_3[k]), \\
\pi_2[k+1] &= \frac{1}{3}(\pi_1[k] + \pi_2[k]) + \frac{1}{2}\pi_4[k], \\
\pi_3[k+1] &= \frac{1}{3}(\pi_1[k] + \pi_3[k]), \\
\pi_4[k+1] &= \frac{1}{3}(\pi_2[k] + \pi_3[k]) + \frac{1}{2}\pi_4[k].
\end{aligned} \tag{4.1}$$

Equation (4.1) can be written in matrix form according to (2.2), where $\pi[0] = \left[\frac{1}{2}, \frac{1}{2}, 0, 0\right]^{\mathrm{T}}$ and

$$P = \begin{bmatrix} 1/3 & 1/3 & 1/3 & 0 \\ 1/3 & 1/3 & 0 & 1/2 \\ 1/3 & 0 & 1/3 & 0 \\ 0 & 1/3 & 1/3 & 1/2 \end{bmatrix}. \tag{4.2}$$

The evolution of the values of $\pi[k]$ computed at each node is plotted in Fig. 4.2. From the plot, it can be seen that the nodes converge to their steady-state values in approximately 8 iterations. For this experiment, the nodes are programmed to perform 14 iterations; thus

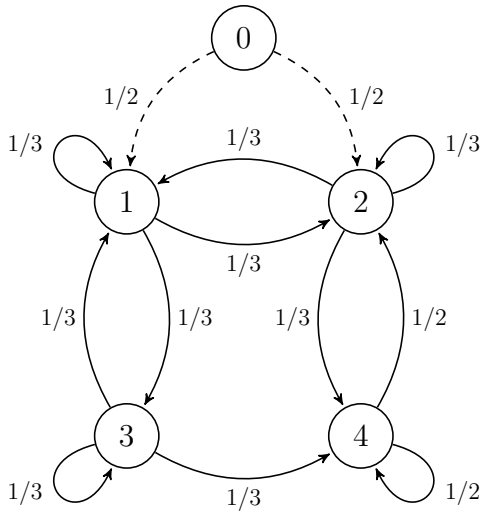

Figure 4.1: Graph of 4-node network with leader

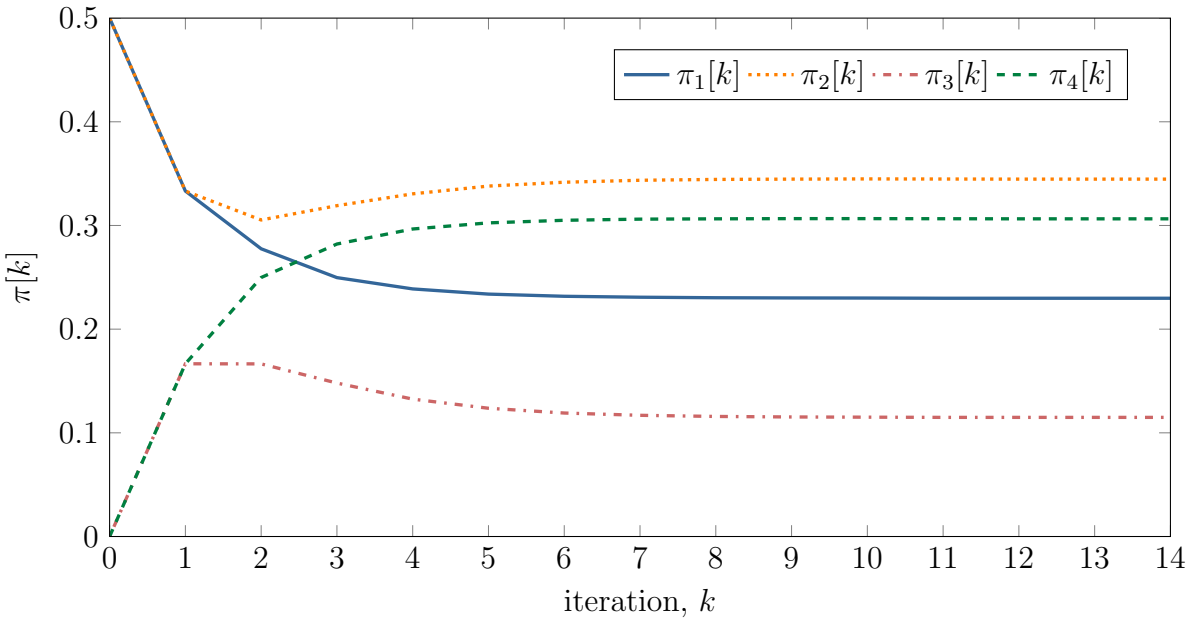

Figure 4.2: Unconstrained results

the vector of final values corresponding to the amount of energy each DSR should provide during interval r is given as $x^r = \pi[14] = \left[0.230, 0.345, 0.119, 0.306\right]^{\mathrm{T}}$. Due to the directed edge between nodes 3 and 4, this is an example where the DSRs do not equally split the total energy demand among themselves.

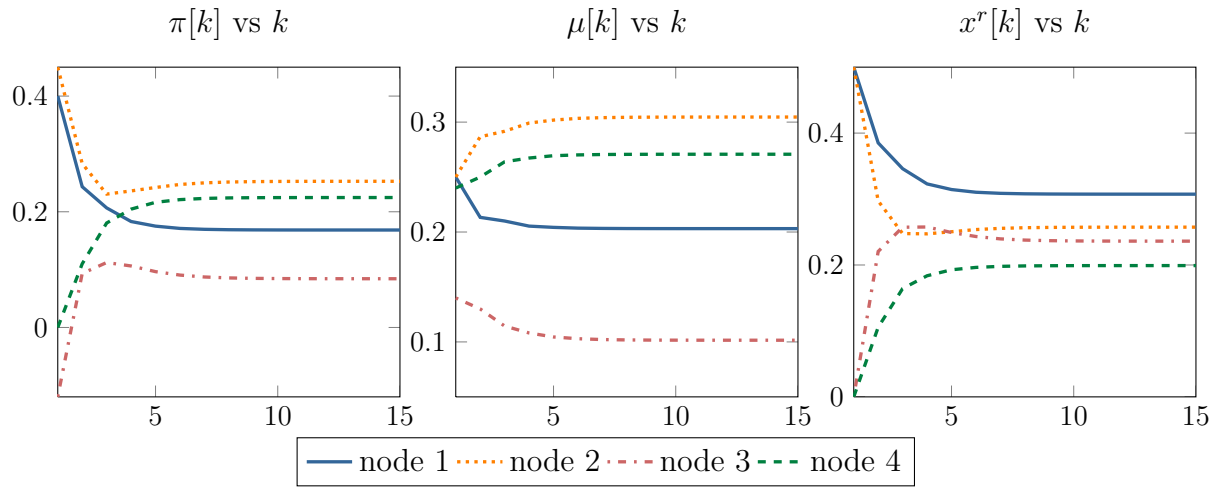

Figure 4.3: Evolution of the distributed algorithm for a network of 4 nodes with constraints

4.2 Constrained Algorithm Results

Similar to the unconstrained example, the 4-node network represented by the graph in Fig. 4.1 is constructed using the hardware testbed to evaluate the convergence of the constrained algorithm. To illustrate the effects of link availability on convergence, we present a case in which the constrained algorithm converges to the correct solution and a case in which it does not.

4.2.1 Correct Convergence

In order to allow sufficient time for nodes to exchange information and compute their next value, a period of 500 ms is apportioned for each iteration. Furthermore, nodes are restricted from transmitting during the first and last 50 ms of each iteration to account for any synchronization errors. As in the unconstrained example, the leader node is indexed by 0 and the energy demand during interval r is chosen to be $\rho_d^r = 1$. The lower and upper constraints are given by the vectors $\underline{x}^r = \left[0.1, 0.05, 0.12, 0\right]^{\mathrm{T}}$ and $\overline{x}^r = \left[0.35, 0.3, 0.26, 0.24\right]^{\mathrm{T}}$, respectively. To ensure a feasible solution, the individual limits are chosen such that the total energy demanded from the DSRs lies within the bounds of the collective constraints, that is, $\underline{\chi}^r = 0.27 < \rho_d^r < \overline{\chi}^r = 1.15$.

Given the amount of energy demanded by the leader and the individual constraints, the initial values for (2.8) and (2.9) are $\mu_1[0] = 0.4, \mu_2[0] = 0.45, \mu_3[0] = -0.12, \mu_4[0] = 0$ and $\sigma_1[0] = \sigma_2[0] = 0.25, \sigma_3[0] = 0.14, \sigma_4[0] = 0.24$ and the constrained algorithm written in matrix form is given as

$$\begin{aligned} \mu[k+1] &= P\mu[k] \\ \mu[0] &= \left[0.4, 0.45, -0.12, 0\right]^{\mathrm{T}} \\ \sigma[k+1] &= P\sigma[k] \\ \sigma[0] &= \left[0.25, 0.25, 0.14, 0.24\right]^{\mathrm{T}}, \end{aligned} \tag{4.3}$$

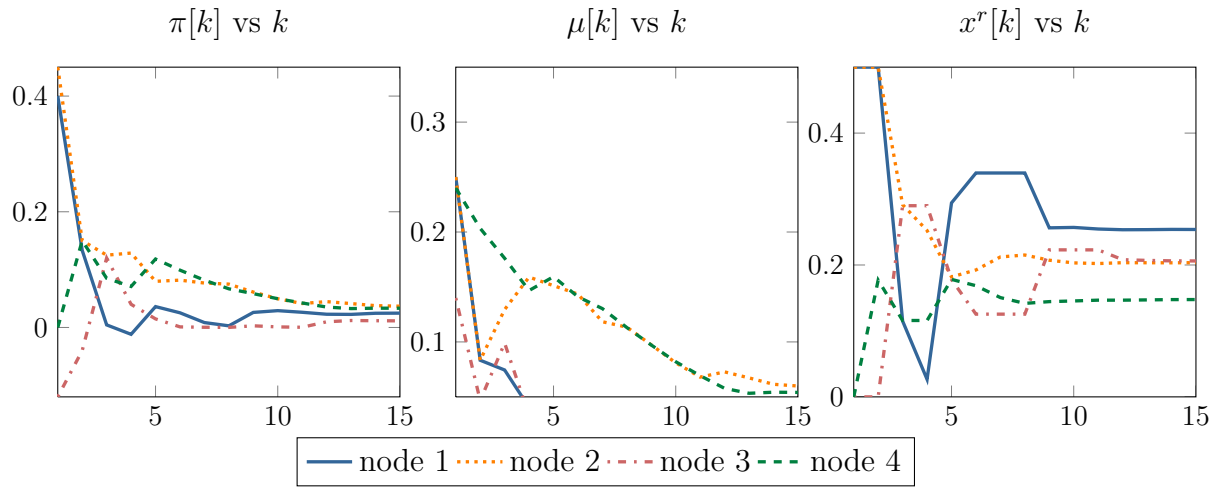

Figure 4.4: Incorrect evolution of the distributed algorithm for a network of 4 nodes with constraints

where P is the matrix given in (4.2).

The evolution of the constrained distributed algorithm is shown in Fig 4.3. Although each node i is not required to compute x_i^r until the iterative process is complete, it is useful to illustrate the evolution of the system. Thus the values of $\mu_i[k]$, $\sigma_i[k]$ and $x_i^r[k]$ for $i = 1, 2, 3, 4$ are shown in the figure. The plots show that the nodes reach their steady-state values in approximately 8 iterations, which given an iteration period of 500ms, requires around 4 seconds. As in the unconstrained case, the nodes are programmed to perform 14 iterations; thus, the nodes compute the amount of energy each DSR should provide during interval r according to (2.10) with $m = 14$ and we have that $x^r = \left[0.307, 0.257, 0.237, 0.199\right]^{\mathrm{T}}$. If we sum the energy provided by all the DSRs, we see that the collective output meets the overall demand, i.e., $\sum_{i=1}^{4} x_i^r = 1 = \rho_d^r$, while no individual constraints are exceeded.

4.2.2 Incorrect Convergence

The iteration period was chosen conservatively in the previous experiment to reduce the probability of packet collisions resulting from nodes broadcasting their values concurrently. Moreover, nodes were restricted from transmitting information during the first and last 50 ms of each iteration to ensure that the algorithm would converge correctly despite synchronization error. To illustrate the sensitivity to these parameters, the 4-node network is tested again using a significantly smaller iteration period of 50 ms with no restrictions on broadcast time.

Using the same initial conditions as in the previous example, the evolution of the values maintained by the nodes is plotted in Fig. 4.4. From these plots it is evident that the loss of packets induced by reducing the iteration period effectively removes the ability of the algorithm to preserve the sum of the values maintained by the nodes, causing $\mu[k]$ and $\sigma[k]$ to quickly converge to zero. Although the values exchanged by the nodes approach zero, the figure illustrates that the value of $x^r[k]$, computed as a function of the ratio of $\mu[k]$ and $\sigma[k]$, tends toward a nonzero steady-state solution. Running the algorithm for

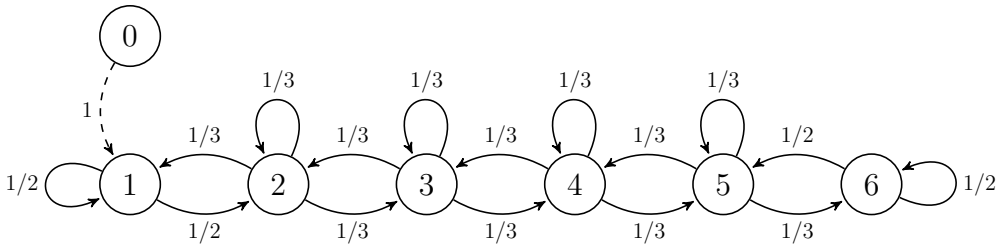

Figure 4.5: Graph of 6-node network with leader

99 iterations (only the first 15 are shown in the figure) results in a steady-state solution of $x^r = \left[0.254, 0.204, 0.206, 0.147\right]^{\mathrm{T}}$. The total energy provided by the DSRs is given as $\sum_{i=1}^{4} x_i^r = 0.811 \neq \rho_d = 1$. Thus there is a mismatch between the collective amount of energy supplied and the total energy demand, and the algorithm is ineffective.

4.3 Robust Algorithm with Constraints Results

The 6-node network with leader node represented by the graph in Fig. 4.5 is created using the hardware testbed to evaluate the robust algorithm with constraints. In order to induce dropped packets, the iteration period is reduced to 40 ms and no restrictions are placed on broadcast time.

For this experiment, the leader is indexed by 0 and the energy demand is chosen to be $\rho_d^r = 1$. Node 1 is the only DSR with the leader in its in-neighborhood, thus all of the energy demand is passed to it initially. The minimum and maximum amount of energy each DSR can provide during interval r are given, respectively, by

$$\underline{x}^r = \left[0.02, 0.1, 0.05, 0.08, 0.12, 0\right]^{\mathrm{T}},$$
$$\overline{x}^r = \left[0.146, 0.208, 0.193, 0.167, 0.229, 0.159\right]^{\mathrm{T}}.$$

The collective lower and upper bounds are chosen to ensure the system is capable of meeting the overall energy demand during interval r, i.e., $\underline{\chi}^r = 0.37 < \rho_d^r < \overline{\chi}^r = 1.102$.

Using the energy demand and the constraints of each DSR, the initial values of the internal states are given by the vectors

$$y[0] = \left[0.98, -0.1, -0.05, -0.08, -0.12, 0\right]^{\mathrm{T}},$$
$$z[0] = \left[0.126, 0.108, 0.143, 0.087, 0.109, 0.159\right]^{\mathrm{T}}.$$

Furthermore, the matrix of weights used by the nodes is given by

$$P = \begin{bmatrix} 1/2 & 1/3 & 0 & 0 & 0 & 0 \\ 1/2 & 1/3 & 1/3 & 0 & 0 & 0 \\ 0 & 1/3 & 1/3 & 1/3 & 0 & 0 \\ 0 & 0 & 1/3 & 1/3 & 1/3 & 0 \\ 0 & 0 & 0 & 1/3 & 1/3 & 1/2 \\ 0 & 0 & 0 & 0 & 1/3 & 1/2 \end{bmatrix}.$$

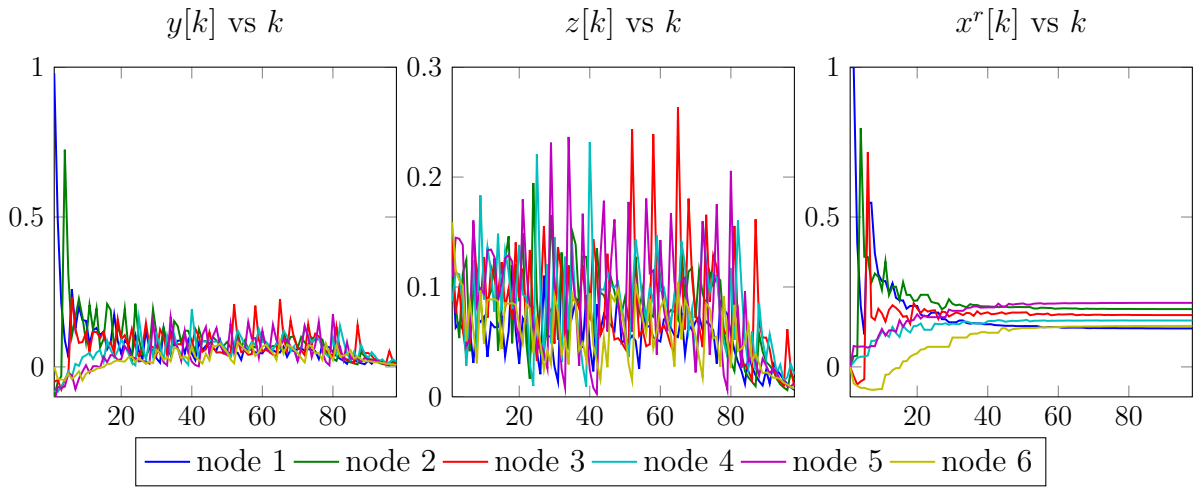

Figure 4.6: Evolution of robust constrained algorithm

The evolution of the internal states and the output of each DSR computed at each node running the robust algorithm is shown in Fig. 4.6. The plots of the internal states $y[k]$ and $z[k]$ show erratic behavior that does not appear to reach steady-state. Despite this, $x^r[k]$ converges to a steady-state solution that meets the overall generation demand. After running 99 iterations, the generation output of each DSR is computed and given by the vector

$$x^r = \left[0.128, 0.193, 0.173, 0.155, 0.214, 0.137\right]^{\mathrm{T}}.$$

If we sum the total amount of generation provided by the DSRs, we see that $\rho^r = \rho_d^r$, while none of the individual resource constraints are violated.

4.4 Determining Feasibility

As mentioned in Section 2.4.2, each node can independently determine if the collective capacity of the available DSRs is sufficient to meet the overall energy demand during interval r. Specifically, after performing the specified number of iterations and computing α_i according to (2.15), each node can determine if the demand for energy is outside the collective bounds of the DSRs if $\alpha_i > 1$ or $\alpha_i < 0$. By taking advantage of this property, it is possible, for instance, to designate a subset of DSRs as reserves which can participate in the distributed algorithm with artificially restricted limits until determining that the capacity of the remaining DSRs has been exceeded. To illustrate the ability of the individual nodes to determine feasibility, we show results for a case in which the resource demand is within the collective limit of the DSRs and one in which it is not. In both cases, the robust algorithm with constraints is used to implement the 4-node network depicted by the graph in Fig. 4.1 and the total demand for energy is chosen to be $\rho_d^r = 1$.

We first demonstrate the case in which the energy demand is within the collective bounds of the DSRs. For this experiment, the leader node is indexed by 0, the energy demand is chosen to be $\rho_d^r = 1$. Let the minimum and maximum capacities of the nodes be given respectively by $\underline{x}^r = \left[0.15, 0, 0.15, 0.1\right]^{\mathrm{T}}$ and $\overline{x}^r = \left[0.3, 0.15, 0.4, 0.25\right]^{\mathrm{T}}$, such that $\underline{\chi}^r = 0.4 \leq \rho_d^r \leq \overline{\chi}^r = 1.1$.

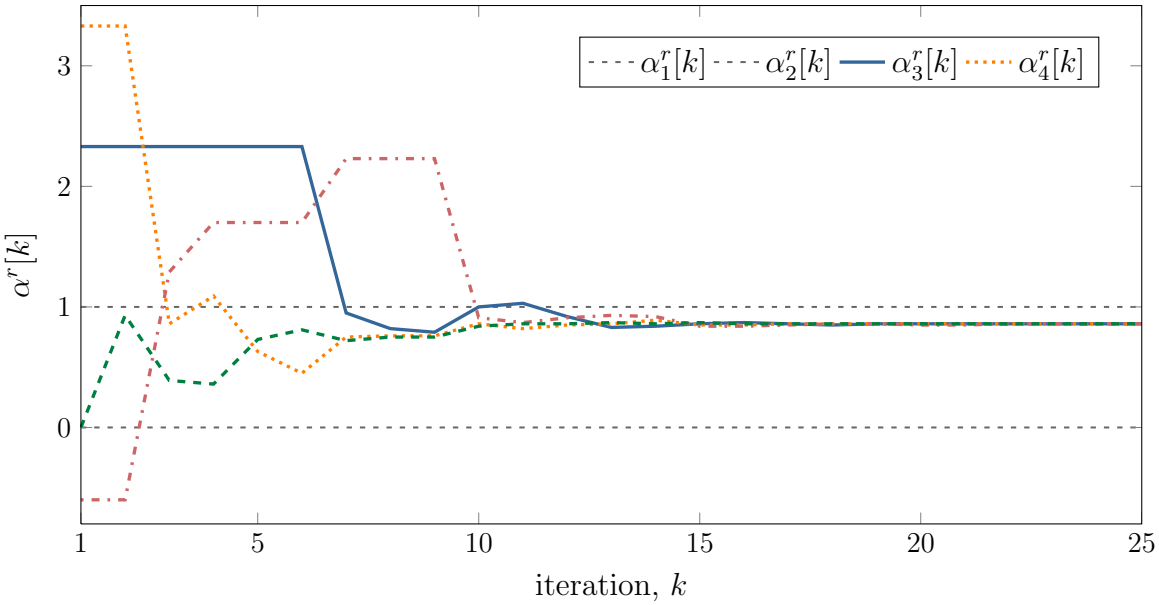

Figure 4.7: Evolution of $\alpha^r[k]$ for a 4-node system with feasible solution

Given the energy demand and the limits of the DSRs, the vectors of initial states are given as $y[0] = \left[0.35, 0.5, -0.15, -0.1\right]^{\mathrm{T}}$, and $z[0] = \left[0.15, 0.15, 0.25, 0.15\right]^{\mathrm{T}}$.

The evolution of $\alpha_i^r[k]$ for $j = 1, 2, 3, 4$ over 25 iterations is shown in Fig. 4.7. From the figure, we see that after approximately 15 iterations, all nodes have converged to a solution in which $\alpha = 0.857$. Thus, the nodes determine the solution is feasible and compute the amount of energy each DSR should provide during interval r according to (2.20), and we have that $x^r = \left[0.279, 0.129, 0.364, 0.228\right]^{\mathrm{T}}$.

We now demonstrate a case in which the collective capacity of the DSRs is insufficient to meet the total demand for energy. Let the energy demand be the same as in the previous case but adjust the minimum and maximum capacity of the nodes to be given respectively by $\underline{x}^r = \left[0.1, 0, 0.1, 0.1\right]^{\mathrm{T}}$ and $\overline{x}^r = \left[0.25, 0.15, 0.3, 0.25\right]^{\mathrm{T}}$, such that $\underline{\chi}^r = 0.3$ and $\overline{\chi}^r = 0.95 < \rho_d^r$. Thus, the vectors of initial states are given as $y[0] = \left[0.4, 0.5, -0.1, -0.1\right]^{\mathrm{T}}$ and $z[0] = \left[0.15, 0.15, 0.2, 0.1\right]^{\mathrm{T}}$.

The evolution of $\alpha_i^r[k]$ for the four nodes over 25 iterations is shown in Fig. 4.8. From this figure, we see that after approximately 15 iterations, all nodes have converged to a solution in which $\alpha^r = 1.167$. Thus, the nodes determine that the solution is infeasible and they cannot adjust their output beyond their maximum capacities.

4.5 Even Splitting Algorithm

In the previous examples demonstrating algorithms that account for constraints, the output of each DSR was computed such that the energy demand was distributed fairly among all DSRs in the system. Specifically, as illustrated by (2.15), after the algorithm has converged, each DSR i determines its generation output based upon its constraints and α_i^r. Since α_i^r is

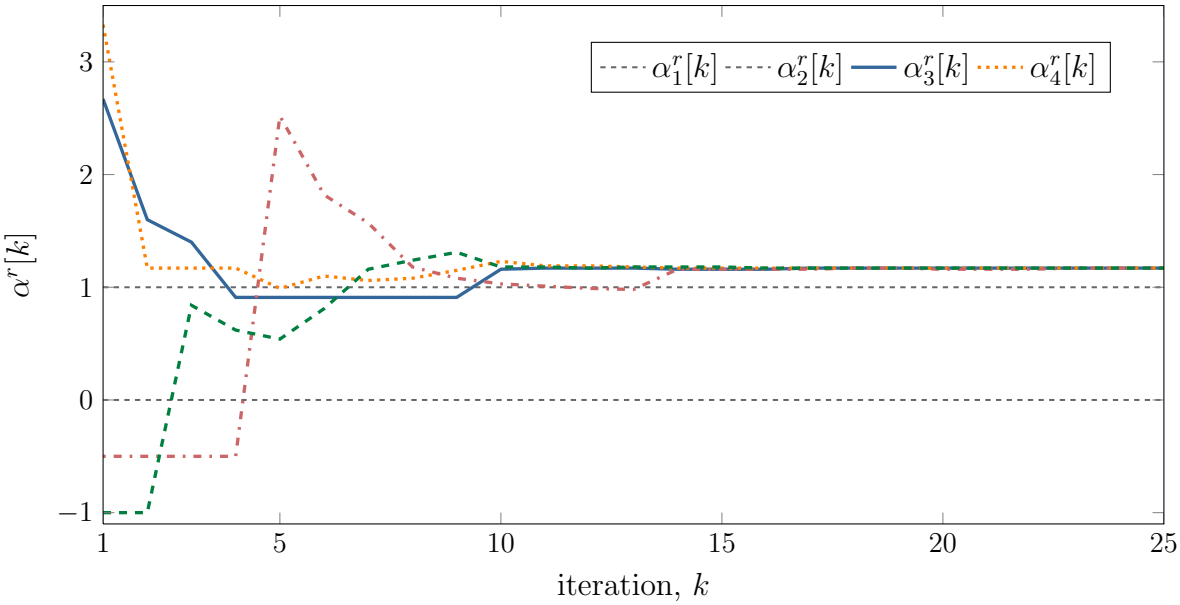

Figure 4.8: Evolution of $\alpha^r[k]$ for a 4-node system with infeasible solution

the ratio of the total demand to the collective capacity of the system, the output of each DSR is chosen to be proportional to the overall loading in the system relative to its constraints. In the absence of constraints, however, the algorithm can be adapted such that the total demand for energy is evenly divided among all DSRs in the system, i.e., $x_i^r = \rho_d^r/n,\ \forall i$.

To demonstrate a case in which the nodes split the overall demand evenly, the 7-node network depicted by the graph in Fig. 4.9 is created using the hardware testbed and the robust algorithm with constraints with $\underline{x}_i^r = 0$ and $\overline{x}_i^r = 1,\ i = 1, \ldots, 7$. Unlike the previous examples, there is no leading node. Rather, each DSR demands the values of energy given by the the following vector

$$\left[0.2, 0.1, 0.05, 0.15, 0.25, 0.35, 0.5\right]^{\mathrm{T}},$$

such that the total energy demand is $\rho_d = 2.1$ and the vectors of initial states are given as

$$y[0] = \left[0.7, 0.1, 0.05, 0.15, 0.25, 0.35, 0.5\right]^{\mathrm{T}},$$
$$z[0] = \left[1.0, 1.0, 1.0, 1.0, 1.0, 1.0, 1.0\right]^{\mathrm{T}}.$$

Given the edges in the graph representing the communication network, the matrix of weights is

$$P = \begin{bmatrix} 1/4 & 1/3 & 0 & 0 & 1/2 & 1/3 & 0 \\ 1/4 & 1/3 & 0 & 0 & 0 & 0 & 0 \\ 0 & 1/3 & 1/2 & 0 & 0 & 0 & 0 \\ 1/4 & 0 & 1/2 & 1/3 & 0 & 0 & 0 \\ 0 & 0 & 0 & 1/3 & 1/2 & 1/3 & 1/2 \\ 1/4 & 0 & 0 & 0 & 0 & 1/3 & 0 \\ 0 & 0 & 0 & 1/3 & 0 & 0 & 1/2 \end{bmatrix}.$$

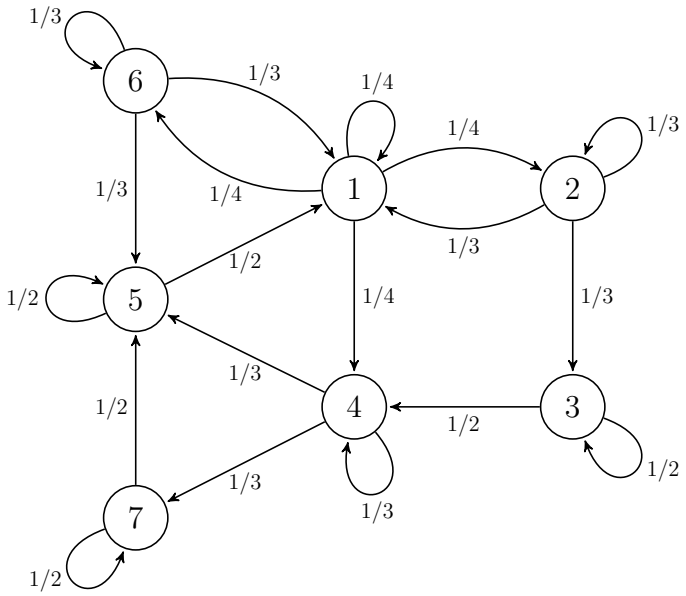

Figure 4.9: Graph of 7-node network

The evolution of $x^r[k]$ for the seven nodes over 35 iterations is shown in Fig. 4.10. From the figure, it can be seen that the nodes converge to a solution after approximately 30 iterations. As expected, all DSRs split the total demand evenly and thus $x_i^r = 0.3 = \rho_d/7,\ i = 1, \ldots, 7$.

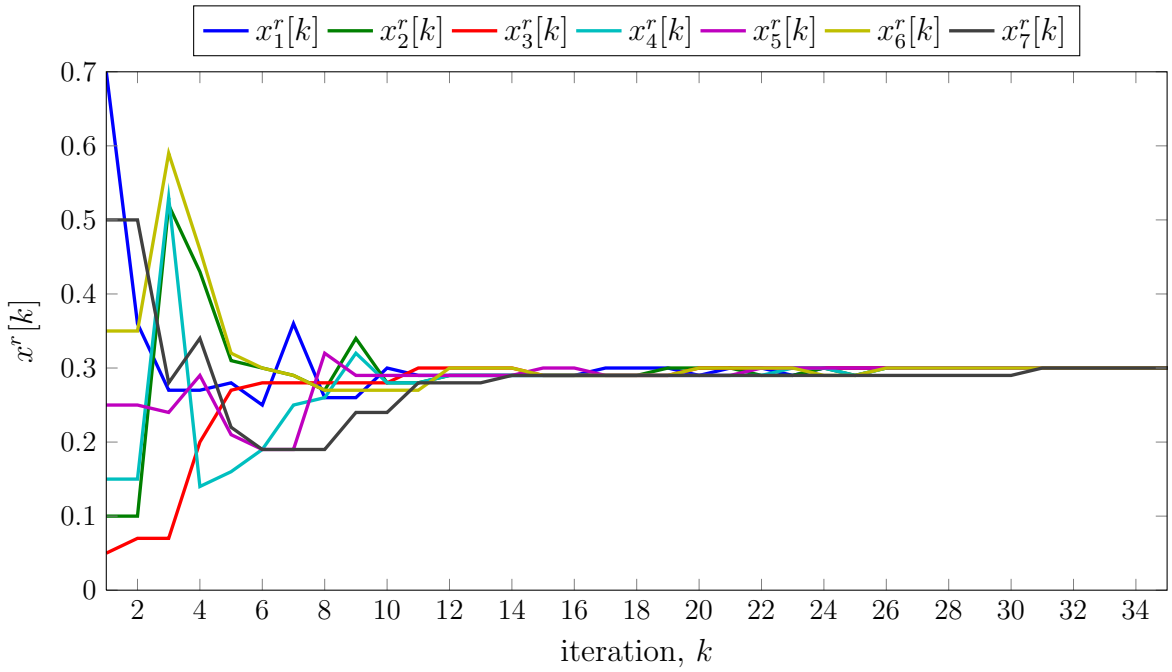

Figure 4.10: Evolution of $x^r[k]$ for 7-node system with even splitting

Chapter 5

Concluding Remarks and Future Work

5.1 Concluding Remarks

In this report, several algorithms suitable for controlling distributed storage resources without the need for a centralized controller were proposed. We began by formulating an unconstrained algorithm that iteratively disperses the total energy demand among the DSRs and analyzed its convergence. We then extended this algorithm to account for individual DSR constraints and discussed how the result could be used by each DSR to ascertain the global state of the system. Finally we adapted the constrained algorithm to be more resilient to imperfect communication links. Each of the proposed algorithms was implemented using a hardware testbed comprised of low complexity devices capable of performing simple computations and exchanging information wirelessly with other nearby devices. Results were presented illustrating the capabilities of the hardware testbed as well as the evolution of the values computed at each iteration for the algorithms

All of the results presented herein were for systems comprised of relatively few DSRs. Despite this, the algorithms are scalable, with only convergence speed being affected by the total number of nodes participating (and the connectivity of the communication network linking them). Furthermore, the application to distributed energy storage is just one of many that would be well-suited for a distributed control architecture similar to the ones proposed in this report. In fact, the algorithms discussed could be adapted for any class of applications in which one wishes to coordinate a set of distributed agents such that they collectively achieve a desired goal. Additionally, the algorithms could be used for applications in which resiliency and self-healing are important since the distributed nature obviates the need for a centralized controller with full knowledge of the network.

5.2 Future Work

One worthwhile future pursuit would be to account for both energy and power constraints. In the formulation of the constrained algorithm, it was assumed that the power rating of each DSR was sufficient to provide the amount of energy demanded over the specified period, i.e.,

$\underline{p}_i \leq x_i^r/\Delta \leq \overline{p}_i$. While this assumption is not unreasonable, it would be useful to account for arbitrary combinations of power and energy constraints to accommodate several different types of energy storage devices.

Another aspect we would like to address is the costs associated with each DSR. While we demonstrated cases in which individual DSR constraints were accounted for, we neglected the incremental costs associated with increasing or decreasing the output of the DSRs. Given a quadratic cost function and upper and lower bounds on the energy output of each DSR, we would like to find a solution that minimizes the total cost while meeting the total demand for energy without violating DSR limits. That is, we would like to use a distributed algorithm to find x_i^r for $i = 1, \ldots, n$, such that

$$\begin{aligned} \text{minimize} \quad & \sum_{i=1}^{n} \frac{(x_i - \alpha_i)^2}{2\beta_i} \\ \text{subject to} \quad & \sum_{i=1}^{n} x_i^r = \rho_d^r \\ & 0 < \underline{x}_i^r \leq x_i^r \leq \overline{x}_i^r, \ \forall i, \end{aligned} \tag{5.1}$$

where $\alpha_i \leq 0$ and $\beta_i > 0$ are real numbers. To achieve this, we plan to expand our work in [19] by implementing the proposed optimal solution utilizing the hardware testbed and using it to optimally control the DSRs.

References

[1] G. Joos, B. Ooi, D. McGillis, F. Galiana, and R. Marceau, "The potential of distributed generation to provide ancillary services," in *Proc. of IEEE Power Engineering Society Summer Meeting*, vol. 3, Seattle, WA, 2000, pp. 1762 – 1767.

[2] M. Baran and I. El-Markabi, "A multiagent-based dispatching scheme for distributed generators for voltage support on distribution feeders," *IEEE Transactions on Power Systems*, vol. 22, no. 1, pp. 52 –59, Feb. 2007.

[3] K. Turitsyn, P. Šandulc, S. Backhaus, and M. Chertkov, "Distributed control of reactive power flow in a radial distribution circuit with high photovoltaic penetration," in *Proc. IEEE Power and Energy Society General Meeting*, july 2010, pp. 1 – 6.

[4] A. D. Dominguez-Garcia, C. N. Hadjicostis, P. T. Krein, and S. T. Cady, "Small inverter-interfaced distributed energy resources for reactive power support," in *Proc. Applied Power Electronics Conference and Exposition*, March 2011, pp. 1616 –1621.

[5] C. Guille and G. Gross, "A conceptual framework for the vehicle-to-grid (v2g) implementation," *Energy Policy*, vol. 37, no. 11, pp. 4379 – 4390, 2009.

[6] A. D. Domínguez-García and C. N. Hadjicostis, "Coordination and control of distributed energy resources for provision of ancillary services," in *Proc. IEEE International Conference on Smart Grid Communications*, Gaithersburg, MD, October 2010, pp. 537 –542.

[7] A. D. Dominguez-Garcia and C. N. Hadjicostis, "Distributed algorithms for control of demand response and distributed energy resources," in *Decision and Control and European Control Conference (CDC-ECC), 2011 50th IEEE Conference on*, dec. 2011, pp. 27 –32.

[8] A. D. Domínguez-García, C. N. Hadjicostis, and N. H. Vaidya, "Distributed algorithms for consensus and coordination in the presence of packet-dropping communication links - part i: Statistical moments analysis approach," in *University of Illinois at Urbana-Champaign. Coordinated Science Laboratory technical report*, September 2011.

[9] D. B. West, *Introduction to Graph Theory*, 2nd ed. Prentice Hall, 2001.

[10] R. Horn and C. Johnson, *Matrix Analysis*. New York, NY: Cambridge University Press, 1985.

[11] (2011, October) Arduino. [Online]. Available: http://www.arduino.cc

[12] (2012, Feb.) Arduino mega 2560. [Online]. Available: http://arduino.cc/en/Main/ArduinoBoardMega2560

[13] "Atmel atmega2560," Feb. 2012. [Online]. Available: http://www.atmel.com/devices/ATMEGA2560.aspx

[14] (2011, October) Digi international inc. [Online]. Available: http://www.digi.com/products/wireless-wired-embedded-solutions/zigbee-rf-modules/point-multipoint-rfmodules/xbee-series1-module.jsp

[15] (2011, October) Sparkfun electronics. [Online]. Available: http://www.sparkfun.com/

[16] ZigBee Alliance. (2011, October) ZigBee Specification. San Ramon, CA. [Online]. Available: http://www.zigbee.org

[17] A. Rapp. (2011, October) xbee-arduino. [Online]. Available: http://code.google.com/p/xbee-arduino/

[18] H. Dai and R. Han, "Tsync: a lightweight bidirectional time synchronization service for wireless sensor networks," *SIGMOBILE Mob. Comput. Commun. Rev.*, vol. 8, pp. 125–139, January 2004. [Online]. Available: http://doi.acm.org/10.1145/980159.980173

[19] A. D. Dominguez-Garcia, S. T. Cady, and C. N. Hadjicostis, "Decentralized optimal dispatch of distributed energy resources," in *Under Review for Conference on Decision and Control (CDC), 2012 51th IEEE Conference on*, dec. 2012.